Aston University

Some pages of this thesis may have been removed for copyright restrictions.

If you have discovered material in Aston Research Explorer which is unlawful e.g. breaches copyright, (either yours or that of a third party) or any other law, including but not limited to those relating to patent, trademark, confidentiality, data protection, obscenity, defamation, libel, then please read our Takedown policy and contact the service immediately (openaccess@aston.ac.uk)

STUDIES OF THE DRYING OF PARTICULATE SLURRIES.

by

Thomas Okpo Kimble Audu, M.Sc., Dip.Chem.Eng.

A thesis

submitted in fulfillment of the requirements for the degree of Doctor of Philosophy.

24 FEB 1976

The Department of Chemical Engineering,
The University of Aston in Birmingham,
Birmingham, U.K.

August, 1973.

SUMMARY

The literature relating to the drying characteristics of pure liquid drops and particulate slurry drops has been reviewed. The experimental investigation was, therefore, divided into three parts:

Pure water drops,

Aqueous sodium sulphate decahydrate drops, and,

Slurry drops from nine detergent formulations.

The value of the constant, Ψ , reported by Ranz and Marshall, was found to be temperature dependent. In the temperature range $26.5 \leqslant T \leqslant 118.5^{o}C$, Ψ , for pure water drops, varied between 0.38 and 0.47. A revised correlation of the mass transfer coefficients is therefore proposed:

$$\frac{k_G d_p}{D_M} = 2.0 + 0.44\left(\frac{T_{au} - T_s}{T_{amb}}\right) - 0.008\ Re^{0.5} . Sc^{0.33}$$

A mathematical model for estimating the variation of crust thickness, for aqueous sodium sulphate drops, with time is proposed:

$$\beta = R - \{R^3 - (1.5G/\pi C_o)(\Delta H_D - \Delta H_U)\ \Delta\theta\}^{1/3}$$

Experimental crust thickness evaluated from stereoscan micrographs showed good agreement with theoretical prediction.

It has been shown that drying characteristics of detergent drops can be evaluated from the porosity:thickness ratio, $\{\varepsilon/\beta\}$. Formulations having large $\{\varepsilon/\beta\}$-ratios dry better than those with smaller values. The mass transfer coefficients were well correlated by:

$$\frac{K_m \beta_m}{D_M \varepsilon^{1.5}} = 0.58\left(\frac{\rho u d_p}{\mu}\right)^{0.05}\left(\frac{\mu}{\rho D_M \varepsilon^{1.5}}\right)^{0.06}$$

The agreement between the experimental and theoretical mass transfer coefficients shows, in addition to the above correlation, that the overall mass transfer coefficient can be predicted from the expression:

$$\frac{1}{K} = \frac{1}{k_G} + \frac{\beta}{D_M \varepsilon^{1.5}}$$

The crust is the controlling resistance to transfer in particulate slurry drops. For aqueous sodium sulphate drops, the crust provides 64.2% of the total resistance while for detergents with thicker, but less porous crusts, the value is 97.5%.

DEDICATION

to

My family.

ACKNOWLEDGEMENT.

The author wishes to express his gratitude to: -

Professor G. V. Jeffreys, Head of the Department of Chemical Engineering, University of Aston in Birmingham, who suggested and personally supervised this research programme.

Mr. A. F. Price, who was an Associate Supervisor of this work.

Dr. J. D. Jenkins and Dr. M. P. Wilson for their helpful advice.

Mr. N. Roberts, Chief Technician in the Department of Chemical Engineering, and his staff for their technical assistance.

Mr. J. Fuggle, Stereoscan Technician in the Department of Metallurgy for his assistance.

The Photographic Technicians of the Communications Media.

The Library staff for their "current awareness" search.

Mr. K. C. Echenim of the University of Besancon, France, for translating one of the papers reviewed from French to English.

Unilever Research, Port Sunlight, for supplying the detergent chemicals.

The Elder Dempster Nigeria Independence Trust for a three year Postgraduate grant.

INDEX

Page

Section One.

Introduction. 1

Section Two.

Literature Survey. 5

2.1. Mass Transfer Across a Phase Boundary. 6

2.1.1 Whitman Two-Film Theory. 7

2.1.2 Higbie Penetration Theory. 8

2.1.3 The Film Penetration Theory. 8

2.1.4 Mass Transfer Coefficients. 9

2.2 Colburn Analogy. 12

2.2.1. The j-Factor of Chilton and Colburn 12

2.2.1.1 Heat Transfer 12

2.2.1.2 Mass Transfer 12

2.2.2 Limits of Applicability. 15

2.3 Drying of Drops containing Dissolved Solids 16

2.3.1 Mechanism of Drying in General 16

2.3.1.1 Diffusion Theory 17

2.3.1.2 Capillary Flow Theory 17

2.3.1.3 Evaporation - Condensation Theory 18

2.3.1.4 Constant Rate Period 18

2.3.1.5 Falling Rate Period 19

2.3.2 Drops of Pure Liquids 20

2.3.2.1 Single Drops 20

2.3.2.2 Single Drops in High Temperature Surroundings 25

2.3.2.3 Clouds of Drops 29

2.3.3 Drops containing Dissolved Solids 32

2.3.3.1 Single Drops containing Dissolved Solids 32

Page

2.3.3.2 Mathematical Models for Single Drops containing Dissolved Solids 36

2.3.3.3 Clouds of Drops containing Dissolved Solids. 43

2.4 Conclusion. 45

Section Three

Mathematical Models. 48

3.1. Pure Water Drops. 49

3.1.1 Assumptions. 49

3.1.2 Mass Transfer Rate. 50

3.1.3 Mass Transfer Coefficient. 50

3.1.3.1 Humidity Driving Force. 50

3.1.3.2 Pressure Driving Force. 51

3.2. Drops Containing Dissolved Solids 53

3.2.1 Assumptions 54

3.2.2 Crust Thickness 54

3.2.3 Mass Transfer Coefficient. 56

3.2.3.1 Crust Coefficient. 57

3.2.3.2 Concentration Driving Force. 58

Section Four.

Experimental Apparatus and Procedure. 60

4.1 Description of Apparatus. 61

4.1.1 Overall Flow System. 61

4.1.2 Drop Suspension Device. 64

4.1.2.1 Less-Viscous Liquids or Slurries. 64

4.1.2.2 More-Viscous Slurries 67

4.1.3 Feeding Device. 67

4.1.4 Shaw Hygrometry. 70

Page

4.1.4.1 Sensing Elements 70

4.1.4.2 Constant Temperature Unit 72

4.1.4.3 The Hygrometer 72

4.1.5 Ancillary Equipment: The Stereoscan. 73

4.2 Experimental Procedure. 74

4.2.1 Instrument Calibration. 74

4.2.1.1 Rotameter 74

4.2.1.2 Dew Point Meter. 74

4.2.2 Experiments. 74

4.2.2.1 Air-Water System. 75

4.2.2.2 Sodium Sulphate-Water-Air System 76

4.2.2.3 Crust Thickness Measurements. 78

4.2.2.4 Detergent-Water-Air System. 79

4.2.2.5 Pressure Drop Test for Determining Porosity of the Crust. 80

Section Five.

Presentation and Analysis of Results. 82

5.1 Pure Water Drops. 83

5.1.1 Effect of Air Temperature. 83

5.1.1.1 Mass Transfer Coefficients. 83

5.1.1.2 Mass Transfer Rate. 83

5.1.2 Effect of Drop Diameter. 89

5.1.2.1 Mass Transfer Coefficient. 89

5.1.2.2 Mass Transfer Rate. 89

5.1.3 Correlations. 89

5.2 Sodium Sulphate Decahydrate Drops. 94

5.2.1 Effect of Air Flow Rate. 97

5.2.1.1 Crust Thickness Rate 97

Page

5.2.1.2 Overall Mass Transfer Coefficient 97

5.2.1.3 Driving Force 97

5.2.2 Effect of Initial Drop Radius 97

5.2.2.1 Crust Thickness Rate 97

5.2.2.2 Overall Mass Transfer Coefficient 104

5.2.2.3 Driving Force 104

5.2.3 Effect of Air Temperature 104

5.2.3.1 Crust Thickness Rate 104

5.2.3.2 Overall Mass Transfer Coefficient 104

5.2.3.3 Driving Force 104

5.2.4 Effect of Initial Moisture Content 111

5.2.4.1 Crust Thickness Rate 111

5.2.4.2 Overall Mass Transfer Coefficient 111

5.2.4.3 Driving Force 111

5.2.5 Comparison of Predicted with Experimental Crust Thickness 111

5.2.6 Sodium Sulphate Micrographs 111

5.3 Detergent Slurry Drops. 121

5.3.1 Determination of Specific Surface Area of Bed 122

5.3.1.1 The B.E.T Method. 122

5.3.1.2 The Geometric Method. 123

5.3.2 Analysis of Mass Transfer Characteristics 129

5.3.2.1 Trend of Curves for Nine Detergent Formulations. 129

5.3.2.2 Effect of Additives on Drying Rate. 132

5.3.3 Detergent Micrographs. 133

5.3.4 Correlation of Mass Transfer Coefficients 133

5.4 Comparison of Experimental Mass Transfer Coefficients with Theoretical values for Transfer through Particulate Slurry Drops. 146

5.4.1 Resistance to Transfer 147

Page.

Section Six.

Discussion. 152

6.1 Pure Water Drops. 153

6.1.1 Effect of Air Temperature on Mass Transfer Coefficient and Mass Transfer Rate. 153

6.1.2 Effect of Drop Diameter on Mass Transfer Coefficient and Mass Transfer Rate. 153

6.1.3 Mass Transfer Correlations. 155

6.2 Aqueous Sodium Sulphate Decahydrate Drops. 156

6.3 Detergent Slurry Drops. 157

6.4 Comparison of the Experimental Techniques. 160

Section Seven.

Conclusions and Recommendations. 162

7.1 Conclusions. 163

7.1.1 Pure Water Drops. 163

7.1.2 Aqueous Sodium Sulphate Drops. 164

7.1.3 Detergent Slurry Drops. 165

7.2 Recommendations. 167

INDEX OF FIGURES.

		Page.
Figure 4.1	Schematic Diagram of Apparatus	62
Figure 4.2	Drop Suspension Device.	65
Figure 4.3	Feeding Device.	69
Figure 4.4	Schematic Diagram of Pressure-Drop Experiment.	81
Figure 5.1	Effect of Air Temperature on Mass Transfer Coefficient.	84
Figure 5.2 } Figure 5.3	Effect of Air Temperature on Mass Transfer Rate.	84
Figure 5.4	Effect of Drop Diameter on Mass Transfer Coefficient.	90
Figure 5.5	Effect of Drop Diameter on Mass Transfer Rate.	90
Figure 5.6	Mass Transfer Correlation for Pure Water Drops Drying in Air at 26.5°C.	91
Figure 5.7	Mass Transfer Correlation for Pure Water Drops Drying in Air at 46.5°C.	91
Figure 5.8	Mass Transfer Correlation for Pure Water Drops Drying in Air at 85.0°C.	92
Figure 5.9	Mass Transfer Correlation for Pure Water Drops Drying in Air at 118.5°C.	92
Figure 5.10	Proposed Correlation for Pure Water Drops. Sh VS. $\left(\frac{T_{au}-T_s}{T_{amb}}\right)^{-0.008} Re^{1/2} Sc^{1/3}$	93
Figure 5.10a	Proposed Correlation for Pure Water Drops. Sh vs. $Re^{1/2} Sc^{1/3}$.	93
Figure 5.11	Effect of Air Flow Rate on Crust Thickness.	98
Figure 5.12	Effect of Air Flow Rate on Overall Mass Transfer Coefficient.	99

		Page
Figure 5.13	Effect of Air Flow Rate on Driving Force.	100
Figure 5.14	Effect of Initial Drop Radius on Crust Thickness.	101
Figure 5.15	Effect of Initial Drop Radius on Crust Thickness.	102
Figure 5.16	Effect of Initial Drop Radius on Crust Thickness.	103
Figure 5.17	Effect of Initial Drop Radius on Overall Mass Transfer Coefficient.	105
Figure 5.18	Effect of Initial Drop Radius on Overall Mass Transfer Coefficient.	106
Figure 5.19	Effect of Initial Drop Radius on Driving Force.	107
Figure 5.20	Effect of Air Temperature on Crust Thickness.	108
Figure 5.21	Effect of Air Temperature on Overall Mass Transfer Coefficient.	109
Figure 5.22	Effect of Air Temperature on Driving Force.	110
Figure 5.23	Effect of Initial Moisture Content on Crust Thickness.	112
Figure 5.24	Effect of Initial Moisture Content on Overall Mass Transfer Coefficient.	113
Figure 5.25	Effect of Initial Moisture Content on Driving Force.	114
Figure 5.26	Comparison of Predicted Crust Thickness with Experimental Crust Thickness.	115
Figure 5.27	Geometric Method for Estimating Specific Surface Areas of Crust.	124
Figure 5.28a	Drying Characteristics of Detergent Drops (Mass Transferred).	(Pocket)

		Page.
Figure 5.28b	Drying Characteristics of Detergent Drops.(Drying Rate).	(Pocket)
Figure 5.28	Combination of Figures 5.28a and b.	(ditto)
Figure 5.29	Proposed Correlation for Particulate Slurries.	144
Figure 5.30	Experimental versus Theoretical Mass Transfer Coefficients. Sodium Sulphate Drops.	150
Figure 5.31	Experimental versus Theoretical Mass Transfer Coefficients. Detergent Formulations.	151

INDEX OF TABLES

		Page
Table 2.1	Values of the coefficients in Mass Transfer Correlations of previous investigators.	46
Table 5.1	Drying Characteristics of Pure Water Drops at an air temperature of 26.5°C	85
Table 5.2	Drying Characteristics of Pure Water Drops at an air temperature of 46.5°C	86
Table 5.3	Drying Characteristics of Pure Water Drops at an air temperature of 85.0°C.	87
Table 5.4	Drying Characteristics of Pure Water Drops at an air temperature of 118.5°C.	88
Table 5.5	Correlations for Pure Water Drops.	89
Table 5.6	Drying Characteristics of Detergent Formulations: - Mass Transferred.	130
Table 5.7	Drying Characteristics of Detergent Formulations: - Drying Rate.	131
Table 5.8	% Composition of Detergent Formulations.	(Pocket)
Table 5.9	Experimental and Calculated Sherwood Numbers for Detergent Formulations.	145
Table 5.10	Hydrated Sodium Sulphate Drops. Experimental and Theoretical Mass Transfer Coefficients; and Resistance to transfer.	148
Table 5.11	Drops of Detergent Formulations. Experimental and Theoretical Mass Transfer Coefficients; and Resistance to Mass Transfer.	149

INDEX OF PLATES

		Page.
Plate 4.1	Experimental Rig.	63
Plate 4.2	Drop Suspension Device for Less-Viscous Liquids	66
Plate 4.3	Drop Suspension Device for More-Viscous Slurries	68
Plate 4.4	Hygrometer and Sensing Element.	71
Plate 4.5	Working Section showing Drop-suspension Device and Guillotine	77
Plate 5.1	Experimental Measurement of Sodium Sulphate Crust Thickness.	95
Plate 5.2	- ditto -	96
Plate 5.3	Internal and External Structure of Sodium Sulphate Crust.	116
Plate 5.4	- ditto -	117
Plate 5.5	Sodium Sulphate Crust showing Cracks and Holes.	118
Plate 5.6	Effect of Initial Moisture Content on Porosity of Sodium Sulphate Crust.	119
Plate 5.7	Line Film as used on the Quantimet for Porosity Determination.	120

STRUCTURE OF DETERGENT FORMULATIONS

Plate 5.8	Formulation A	135
Plate 5.9	Formulation B	136
Plate 5.10	Formulation C	137
Plate 5.11	Formulation D	138
Plate 5.12	Formulation E	139
Plate 5.13	Formulation F	140

Page.

Plate 5.14 Formulation G 141

Plate 5.15 Formulation H 142

Plate 5.16 Formulation I 143

Section One.

Introduction.

1. Introduction.

Evaporation from pure liquid drops and drops containing suspended or dissolved solids is important in industrial operations such as the spray drying of slurries. The process involves simultaneous heat and mass transfer. The heat for evaporation is supplied to the drop by convection from the hot gas stream to the drop surface, and by conduction into the drop from which evaporation occurs by diffusion and convection back into the gas stream.

A review of the literature reveals that a study of the drying of drops can be achieved in a number of ways, from:

(1) Single stagnant drops from non-crust-forming liquids, e.g. distilled water,

(2) pure liquids in single stationary celite spheres of known porosity,

(3) single stagnant drops containing dissolved or suspended solids, e.g. sodium sulphate,

(4) sprays of pure liquid drops,

and, (5) sprays of drops containing suspended or dissolved solids,

drying in a hot current of air or superheated steam for drops in categories (1) through (3) in addition.

Although it has been claimed (41) that mass transfer correlations from experimental results obtained in categories (1) through (3) are applicable to what occurs in spray drying of slurry drops, single drops rotating in a wind tunnel will be expected to simulate more closely, conditions in a spray tower.

In order to understand evaporation from aqueous drops containing suspended or dissolved solids, a study of the drying characteristics of single drops of pure solvent is essential. That is initially a free liquid interface is presented to the air stream during drying of the latter and evaporation proceeds as for pure water drops until the drop liquid concentrates to a point when a crust forms. Then it no longer presents this liquid interface.

The experimental investigation has therefore been divided into three subsections involving the drying characteristics of:

(1) Pure water drops, to compare results with previous work (39, 40, 54)

(2) Aqueous sodium sulphate drops, representing a crust-forming solution of determinable properties (44, 45)

and (3) Slurry drops from nine detergent powder formulations, to provide useful information for correlating mass transfer coefficients applicable to design of spray driers.

In order to pursue the above programme, a critical discussion of the literature pertinent to the subject matter and other related topics was undertaken. Thus in Chapter 2.1, is discussed mass transfer across a phase boundary, since drying of slurry drops is a process where material is transferred across a phase boundary. Drying of drops is discussed in Chapter 2.3; it appears that, Ranz and Marshall's correlations (40) for heat and mass transfer, have been widely accepted as applicable to conditions operating in a spray drier. Actually, their

correlations apply to heat and mass transfer through a continuous liquid interface and are correlated through the j-factors. However, since heat and mass transfer through a crust are different from those of a pure liquid drop, these correlations cannot be expected to apply after a crust forms and therefore more pertinent correlations are presented in this thesis.

A mathematical model for estimating crust thickness is developed in Chapter 3, and, theoretical and experimental values are compared in Chapter 5.

The results of the study are presented graphically in Chapter 5, and, where applicable, mass transfer correlations have been submitted.

Section Two

Literature Survey

Chapter 2.1 Mass Transfer Across a Phase Boundary

Chapter 2.2 Colburn Analogy

Chapter 2.3 Drying of Drops containing Dissolved Solids.

Chapter 2.4 Conclusion

2.1 Mass Transfer across a Phase Boundary.

During evaporation of a liquid droplet into a still gas, vapour is transferred from the surface to the bulk of the gas due to the concentration gradient (1). The process continues until all the liquid has evaporated or until the gas is saturated and the concentration gradient reduced to zero.

The first work reported on mass transfer from spherical particles was that of Maxwell (2) who solved the equations describing radial molecular diffusion analytically to obtain an expression for the mass transfer coefficient, k_x:

$$k_x = 2 \frac{C_f D}{d} \qquad ((2.1))$$

These theoretical treatments related to mass transfer within a single phase in which no discontinuities existed. However, in most of the important applications of mass transfer such as drying of drops containing dissolved solids, material is transferred across a phase boundary.

Some mechanisms were suggested (1) to represent conditions in the phase boundary region, the earliest being the Two-Film Theory propounded by Whitman (3). He suggested that the resistance to transfer in each phase could be regarded as lying in a thin film near the interface. Higbie (4) suggested the Penetration Theory in which the transfer process was largely due to a combination of eddy mixing in the liquid and molecular

diffusion across the interface, where unsteady-state transfer took place for a fixed period at the freshly-exposed surface. Danckwerts (5) provided a modification of the theory by considering that the material brought to the surface would remain there for varying periods of time. Toor and Marchello (6) produced a more general theory, the Film-Penetration Theory showing that each of the earlier theories was a particular limiting case of their (6) own.

2.1.1 Whitman Two-Film Theory (3)

The Whitman Two-Film Theory was the first serious attempt to represent conditions occurring when material was transferred from one fluid stream to another. It was assumed that turbulence ceased at the interface and that a laminar layer existed in each of the two fluids. In the presence of turbulent eddies, resistance to transfer became progressively smaller. The theory was based on the assumption that the zones in which resistance to transfer existed could be replaced by two hypothetical films, one on each side of the interface and, in which the transfer was solely by molecular diffusion.

The mass transfer was treated as a steady-state process, thus limiting the theory to the case where the time taken to establish the concentration gradients was very small compared with the time of transfer or where the volume of the film was negligible.

2.1.2 Higbie Penetration Theory.

Higbie (4) studied the rate of absorption of pure gas into a still liquid during short exposure periods to determine whether, or not, a resistance to transfer existed at the interface when a pure gas was absorbed in a liquid. The Penetration Theory was based on the assumption that the eddies in the fluid brought an element of fluid to the interface where it was exposed to the second phase for a definite time interval, after which the surface element was mixed with the bulk again. It was assumed that equilibrium was immediately attained by the surface layer and that unsteady state molecular diffusion into the element occurred while it remained exposed. The element then remixed with the bulk of the liquid after a fixed time interval.

However, the existence of velocity gradients within the fluid was completely ignored and the fluid at all depths was assumed to be moving at the same rate as the interface.

Danckwerts (5) suggested a modification to the theory; the Random Surface Renewal approach. Each element of the surface would randomly be exposed and the probability of any element of surface becoming destroyed and mixed with the bulk of the fluid was independent of the age of the element.

2.1.3 The Film-Penetration Theory.

This theory due to Toor and Marchello (6) included

some of the principles of both the Two-Film Theory of Whitman (3) and Higbie (4) Penetration Theory. Toor and Marchello (6) considered the mass transfer as an unsteady-state process and assumed that resistance to mass transfer was within a laminar film at the interface, as in the Two-Film Theory. It was also assumed that the surface renewal occurred at intervals due to eddies. For short exposure times, the process could be approximated by the Penetration Theory while for prolonged exposure, when a steady concentration gradient had developed, the conditions were similar to those of the Two Film Theory.

As a result of their investigation, Toor and Marchello (6) established that neither the Two-Film Theory nor the Penetration Theory could be treated in isolation; both occurring, depending on the exposure periods.

2.1.4 Mass Transfer Coefficients.

The theories already discussed established that if bulk flow was absent, mass transfer rate was directly proportional to the driving force expressed as a molar concentration difference between the interface and the bulk phase:

$$N_A = k'_x (C_i - C_o) \qquad ((2.2))$$

where N_A was the mass transfer rate per unit area, k'_x the mass transfer coefficient and C_i and C_o were the molar concentrations of the diffusing species in the

interface and the bulk phase respectively.

When mass transfer occurred across a phase boundary (1) and material did not accumulate at the interface, the mass transfer rate on either side of the phase boundary could be equated:

$$N_A = k_1' (C_{o1} - C_{i1}) = k_2' (C_{i2} - C_{o2}) \qquad ((2.3))$$

but if there was no resistance to transfer at the interface, then, C_{i1} and C_{i2} could be replaced by the equilibrium values C_{e1} and C_{e2}:

$$N_A = K_1 (C_{o1} - C_{e1}) = K_2 (C_{e2} - C_{o2}) \qquad ((2.4))$$

where C_{e1} was the concentration in phase 1 in equilibrium with C_{o2} in phase 2, and C_{e2} was the concentration in phase 2 in equilibrium with C_{o1} in phase 1; K was the mass transfer coefficient for the overall process.

For a linear equilibrium relationship,

$$H = \frac{C_{i1}}{C_{i2}} = \frac{C_{e1}}{C_{o2}} = \frac{C_{o1}}{C_{e2}} \qquad ((2.5))$$

where H is a proprotionality constant otherwise known as Henry's law constant.

Equations ((2.3)), ((2.4)) and ((2.5)) could be combined to yield the series relationship of the resistances to mass transfer:

$$\frac{1}{K} = \frac{1}{Hk_1'} + \frac{1}{k_2'} \qquad ((2.6))$$

These equations are valid (1) if the transfer rate is linearly related to the driving force defined as the concentration difference ΔC, or the pressure difference, ΔP according to Hinchley and Himus (7); and the equilibrium relationship is a straight line. They are, therefore, applicable for the Two-Film Theory (3), the Penetration Theory (4) and the Film-Penetration Theory (6).

The above theories could be applied satisfactorily to problems involving mass transfer between a fluid and the surface of a solid, such as the drying of drops containing dissolved solids. In such a case the fundamental assumption that turbulence ceased (1) at the interface would be justified. Although in the neighbourhood of a solid surface, appreciable velocity gradients would exist within the fluid and the calculation of transfer rates could become complex if the velocity gradients were taken into account, the rotation of the so-called solid surface would minimise that.

2.2 Colburn Analogy: Colburn (8) produced a method for correlating forced convection heat transfer data and compared the resulting correlation with fluid friction:

$$St.Pr^{2/3} = 0.023\ Re^{-0.2} \qquad ((2.7))$$

where St is the Stanton number, Pr is the Prandtl number and Re is the Reynolds number.

Equation ((2.7)) formed the basis of analysis which produced the j-factors of Chilton and Colburn.

2.2.1 The j-Factor of Chilton and Colburn.

2.2.1.1 Heat Transfer: Chilton and Colburn (9) correlated their results in the dimensionless form:

$$Nu = 0.023\ Re^{0.8} Pr^{0.33} \qquad ((2.8))$$

for heat transfer by convection to a fluid flowing through a tube. Nu is the Nusselt number.
By dividing both sides of equation ((2.8)) by the product Re. Pr, they obtained a correlation for the very-well known j-factor for heat transfer, jh

$$jh = 0.023\ Re^{-0.2} \qquad ((2.9))$$

They found that a plot of jh against Re gave approximately the same curve as the friction chart for flow through tubes.

2.2.1.2 Mass Transfer: Under forced convection conditions, by analogy to heat transfer, the rate of mass

transfer to, or from, a surface could be expressed in the form of three dimensionless groups:

$$\frac{k\, d_p}{D} = f(Re\ Sc) \qquad ((2.10))$$

where k is the mass transfer coefficient, d_p, the drop or particle diameter, D is the diffusivity and Sc is the Schmidt number.

By analogy with the derivation given for heat transfer, Chilton and Colburn (9) deduced the j-factor for mass transfer.

$$jd = \frac{k\, p_{bm}}{G_M}\ Sc^{2/3} \qquad ((2.11))$$

where k is the mass transfer coefficient, p_{bm} is the logarithm mean partial pressure of the inerts and G_M is the superficial mass velocity of the fluid.

Several workers carried out experiments to establish the relation between jh and jd. Gilliland and Sherwood (10) vapourised nine different liquids into air in a wetted-wall column and their results were plotted on a log-log scale as,

$$\frac{k\, p_{bm}}{G_M} \text{ against Re.}$$

By introducing the Schmidt group, the data could be correlated as,

$$\left(\frac{k\ p_{bm}}{G_M}\right)\left(\frac{\mu}{\rho D}\right)^{0.56} = 0.023\ Re^{-0.17} \qquad ((2.12))$$

where μ is the viscosity of the air, ρ, the density of the air and D is the diffusivity of water vapour into air.

The index of the Schmidt group, $\left(\frac{\mu}{\rho D}\right)$, was much less than the index of 0.67 for the Prandtl group as obtained with heat transfer, but the range of values of Schmidt number was very small and insufficient to provide a confirmation. However, the experimental work of Maisel and Sherwood (11) on the evaporation of water into air from flat plates, of water into carbon dioxide and into helium from cylinders, of benzene and carbon tetrachloride into air from cylinders, and of benzene into air from spheres also showed a good agreement with equation ((2.11)) of Chilton and Colburn (9).

Sherwood and Pigford (12) showed that if the data of Gilliland and Sherwood (10) and others were plotted with the Schmidt number raised to the power of 0.67, a reasonably good correlation was obtained. Although the data for mass transfer were more scattered than that of heat transfer, it was justifiable to assume that both jd and jh were near enough equal to $R_f/(\rho u^2)$, the friction factor.

The experimental work of Linton and Sherwood (13) on rates of solution of benzoic acid, cinnamic acid, and β-naphtol in water, under turbulent flow, established the true influence of Schmidt number for liquid phase mass transfer. For the range $100 \leq Sc \leq 3000$, the results confirmed the index of 0.67 for the Schmidt group in equation ((2.11)).

2.2.2 Limits of Applicability.

The j-Factors for heat and mass transfer have been shown to be approximately equal; hence values of mass transfer coefficients could be calculated from the corresponding values of the heat transfer coefficients. For the cases considered (9), the drag was almost entirely viscous drag at the surface. It is important to note that transfer in the liquid phase was from a vapour-liquid interface.

Sherwood (14) investigated mass transfer and friction in turbulent flow and calculated, approximately, the skin friction, (viscous drag at the surface), by subtracting the form drag, (additional drag caused by the eddies set up as a result of the fluid impinging on an obstruction), from the total drag force. It was only after isolation of the form drag from the total drag force that he obtained reasonable agreement between the corresponding value of $R_f/(\rho u^2)$ and jh and jd.

Consequently when a droplet containing dissolved solids is being dried in a wind tunnel, and concentrates to such a point where it no longer presents a free vapour-liquid interface to the air stream, when a crust forms, the j-Factors cannot be expected to apply any longer. This is due to the additional drag (1) caused by the eddies set up as a result of the air impinging on an obstruction - the crust of a droplet.

2.3 Drying of Drops containing Dissolved Solids.

Various theories available in the literature are discussed to provide a general relationship that governs drying of drops. More work appears to have been done on the less complex case of drying of pure liquid drops than on drops containing dissolved solids. However a review of the literature available on drying of pure liquid drops could aid the interpretation of results from more complex systems.

The general mechanisms of drying are also considered.

2.3.1 Mechanism of Drying in General.

The drying process consists of both the transfer of moisture within the drop and the evaporation of moisture from the surface into the surrounding medium (15). Of the several theories so far suggested (16), the diffusion theory, capillary flow theory and evaporation-condensation theory appear to have gained general recognition. Although more than one of these mechanisms of flow might be effective at any one time, generally only one predominated at any given time.

Keen (17), Fisher (18, 19), Sherwood (20, 21, 22), and Sherwood and Comings (23) indicated that under constant environmental conditions the drying process could be divided into a constant rate and one or two falling rate periods.

2.3.1.1 Diffusion Theory.

Several research workers (20, 21, 22, 23, 24, 25, 26) proposed explicitly the movement of moisture by diffusion as the principal flow mechanism. Sherwood (21) established that, if the theory of diffusion was assumed valid then, the drying process could be visualised in two distinctly different ways: -

(a) the diffusion of liquid from the interior to the solid surface, followed by vapourisation of the liquid at the surface and diffusion of the vapour into the surrounding air; or

(b) vapourisation of the liquid at a point beneath the surface of the solid structure, followed by diffusion of water vapour from that point through the porous solid to the surface and thence out into the air.

For case (a), a stagnant air film on the solid surface would present a resistance to the passage of vapour from the surface into the air. If the surface resistance was negligible compared with the interior resistance to liquid diffusion, the overall drying rate would be affected to the same degree by the variables affecting the latter, such as thickness of the crust.

2.3.1.2 Capillary Flow Theory.

During drying, liquid flows resulting from capillarity applies to liquids not held in solution (27). The basic fundamentals of the capillary flow theory were

laid down by Buckingham (16) who introduced the concept of capillary potential and postulated the mechanism of unsaturated capillary flow. Hougen, McCauley and Marshall (28) discussed the conditions under which capillary and diffusional flow might be expected in a drying solid, and analysed the published experimental moisture-gradient data for the two cases. Their curves indicated that capillary flow was typified by a moisture gradient involving a double curvature and point of inflexion.

2.3.1.3 Evaporation-Condensation Theory.

The evaporation condensation theory assumed that migration of moisture took place entirely, in the gaseous phase, in the pores (16). Other investigators (29, 30) proved that when the system was subjected to a temperature gradient, even at relatively high pore saturation, the assumption was essentially correct. Henry (31), Cassie et al (32) and Walker (33) used the evaporation-condensation mechanism in describing the movement of moisture in beds of textile materials.

2.3.1.4 Constant Rate Period.

In the constant rate period, it is assumed that drying takes place from a saturated surface of the material by diffusion (34) of water vapour through a stationary air film into the air stream, at an approximately constant rate (27). Gilliland (35) confirmed this by showing that the rates of drying of

water, whiting pigment, brass filings, brass turnings, fine sand and clay, were substantially constant under constant drying conditions. The mechanism of moisture removal was equivalent to evaporation from a body of water and was essentially independent (27) of the nature of the solids. However, Wenzel and White (36) showed that the increased roughness of the solid surface might lead to higher rates of evaporation than from a free liquid.

The constant rate period for direct or convection drying is controlled (27) by the external conditions of air velocity, temperature and humidity.

Immediately after the constant rate period is the falling rate period.

2.3.1.5 Falling Rate Period.

During the falling rate period, the surface is no longer completely wetted as will be expected when a crust forms during the drying of drops containing dissolved solids. The influence of external variables diminishes while the internal mechanism of moisture flow controls (37).

Studies of internal moisture movement indicated the possibility of several controlling mechanisms, diffusion and capillarity being postulated as the more significant ones.

The falling rate period has an important effect on the time of drying and hence on the dimensions of the dryer because the time required for this period is usually quite long.

2.3.2 Drops of Pure Liquids.

Dimensional analysis has shown that a simple (43) correlation for mass transfer from spheres in free motion exists:

$$Sh = a + \psi Re^{q} Sc^{z} \qquad ((2.13))$$

The earliest work on the evaporation of falling drops was initiated by Froessling (39). He applied the concept of the boundary layer equations for a blunt-nosed body of revolution to his data and proposed the following empirical correlation for the rate of mass transfer from spheres,

$$Sh = 2.0 + 0.552\ Re^{0.5} \cdot Sc^{0.33} \qquad ((2.14))$$

The value of a = 2.0 relates to the condition, Re = 0, that is at zero relative velocity for mass transfer by molecular diffusion.

2.3.2.1 Single Drops: Ranz and Marshall (40) investigated the rate of evaporation from a single stationary liquid drop suspended in a moving air stream with $0 \leqslant Re \leqslant 200$, and correlated the experimental results for drops of pure water and benzene and obtained a new value for ψ in equation ((2.13)). Thus for mass transfer,

$$Sh = 2.0 + 0.6\ Re^{0.5} \cdot Sc^{0.33} \qquad ((2.15))$$

and for heat transfer by analogy to mass transfer,

$$Nu = 2.0 + 0.6\ Re^{0.5}\ .\ Pr^{0.33} \qquad ((2.16))$$

where $Sh = K_G d_p / D_M$ = Sherwood Number,

$Re = \rho\ u d_p / \mu$ = Reynolds Number

$Sc = \mu / (\rho\ D_M)$ = Schmidt Number

$Nu = h d_p / k_T$ = Nusselt Number

k_G = film mass transfer coefficient (cm/s),

d_p = drop diameter (cm),

D_M = molecular diffusivity (cm^2/s),

ρ = gas density (g/cm^3),

μ = gas viscosity (g/(cm.s.)),

h = film heat transfer coefficient ($cal/(cm^2 s\ ^oC)$),

k_T = thermal conductivity of gas (cal/(cm.s.^oC)),

$Pr = \mu C_p / k_T$ = Prandtl Number,

C_p = specific heat of gas (cal/($g\ ^oC$))

Equations ((2.15)) and ((2.16)) compare favourably with equation ((2.14)) of Froessling (39).

However, to account for buoyancy effects, Ranz and Marshall (40) defined the velocity term in Re as a vector sum, $u + u_{fc}$; where u_{fc} was the velocity component due to free convection, and

$$u_{fc} = (d_p\ g_c\ \gamma\ \Delta T)^{0.5} \qquad ((2.17))$$

On substituting this velocity term into Re, a modified Reynolds number was obtained as,

$$Gr = \frac{(d_p^3\ \rho^2\ g_c\ \gamma\ \Delta T)^{0.5}}{\mu^2} \qquad ((2.18))$$

where Gr = Grashof Number,

γ = coefficient of cubical expansion of the gas,

g_c = acceleration due to gravity

ΔT = temperature difference between drop and gas.

It appears, therefore, that for natural convection, equations ((2.15)) and ((2.16)) apply, only after $Gr^{0.25}$ has been substituted for Re in both equations.

Thus for natural convection,

$$Sh = 2.0 + 0.6\ Gr^{0.25}\ .\ Sc^{0.33} \qquad ((2.19))$$

$$Nu = 2.0 + 0.6\ Gr^{0.25}\ .\ Pr^{0.33} \qquad ((2.20))$$

However, Pei, Narasimhan and Gauvin (41), from their study of evaporation from drops and particles in high temperature surroundings, showed that forced and natural convection were non-additive and that the transition from one to the other was only gradual.

In the investigation due to Schlünder (44), the drop was introduced from a capillary onto the fused junction of a thermocouple in a specially designed heating chamber. A photographic technique (45) for determining the drop diameter and the thermocouple deflection was adopted. The thermocouple deflection was calibrated to provide the change in weight of the drop and hence the rate of evaporation.

The experimental results were correlated in a similar way to Ranz and Marshall's (40) except that the Reynolds number was modified to include the effects of both free and forced convection. Thus

$$Re^* = \frac{\rho u L'}{\mu} + (\tfrac{1}{2}\, Gr)^{0.5} \qquad ((2.21))$$

where $L' = \pi r$ = the characteristic length upon which the flow impinged; and r = the droplet radius.

The proposed correlation was

$$\frac{k_G L'}{D_M} \left(\frac{\Delta P_{LM}}{p}\right) = \pi + 0.6\ (Re^*)^{0.5}\ .\ (Sc)^{0.32} \qquad ((2.22))$$

for mass transfer, and

$$\frac{h\ L'}{k_T} = \pi + 0.6(Re^*)^{0.5}\ .\ (Pr)^{0.33} \qquad ((2.23))$$

where ΔP_{LM} = log. mean pressure driving force, and p = average partial pressure of non-diffusing gas in the film surrounding the drop.

The analysis provided in equation ((2.21)) has ignored the non-additiveness (41) of effects due to free and forced convection. However, the theory that thermal equilibrium was only possible when:

(i) the vapour pressure at the surface of the drop depended only on the temperature of the drop,

(ii) radiation transfer was negligible, and

(iii) the ratio $D_M : k_T/(\rho C_p)$ was constant, was confirmed by practical results. With the above conditions prevailing, and at $Re \ll 10$, the drop surface decreased linearly with respect to time.

That is

$$- \frac{d(r^2)}{d\theta} = \text{constant} \qquad ((2.24))$$

Should the above conditions fail to be satisfied however, the drop temperature and equation ((2.24)) would change as evaporation progressed.

Tudose et al (46) carried out an experimental research on the heat and mass transfer from hemispherical droplets of water, ethanol and carbon tetrachloride within a pulsed gas current. The experiments were conducted in a cylindrical glass tube 2.02 cm. in diameter and 82 cm. long. A capillary tube of 0.5 cm. outside diameter was introduced into the cylinder at 48 cm. from the air inlet. The hemisphere was formed at the end of this second tube. An optical method was used to measure the oscillations of the drop and also the amount of liquid fed in to maintain the drop at constant volume. This technique is similar to that of Ranz and Marshall (40). Heat and mass transfer coefficients were calculated from Ranz and Marshall correlations (40) yet again.

The results indicated the possibility of increasing heat and mass transfer by means of throbs. The intensification curves presented maxima due to the resonance phenomena corresponding to the droplets maxima of deformation.

Golli et al (47) studied, by an optical method, evaporation of liquid droplets suspended in a gas in turbulent flow. The optical technique was mainly a photoelectric measurement which was calibrated for the

intensity of light diffused by the drop during evaporation. Thus unlike in previous investigations (40, 41, 45, 49), both the weight of the drop and the droplet size were measured simultaneously as the experiment progressed. They found that the change in surface area of the droplets was a linear function of time, thus supporting the findings of Schlünder (44). They also concluded that the molecular diffusion coefficient of Maxwell's law (2) was still applicable even in a turbulent air stream.

2.3.2.2 Single Drops in High Temperature Surroundings.

Ranz (48) analysed the evaporation of a drop of volatile liquid in high temperature surroundings in terms of the rate of heat transfer, and, from a heat balance, produced an expression similar to that of Marshall (49) without considering the temperature variation of thermal conductivity. It became apparent that for high temperature work, transient heat and mass balances were necessary.

Hoffman and Gauvin (50) studied the rate of evaporation from liquid droplets such as, water, methanol, cumene, pentane and benzene in an electrically heated stainless steel sphere. The gaseous environment was mainly the superheated vapour of the liquid under investigation. Compared with the findings of Pei et al (41), the evaporation rate of stationary droplets in high temperature surroundings did not seem to be governed by the rate of heat transfer by natural convection since there was no dependence of the Nusselt number or the Grashof number (41).

The evaporation rate was satisfactorily predicted over the range $0.03 < B < 1.0$ by,

$$\left(\frac{dm}{d\theta}\right)\left(\frac{C_p}{\pi d_p k_T}\right) Pr^{-0.33} = 3.2\ B^{0.97} \qquad ((2.25))$$

where $(dm/d\theta)$ = evaporation rate,

$B = C_p\ \Delta T/\lambda$ = Transfer Number, and

λ = latent heat of vapourisation.

The droplet diameter used in equation ((2.25)) was taken as being equivalent to the cube root of the volume of an ellipsoid and this diameter should be preferred to the mean of the smallest and largest diameters used by Audu (38). However, the experimental data (50) were obtained under unsteady-state conditions with the droplet diameter continuously changing.

Downing (51) investigated the evaporation of drops of pure liquids at elevated temperatures in the range $27^{o} \leqslant T \leqslant 340^{o}C$ Drop diameters of the order of 0.1 cm. and Reynolds number from 24 to 325 were employed. A modified apparatus similar to that of Charlesworth and Marshall (45) was used.

An unsteady-state heat and mass balance (40, 44, 45) was performed and the mass transfer data were shown to be very sensitive to the values estimated for the wet bulb temperatures. Hence the evaporation rates were correlated in terms of heat transfer rates rather than mass transfer rates. However, it was necessary to introduce a correction factor of approximately 35% of the value of the Nusselt number as predicted by the film theory.

At higher rates of heat and mass transfer, Ranz and Marshall's correlations (40) must be modified. One such modification was presented by Downing (51) for heat and mass transfer.

$$Sh = M(2.0 + 0.6\ Re^{0.5}\ Sc^{0.33}) \qquad ((2.26))$$

$$Nu = MN\left(\frac{1}{B}\right)\ \ln(1 + B)\ (2.0 + 0.6\ Re^{0.5}\ Pr^{0.33}) \qquad ((2.27))$$

Equations ((2.26)) and ((2.27)) represent the correlations for mass and heat transfer respectively.
where $M = 1 - 0.4(1 - T_1/T_o)$, and
$N = 1 - 0.4(1 - (1/B)\ \ln\ (1 + B))$; M and N being empirical factors. As a result of these modifications, it was possible to calculate high temperature humidity charts for the four liquids studied, namely, acetone, benzene, hexane and water.

For water drops evaporating into superheated steam at $9 \leqslant Re \leqslant 120$ and $0.7 \leqslant p \leqslant 1.0$, Toei et al (52) produced correlations, for heat and mass transfer, similar to those of Ranz and Marshall (40);

$$Nu = 2.0 + 0.65\ Re^{0.5}\ Pr^{0.33} \qquad ((2.28))$$

$$Sh\ \left(\frac{p\ LM}{p}\right)^{-0.2} = 2.0 + 0.65\ Re^{0.5}\ Sc^{0.33} \qquad ((2.29))$$

These correlations agreed favourably with those of Hughmark (53) who concluded that, for $1 \leqslant Re \leqslant 450$ and Sc or $Pr \leqslant 250$, Ranz and Marshall's correlations were applicable.

Lee and Ryley (54) suspended a water drop from a fine horizontal glass fibre within a steam flow of controlled velocity, pressure and superheat, and observed the rate of evaporation for droplet Reynolds number in the range $64 \leqslant Re \leqslant 250$. For this Reynolds range, the drop was shown to be surrounded by a thin boundary layer of saturated vapour superheated by the heat transferred from the atmosphere to the drop. They confirmed the correlation of Ranz and Marshall (40) for heat transfer but correlated the mass transfer data according to,

$$Sh = 2.0 + 0.738\ Re^{0.5}\ .\ Sc^{0.33} \qquad ((2.30))$$

The coefficient of $Re^{0.5}\ .\ Sc^{0.33}$ differs from that of Ranz and Marshall (40), but it should be noted, however, that the gaseous media were different. Ranz and Marshall (40) conducted their experiments in air at moderate temperatures, and not in superheated steam.

Trommelen and Crosby (55) evaporated drops of distilled water in both air and superheated steam. Their results supported the findings of Toei et al (52) and indicated that the accepted correlation (40) of heat transfer coefficients applicable for evaporation of small drops of pure liquid in air was also valid for evaporation in a superheated vapour. Lee and Ryley's data also confirmed this finding.

Recently Matlosz et al (56) investigated liquid drop evaporation in a high temperature, $T \leqslant 548$ K, and high pressure environment and obtained reproducible temperature-time and radius-time histories for n-hexane droplets

evaporating in a nitrogen, and also argon gas environment. A model was formulated that accounted for the transient character of the phenomena, the effect of the motion of the droplet boundary on the governing equations, and also for the effects of the non-ideal gas behaviour in the boundary conditions.

Their results, when compared with the model suggested a different mechanism for mass transfer since the ratio of the effective diffusivity to the molecular diffusivity, as calculated from existing correlations (40, 52), departed from unity at high chamber pressures.

2.3.2.3 Clouds of Drops:

Marshall (49) discussed heat and mass transfer phenomena to and from clouds of pure liquid droplets, and presented a stepwise procedure for calculating drop size distribution. The method was based on an assumed Nusselt number of 2.0.

Dlouhy and Gauvin (57) studied the evaporation and drying rates of atomised drops in an experimental concurrent spray drier 8 inches in diameter and 14 feet high. Owing to the presence of liquid droplets, the droplet temperature was measured with shielded mercury-in-glass thermometers. A volumetric technique was adopted for measuring humidities because of the inherent anomalies and errors introduced when wet bulb thermometry is used. This technique involved absorbing water vapour from a known volume of air in contact with magnesium perchlorate and noting the change in volume. The droplet size and size

distribution were measured with the aid of an immersion technique, and the drops so-collected were photographed and counted. The rate of evaporation was predicted from heat and mass balances. The Nusselt number was found to be 2.07 ± 0.06 while the Sherwood number was 1.89 ± 0.06. Although the values compared very well with those at zero relative velocity, they suggested that their value of Sherwood Number was less than $Sh = 2.0$ due to the uncertainties in determining diffusivities.

Manning and Gauvin (58) determined the rate of heat and mass transfer in the nozzle zone of water sprays produced by internal mixing pneumatic nozzles and hollow-cone nozzles. The drop size distribution was measured using the method of Dlouhy and Gauvin (57). The evaporation history of the spray was followed by measuring colourimetrically, the increase in concentration of a red dye added to the feed water. The spray temperature was measured by a shielded mercury-in-glass thermometer similar to Dlouhy and Gauvin's (57) for similar reasons. The air velocity was measured graphically and a volumetric method (59) was used for humidity measurements.

Although this investigation was fully representative of spray drier conditions, drops smaller than 10μ could not be measured. Also any errors introduced during the cinematographic measurements of the drop velocity and diameter would tend to magnify when estimating the air velocity graphically. A direct method for velocity measurements is preferred.

The scatter of points about the correlation line was considerable when the data were fitted to Ranz and Marshall's correlation for heat transfer (40).

Bose and Pei (59) investigated the rate of evaporation of pure water droplets in a co-current spray drier and attempted to extend the work of Dlouhy and Gauvin (57) in evaluating the heat and mass transfer coefficients of droplets in a spray dryer with droplet sizes comparable to those used in some industrial applications. The sampling techniques used for drop size, temperature and humidity measurements were similar to those of Dlouhy and Gauvin (57).

The results indicated that the relative velocity between the droplets and the air stream had a significant effect on the evaporation rate, thus contradicting Dlouhy and Gauvin (57), but agreeing with Ranz and Marshall (40).

Recently, Dickinson and Marshall's (60) investigation of sprays of pure liquid drops has shown that at low velocities, sprays with less uniform drop size distributions evaporated more rapidly in the initial interval of time than more uniform sprays with the same mean diameter, because the many smaller drops initially present evaporated at higher rates. The air temperature fell as the spray evaporated, and the rate of evaporation decreased. However, at high spray velocities, it was found that the distance travelled by the spray to achieve a given degree of evaporation was much greater, especially at the start.

The velocity effect was more significant at higher initial velocities and at higher temperature differentials.

2.3.3 Drops Containing Dissolved Solids.

In the presence of dissolved solids, the vapour pressure of the solvent is lowered and the surface temperature of the drop rises above the thermodynamic wet bulb temperature. If the drop surface is saturated, that is, it contains a film of free-water, evaporation will take place as for drops of pure liquids. However, in the event of a crust forming, the dynamic equilibrium is off-set and the drop temperature increases.

Ranz and Marshall (40) included, in their work on evaporation of pure liquid drops, some experiments on evaporation from droplets of solutions and suspensions; and concluded that drying proceeded during the first period as if the entire droplet were saturated. The resistance to mass transfer was mainly in the boundary-layer of stagnant gas surrounding the drop, and entrained (61) submicroscopic droplets from the evaporating surface. However, the first major work on the drying of single stationary drops containing dissolved solids was that of Charlesworth and Marshall (45).

2.3.3.1 Single Drops Containing Dissolved Solids:

Charlesworth and Marshall (45) studied specifically evaporation from single drops containing dissolved solids. The drop in each case was suspended in a controlled air stream at moderate temperatures and the weight was recorded by means of a specially designed sensitive balance consisting of a glass filament

attached to a cathetometer. The droplets were formed from a microburette whose tip was fitted with a glass capillary coated with Dri-film and then transferred to the suspension filament. For experiments involving temperature history of the drop, the drop-suspension filament and a thermocouple connected to a quick-response recording potentiometer, were mounted in a fork of glass tubing. The evaporating droplets were observed under magnification in silhouette on the ground-glass background of a microscope camera.

They produced a rigorous mathematical model from transient heat and mass balances like Ranz (48) but, however, assumed that transfer in the droplet was by diffusion only, and concentration gradients were spherically symmetrical. This assumption is not strictly true. A summary of the model is given in section 2.3.3.2.

The mechanism (45) of formation of particles dried from drops was advanced and the changes in appearance of drops during drying were presented. A crust did not form immediately due to the initial heat-up transients necessary for evaporation from the surface of the drop, the first sign of a solid phase being evidenced by the formation of crystals at the bottom of the drop (62). As drying progressed, more crystals appeared, forming a surface crust which grew steadily up the sides of the droplets. This mode of crust formation will not be expected for a rotating drop, since some areas of the crust may redissolve and then reform (45).

The results of further drying after the crust had

formed completely depended on the nature of the solute and the surrounding air temperature. Several different phenomena were possible depending on whether the surrounding temperature was below or above the boiling point of the solution.

However, in virtually all the cases, the final particle consisted of a hollow, thin nearly-spherical crust which was quite smooth outside, but rough and uneven inside, the inner core, containing an open network of large crystals.

Schlünder (44) carried out a theoretical and experimental investigation on evaporation from drops of salt solutions under steady and unsteady-state conditions and produced a mathematical model, similar to that of Charlesworth and Marshall (45). The model is described later.

The experimental study on lithium chloride drops showed a very good agreement with the theoretical calculations and the rate of evaporation was shown to be a function of the mean salt concentration. However, certain peculiarities were observed which could not be explained by the diffusion theory. It was noticed that, for weak salt solutions, there was a high resistance to salt diffusion while, at higher salt concentrations, this phenomenon disappeared. Although this phenomenon had no major influence on the rate of evaporation, Schlünder suggested that this could be due to the initial formation of a highly concentrated boundary layer on the drop surface before diffusion into the drop interior could occur.

Trommelen and Crosby (55) determined the loss in weight and temperature variation as a function of time for droplets of a number of aqueous solutions and suspensions in both drying media for the systems, which included sodium sulphate and a commercial detergent.

It was found that drops of sodium sulphate solution with a nominal size of 1.5 - μ litres, dried more rapidly in steam than in air at temperatures of about 150°C. No depression of the dynamic equilibrium temperature similar to the wet bulb temperature occurred for drying in air. Instead, as was reported by Schlünder (44), the drop temperature rose from its initial value to near the boiling point of water. At about 145°C, the progress of drying varied from one drop to another, an observation also recorded by Charlesworth and Marshall (45).

However, for the case of 2 - μ litre drops of the commercial laundry detergent, drying occurred considerably-more rapidly in air than in superheated steam at 150°C, a reverse of what happened in the drying of drops of sodium sulphate solution.

In both cases occasional ruptures in the shell occurred. While no visual differences were observed between the final particles obtained from drying sodium sulphate drops in air and steam, it appeared that for the detergent drops, an atmosphere of superheated steam produced high density particles.

Recently, Abdul-Rahman et al (63) investigated the effects of dissolved and dispersed gases on the drying of single macrodrops of sodium caseinate. Their idea was to simulate drying of freely moving droplets by

mechanically supporting the drop in a uniform velocity field of drying air at constant temperature, humidity and velocity.

The technique of Charlesworth and Marshall (45) was adopted for measuring the moisture content and temperature of the drop, while the instantaneous weight of the drop was determined by the technique of Trommelen and Crosby (55).

Their results showed that foaming increased the rate of drying markedly for drops of equal mass and volume compared to non-foamed drops. However this work was mainly a duplication of Trommelen and Crosby's investigation with the exception of the fact that foamed and non-foamed drops were the materials studied.

2.3.3.2 Mathematical Models for Single Drops Containing Solids:

The presence of non-volatile dissolved solids in a drop greatly increases the complexity of the process of evaporation from droplets having a velocity relative to the surrounding air, and this complexity was demonstrated by Charlesworth and Marshall (45), and Schlünder (44) in the models proposed.

(i) Model of Charlesworth and Marshall:

Charlesworth and Marshall (45) assumed that transfer in the drop was by diffusion only and also that the concentration gradients were spherically symmetrical. These assumptions can hold only when there is a negligible relative velocity between the drop and the air.

They based their model on the continuity equation relating to a sphere. Thus,

$$\frac{\partial C}{\partial \theta} = D \left(\frac{\partial^2 C}{\partial r^2} + \frac{2}{r} \frac{\partial C}{\partial r} \right) \qquad ((2.31))$$

Equation ((2.31)) was integrated by introducing two boundary conditions of the form of equations ((2.32)) and ((2.33)).

$$C(r,\theta) = C_o \quad 0 < r < x_o/2 \qquad ((2.32))$$

$$D \left(\frac{\partial C}{\partial r}\right)_{r = x/2} = - \frac{\frac{dm}{d\theta} \bar{v} C}{\pi x^2} \qquad ((2.33))$$

Equation ((2.32)) was based on the assumption that the droplet was initially of uniform concentration, while equation ((2.33)) was based on the assumption that the solute would accumulate in the surface layer of the droplet as a result of evaporation and droplet shrinkage.

Charlesworth and Marshall then assumed that the evaporation rate, $dm/d\theta$, from a drop of solution was equal to that from a pure-water drop of the same size. Thus

$$- \frac{d(x^2)}{d\theta} = - \frac{dm}{d\theta} \cdot \frac{4 \bar{v}}{\pi x} \qquad ((2.34))$$

At low Reynolds numbers and for small drops it could be deduced from Ranz and Marshall's (40) correlations that $d(x^2)/d\theta$ was approximately constant. Therefore an evaporation constant, Z, defined by equation (2.35))

was introduced.

$$-\frac{d(x^2)}{d\theta} = 8Z \qquad ((2.35))$$

Combining equations ((2.34)) and ((2.35)) gave

$$-\frac{dm}{d\theta} = \frac{2\pi x Z}{\bar{v}} \qquad ((2.36))$$

By substituting equation ((2.36)) into ((2.33)), the boundary condition was expressed as,

$$\left(\frac{\partial c}{\partial r}\right)_{r = x/2} = \frac{2\gamma C}{x} \qquad ((2.37))$$

where $\gamma = \frac{Z}{D}$ = a dimensionless constant.

Charlesworth and Marshall (45) then obtained the solution of equation ((2.31)), with the aid of equations ((2.32)) and ((2.37)), as

$$C(r,\theta) = 2C_o\gamma\left(\frac{\cosh\phi \sinh\left(\frac{2\phi r}{x}\right) \exp\left(\frac{4\phi^2 D\theta}{x^2}\right)}{\phi(\sinh^2\phi - \gamma)} - \sum_{n=1}^{\infty} \frac{\cos\alpha_n \sin\left(\frac{2\alpha_n r}{x}\right) \exp\left(\frac{-4\alpha_n^2 D\theta}{x^2}\right)}{\alpha_n(\sin^2\alpha_n + \gamma)}\right) \qquad ((2.38))$$

where ϕ = positive real root of

$$\tanh y_1 = \frac{y_1}{\gamma+1} \qquad ((2.39))$$

and α_n (n = 1, 2, 3 .....) are the positive real roots of

$$\tan y_2 = \frac{y_2}{\gamma+1} \qquad ((2.40))$$

Compensation for the change in drop size was made by the relation

$$x^2 = x_o^2 - 8Z\theta \qquad ((2.41))$$

Now, Charlesworth and Marshall postulated that a crust appeared as soon as the surface became saturated and the time of formation of the crust was that at which

$$C(x/2,\theta_c) = C_s \qquad ((2.42))$$

Equations ((2.38)) and ((2.42)) were too complex to be solved for the time of formation of the crust, θ_c. But if the term under the summation sign of equation ((2.38)) were omitted, then, the values of $C(x/2,\theta_c)$ would be high. However, the discrepancy was countered by setting

$$\frac{2\ \gamma \cosh \phi \sinh \phi}{\phi(\sinh^2\phi - \gamma)} \doteq 1$$

Thus the final simplified expression became

$$C(x/2,\ \theta) = C_o \exp \frac{4\phi^2 D\theta}{x_o^2 - 8Z\theta} \qquad ((2.43))$$

By using equations ((2.42)) and ((2.43)), Charlesworth and Marshall evaluated the time for crust formation, θ_c as

$$\theta_c = \frac{\frac{xo^2}{4D} \ln \left(\frac{Co}{C_s}\right)}{\phi^2 + 2\gamma \ln\left(\frac{C_s}{Co}\right)} \qquad ((2.44))$$

where x_o = initial diameter of drop (cm)

C_o = initial concentration of solute $\left(\frac{g.solute}{cm^3\ soln}\right)$

C_s = saturation concentration of solute $\left(\frac{g.Solute}{cm^3 soln}\right.$

ϕ = positive real root of $\tanh y_1 = \frac{y_1}{\gamma+1}$

γ = dimensionless constant Z/D

D = diffusivity (cm^2/s)

Z = evaporation constant (cm^2/s)

(ii) Schlünder's (44) Model

Schlünder started with the same basic equation used by Charlesworth and Marshall (45).

That is,

$$D\left(\frac{\partial^2 C}{\partial r^2} + \frac{2}{r}\frac{\partial C}{\partial r}\right) = \frac{\partial C}{\partial \theta} \qquad ((2.31))$$

and the boundary conditions were

$$D\left(\frac{\partial C}{\partial r}\right)_{r = R(\theta)} = C_R \frac{dR}{d\theta} \qquad ((2.45))$$

$$\left(\frac{\partial C}{\partial r}\right)_{r = 0} = 0 \qquad ((2.46))$$

with the initial condition

$$C(r,0) = C_o \qquad ((2.47))$$

A solution was not possible with the boundary conditions of equations ((2.45)) because $R = f(\theta)$. As a first approximation, $R(\theta)$ was set equal to R = constant, and $dR/d\theta = W_k$ = constant. Thus $dR/d\theta$ was no longer an effective change in the radius of the drop but a volumetric rate of evaporation $G_w/\gamma_w F$. The ratio of the surface to mean concentration was then given by:

$$\frac{C_R}{C_m} = \frac{Pe+1}{3Pe} \; \frac{A_n \exp(-n^2 D\theta/\bar{R}^2).\sinh n + \sum_1^\infty A_k \exp(-m_k^2 D\theta/\bar{R}^2).\sin m_k}{A_n/n.\exp(-n^2 D\theta/\bar{R}^2).\cosh n + \sum_1^\infty A_k/m_k.\exp(-m_k^2 D\theta/\bar{R}^2).\cos m_k}$$

((2.48))

with $$\frac{n}{Pe + 1} = \tanh n \qquad ((2.49))$$

$$\frac{m_k}{Pe + 1} = \tanh m_k \qquad ((2.50))$$

$$A_n = \frac{2(\sinh n - n \cosh n)}{n(n - \sinh n \cosh n)} \qquad ((2.51))$$

$$A_k = \frac{2\ Pe}{(Pe + 1 - m^2_k/\sin^2 m_k)\sin m_k} \qquad ((2.52))$$

where

$$Pe = \frac{W_k \bar{R}}{D} = \text{Peclet Number} \qquad ((2.53))$$

For long times C_R/C_m approaches the asymptotic value, that is,

$$\lim_{\theta \to \infty} \left(\frac{C_R}{C_m}\right) = (Pe + 1)^2 \tanh^2 n/3Pe \qquad ((2.54))$$

However, equation ((2.48)) did not converge well for short times; therefore, Schlünder chose a moving co-ordinate system with the origin at the surface to describe the following differential equations for convective mass transfer:

$$D \frac{\partial^2 C}{\partial x^2} + W_k \frac{\partial C}{\partial x} = \frac{\partial C}{\partial \theta} \qquad ((2.55))$$

with the boundary conditions:

$$D \left(\frac{\partial C}{\partial x}\right)_{x = o} = W_k \, C(0,\theta) \qquad ((2.56))$$

$$C(\infty,\theta) = C_o = C(x,0) \qquad ((2.57))$$

The equation was then solved with the aid of Laplace transforms with the same assumption that $dR/d\theta$ = constant. The solution was expressed as

$$\frac{C_R}{C_m} = 1 + \frac{1}{2}\left(1 + \frac{2}{\sqrt{\pi}}\right) Pe \sqrt{\left(\frac{D\theta}{R^2}\right)} \qquad ((2.58))$$

Thus the change in concentration ratio is directly proportional to Pe and $\sqrt{\theta}$.

Schlünder used equations ((2.58)) and ((2.54)) to describe the surface concentrations of drops containing dissolved solids. The lowest value of C_R was at complete mixing of the drop when $C_R = C_m$, and the highest value was when transfer of solute was by diffusion, and $C_R > C_m$.

2.3.3.3 Clouds of Drops containing Dissolved Solids:

Duffie and Marshall (62) studied the factors influencing the properties of spray-dried materials, for example sodium silicate, in a spray tower arranged for counter current flow. With the aid of photo-micrographs, it was possible to study the appearance of the dried product. They suggested that, when the evaporation rate was greater than the rate of diffusion of solute back into the drop, the product would

concentrate in a spherical shell giving rise to hollow particles.

Crosby and Marshall (64), using the same tower as Duffie and Marshall (62) investigated the effects of drying conditions on the properties of spray-dried particles; an extension of Duffie and Marshall's work.

2.4. Conclusion.

The drying of drops is a very complex process and it is rather difficult to design experimental techniques to simulate drying conditions existing in a practical spray drier. It is now evident that for a single stationary drop (40, 41, 44, 45, 52, 55) drying in either air or superheated steam, the weight change of the drop during drying, the temperature history and a visual observation of the appearance of the drop are required, while for a cloud of drops (50, 57, 62, 64), drop-size distribution and drop velocities are required in addition. The conventional method of measuring air humidities by wet and dry bulb thermometers has been replaced, in most of the papers discussed, by a volumetric technique incorporating the absorption of water vapour by magnesium perchlorate and noting the change in volume (57, 58, 62, 64). The droplet weight was measured by a rather ingeneous device (45, 55). Drop size distribution measurements and visual observation were achieved by the continued use of sophisticated photographic techniques. At high temperatures, transient heat and mass balances were inevitable (41, 48, 50 - 52, 54, 55). A mechanism for the formation of crusts from droplets containing dissolved solids was initiated by Ranz and Marshall (40) and progressed by Charlesworth and Marshall (45), and Duffie and Marshall (62).

The following correlations were proposed by Froessling (39)

$$Sh = 2.0 + \psi Re^{q} . Sc^{Z} \qquad ((2.13))$$

and the values of the coefficient and exponents are tabulated in Table 2.1

TABLE 2.1

Coefficients	ψ	q	Z
Ranz and Marshall (40)	0.6	1/2	1/3
Froessling (39)	0.552	1/2	1/3
Toei et al (52)	$0.65(\frac{p_{BM}}{p})^{0.2}$	1/2	1/3
Hughmark (53)	0.6	1/2	1/3
Lee and Ryley (54)	0.74	1/2	1/3

Concluding, for drying of stationary drops, (40, 45, 55), measuring techniques are not homogeneous since the weight, temperature and size changes cannot be recorded simultaneously. This will introduce errors when heat and mass transfer data are correlated.

Most of the work presented support the correlations of Ranz and Marshall (40). These correlations apply to heat and mass transfer through a continuous liquid interface and are related through the j-factors. However, since the heat and mass transfer paths through the crust of a droplet will be different, it will be expected that not only will the respective correlations be different but also will they not be related by the Chilton-Colburn analogy.

The primary objective in this investigation is therefore to establish working correlations for mass transfer coefficients that will form a basis for further

study aimed at explaining the mechanism of the transport processes through crusts formed in spray drying.

Section Three

Mathematical Models

Chapter 3.1 Pure Water Drops

Chapter 3.2 Drops Containing Dissolved Solids.

3. Mathematical Models

Two models are described: one for pure water drops and the other for drops containing dissolved solids.

3.1 Pure Water Drops

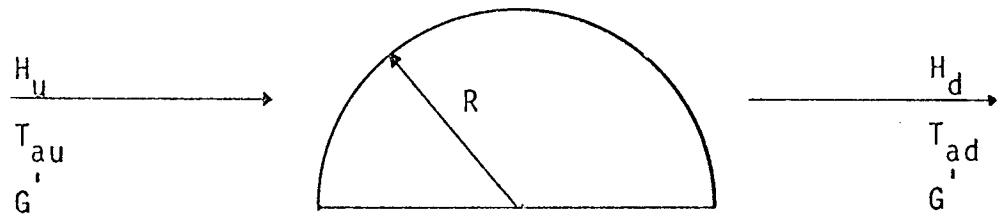

H_u = upstream air humidity

H_d = downstream air humidity

T_{au} = upstream air temperature

T_{ad} = downstream air temperature

R = drop radius

G' = wet air flow rate

3.1.1 Assumptions: (a) The drop radius R is kept constant.

(b) The physical properties of air are constant.

(c) The air flow rate is constant.

(d) The air temperature is also constant.

3.1.2 Mass Transfer Rate: From a mass balance, the amount of water evaporated per unit weight of air is,

$$\Delta H = H_d - H_u \qquad ((3.1))$$

Thus the rate of evaporation, N_A, is the product of the dry air mass flow rate G, and ΔH:

$$N_A = \frac{G.\ \Delta H}{A} \qquad ((3.2))$$

where A = area for mass transfer

$$G = \frac{G'}{1 + H_u} \qquad ((3.3))$$

3.1.3 Mass Transfer Coefficient: As already stated in section 2.14, the rate of mass transfer is directly proportional to the driving force, and the proportionality constant was denoted k. The driving force used here is not a concentration difference but a humidity driving force.

3.1.3.1 Humidity Driving Force: The humidity driving

force is defined (38) as,

$$(\Delta H)_s = H_s - H_u \qquad ((3.4))$$

where H_s = the saturation humidity at the drop temperature T_s.

The rate of mass transfer becomes, therefore,

$$N_A = k_H (H_s - H_u) \qquad ((3.5))$$

where k_H is the mass transfer coefficient in terms of humidity driving force.

<u>3.1.3.2 Pressure Driving Force</u>: Equation ((3.4)) can be transformed to yield the pressure driving force ΔP by converting the humidities to pressure analogues (27). Thus

$$p = \frac{HP}{(M_w/M_a)} + H \qquad ((3.6))$$

where p = partial pressure of water vapour; P = total pressure: H = humidity; M_a = molecular weight of air and M_w = molecular weight of water vapour.

According to Hinchley and Himus (7) the rate of

evaporation is directly proportional to the pressure driving force:

$$N_A = k_p \, (p_s - p) \qquad ((3.7))$$

where k_p is the mass transfer coefficient,

p_s = vapour pressure of water at wet bulb temperature,

p = partial pressure of water vapour in the environment,

N_A = mass transfer rate per unit area.

The mass transfer coefficient is obtained from equation ((3.7)) after substituting for N_A from equation ((3.2)):

$$k_p = \frac{G.\Delta H}{A(p_s - p)} \qquad ((3.8))$$

The units of k_p are g /(cm^{2}s atm).

However, equation ((3.8)) can be modified to yield,

$$K_G = \frac{R_c . \; G. \; \Delta H \; (T_{au} + 273.16)}{A. \; M_w \; (p_s - p)} \qquad ((3.9))$$

where

K_G = mass transfer coefficient, (cm/s)

R_c = universal gas constant (cu. cm. atm/(g.mol.K))

G = dry air flow rate (g/s)

ΔH	=	gram of water vapour/gm of air (g/g)
T_{au}	=	upstream air temperature (^{o}C)
273.16	=	constant for converting T_{au} to degrees K
A	=	$2\pi R^2$, mass transfer area (cm^2)
π	=	constant (-)
R	=	drop radius (cm)
M_w	=	molecular weight of water vapour (g/g.mol)
P_s	=	vapour pressure of water at wet bulb temperature (atm.)
p	=	partial pressure of water vapour (atm.)

3.2 Drops containing Dissolved Solids.

Predicting evaporation rates from drops containing dissolved solids has been treated mathematically by many investigators (29, 40, 41) as an unsteady-state problem. However, this investigation looks at the problem from a steady state situation

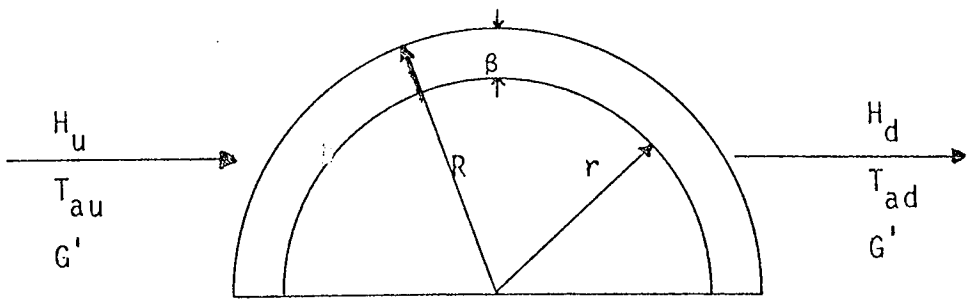

β = crust thickness

r = internal crust radius

3.2.1 Assumptions: (a) There is a receeding interface between the solution and the crust. As drying proceeds, the crust grows inwards and the external radius of the drop remains constant. Thus the internal radius, r, is a function of time, θ.

$$r = f_1 (\theta) \qquad ((3.10))$$

(b) The moisture evaporated at any time is a function of the thickness of the crust, β, and the core concentration is constant:

$$C = f_2 (R - r) = f_2 (\beta) \qquad ((3.11))$$

(c) The holdup of the solvent in the crust is zero.

(d) The crust, once formed, is porous and hence pore diffusion is the mechanism of moisture movement from the interior of the drop to the exterior, where the vapour comes into contact with the hot air stream.

3.2.2 Crust Thickness: From a mass balance, the amount of water vapour evaporated during any time interval is,

$$\Delta W = G(\Delta H_d - \Delta H_u)\Delta\theta \qquad ((3.12))$$

But ΔW is also equal to the product of the initial moisture content and the volume of the crust. This is represented mathematically for a hemispherical drop as:

$$\Delta W = \frac{2}{3} \pi C_o (R^3 - r^3) \qquad ((3.13))$$

Equating ((3.12)) and ((3.13)) yields,

$$\frac{2}{3} \pi C_o (R^3 - r^3) = G(\Delta H_d - \Delta H_u)\Delta\theta \qquad ((3.14))$$

and so the crust thickness, β, becomes:

$$\beta = R - (R^3 - \frac{3G}{2\pi C_o}(\Delta H_d - \Delta H_u)\Delta\theta)^{1/3} \qquad ((3.15))$$

where β = crust thickness (cm)

R = external drop radius (cm)

G = dry air mass flow rate (g/s)

$\Delta H_d = H_{di} - H_{do}$ $(i = 1, n)$ (g/g)

$\Delta H_u = H_{ui} - H_{uo}$ $(i = 1, n)$ (g/g)

$\Delta\theta$ = time interval (s)

C_o = initial moisture content (g. water/cm^3 solution)

π = constant (-)

The thickness can thus be predicted from equation ((3.15))

3.2.3 Mass Transfer Coefficient.

The overall resistance to transfer of water-vapour from the crust surface to the air is obtained by treating the resistances to mass transfer through the crust and the boundary-layer air as a series system. Thus

$$\frac{1}{K_{ca}} = \frac{1}{H_c k_G} + \frac{1}{k_c} \qquad ((3.16))$$

where K_{ca} = overall mass transfer coefficient from the crust surface to the air stream, (cm/s);

k_G = film mass transfer coefficient for pure water drops, deduced from equation ((3.9)), (cm/s);

H_c = Henry's Law constant (section 2.14), (-)

Since the overall drying process is controlled by the resistance of the crust, that is,

$$\frac{1}{k_c} >> \frac{1}{K_G} \quad , \qquad ((3.16a))$$

equation ((3.16)) can be written as

$$\frac{1}{K_{ca}} \simeq \frac{1}{k_c} \qquad ((3.16b))$$

In the presence of liquid water, the air in the crust voids is saturated with water vapour at the local crust temperature but remains constant. Hence the use of

k_G from equation ((3.9)) is valid.

3.2.3.1 Crust Coefficient: By analogy to the Two Film Theory (3) the crust mass transfer coefficient is defined as,

$$k_c = \frac{D_e}{\beta} \qquad ((3.17))$$

since the hold-up of solvent in the crust is negligible. D_e = effective diffusivity of water vapour through the crust of thickness, β.

The effective diffusivity (42) is proportional to the molecular diffusivity, D_M, porosity, ε , the constriction factor, σ, and the tortuosity factor, τ . These quantities are related to D_e according to the expression:

$$\frac{D_e}{D_M} = \frac{\varepsilon\sigma}{\tau} \qquad ((3.18))$$

The porosity factor, ε, is included to account for the effective reduction in the area for the diffusion of moisture at a particular point in the porous medium. The tortuosity factor is a measure of the ratio of the

distance which a diffusing species must travel on the average, and the linear distance between the two points in the solid. The constriction factor takes into account the fact that channels are not uniform in cross-section but vary with position.

The tortuosity and constriction factors are functions of the porosity, and Bruggeman's equation predicts,

$$\frac{\sigma}{\tau} = \varepsilon^{\frac{1}{2}} \qquad ((3.19))$$

When equation ((3.19)) is substituted into equation ((3.18)), the effective diffusivity becomes,

$$D_e = D_M \varepsilon^{1.5} \qquad ((3.20))$$

From equation ((3.17)) and ((3.20)), the mass transfer coefficient of the crust becomes,

$$k_c = \frac{D_M \varepsilon^{1.5}}{\beta} \qquad ((3.21))$$

<u>3.2.3.2 Concentration Driving Force:</u> Equation ((3.12)) can be written in the form,

$$\frac{1}{A}\frac{dW}{d\theta} = \frac{G}{A}(\Delta H_d - \Delta H_u) = N_A \qquad ((3.22))$$

But by definition (1)

$$N_A = k_{ca}\Delta C \qquad ((3.23))$$

therefore by substituting for N_A from ((3.22)) into ((3.23)) the concentration driving force, ΔC is,

$$\Delta C = \frac{G}{A\ K_{ca}} (\Delta H_d - \Delta H_u) \qquad ((3.24))$$

where ΔC is the concentration driving force, (g/cm^3) K_{ca} is the overall mass transfer coefficient, (cm/s), given by equation ((3.16)) after replacing k_G and k_c by equation ((3.9)) and ((3.21)) respectively.

Section Four

Experimental Apparatus and Procedure

Chapter 4.1 Description of Apparatus

Chapter 4.2 Experimental Procedure

4.1 Description of Apparatus

4.1.1 Overall Flow System: A schematic diagram of the overall flow system is shown in figure 4.1; and in plate 4.1 is presented a photograph of the equipment. The wind tunnel was 183 cm (6 feet) long and was constructed from mild steel ducting having a 2.54 by 2.54 cm (1 inch x 1 inch) square cross-section, with the exception of a 20 cm (8 inch) long working T-section made from perspex with a square cross-section of 2.54 cm x 2.54 cm. The entire mild steel portion of the tunnel was insulated with asbestos.

Compressed air from the laboratory supply mains was passed through the system via a Birlec air dryer containing a fixed bed of molecular sieve as dessicant. An air receiver was connected between the mains air line and the dryer. Two pressure regulators were installed, one upstream and the other downstream of the air receiver to damp out any fluctuations in the mains pressure.

The air flow rate, measured at the inlet to the wind tunnel with a Metric type 18A rotameter, could be controlled from approximately 11 to 116 dm^3/min with a 2.54 cm globe valve connected to the outlet of the dryer.

The air was heated with a 1 kW electric heater mounted in the tunnel at the rotameter outlet. The air temperature was controlled with a 3A, 90Ω Cressall Torovolt resistor between 0^oC and 600^oC.

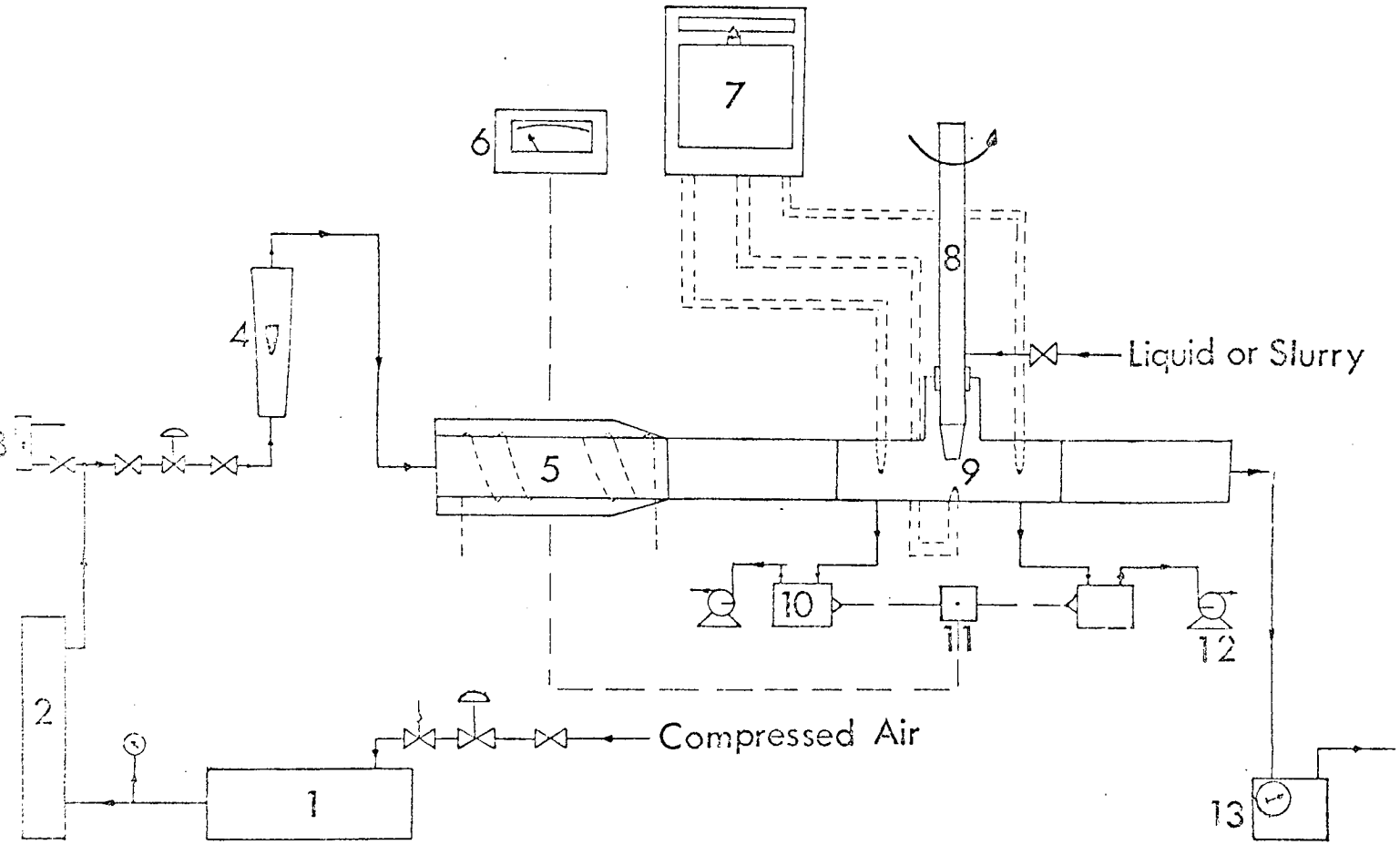

KEY

1	Air Receiver
2	Birlec Air Dryer
3	Fischer Purgerator
4	Rotamer Type 18 A
5	Air Heater
6	Hygrometer
7	Temperature Recorder
8	Drop-Suspension Device
9	Perspex T-piece
10	Constant Temperature Un
11	Dipole Valve
12	Sample Pump
13	Gas Meter

FIGURE 4·1

SCHEMATIC DIAGRAM OF APPARATUS.

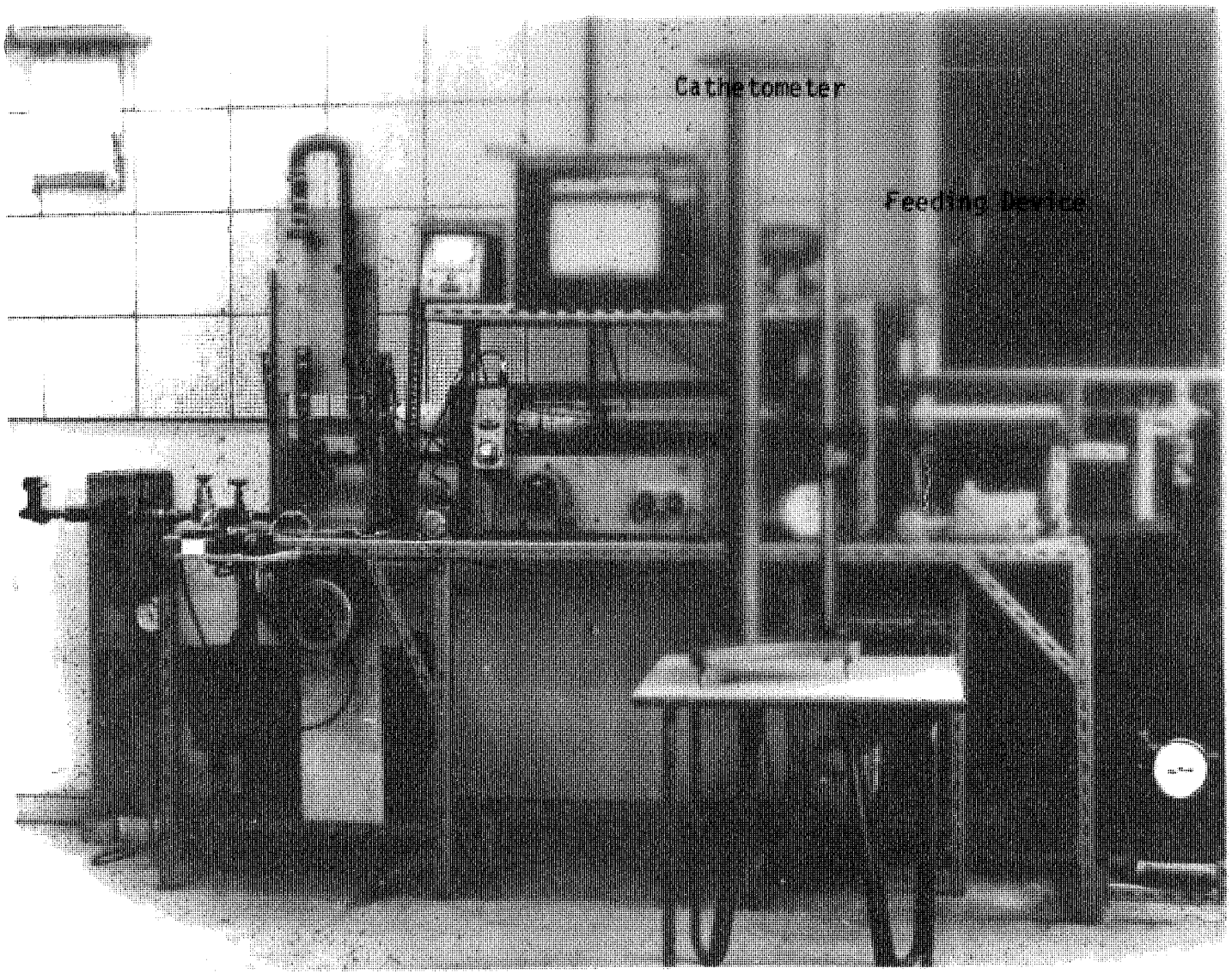

Plate 4.1 Experimental Rig.

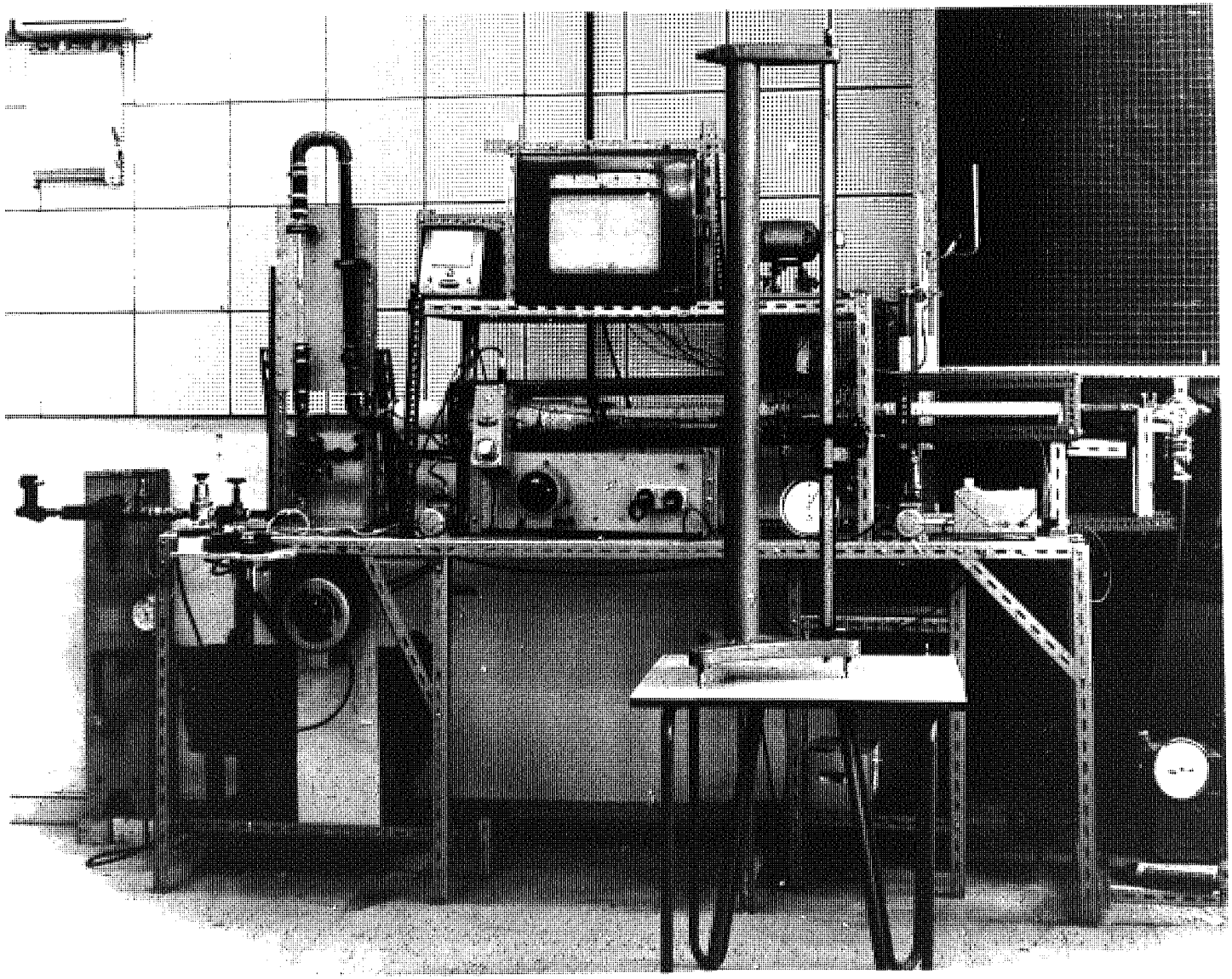

Plate 4.1 Experimental Rig.

The air temperature was measured at points 10 cm. upstream and 10 cm. downstream of the drop, and directly below the drop support device with three chromel-alumel thermocouples connected to an Elliot Automation strip-chart recorder. The central thermocouple was such that it could be traversed vertically into the drop when the drop temperature was measured.

Air humidities, both upstream and downstream of the drop, were measured with a Shaw Dew-Point meter.

4.1.2 Drop Suspension Device.

4.1.2.1 Less-Viscous Liquids or Slurries: The drop-suspension device shown in figure 4.2 and plate 4.2 was essentially a 0.95 cm. o.d. stainless steel tube with a 0.16 cm. diameter hole situated 10 cm. from the nozzle. The tube was introduced into a 2.54 cm. diameter cylindrical T-piece brazed onto a 7.6 cm. diameter plate, and positioned such that the 0.16 cm. diameter hole was enclosed within the cylinder. A liquid-tight seal between the tube and cylinder was provided by Crane Mechanical seals, type IABR171/Z, which allowed the tube, but not the cylinder, to rotate when coupled directly to the vertical shaft of a 1-phase, 50 Hz Parvalux electric motor with a maximum speed of 100 r.p.m.'s. The speed was controlled with a 27 Ω, 10A Cressall Torovolt resistor wired into the armature of the motor.

Figure 4.2 Stainless-Steel Drop-Suspension Device.

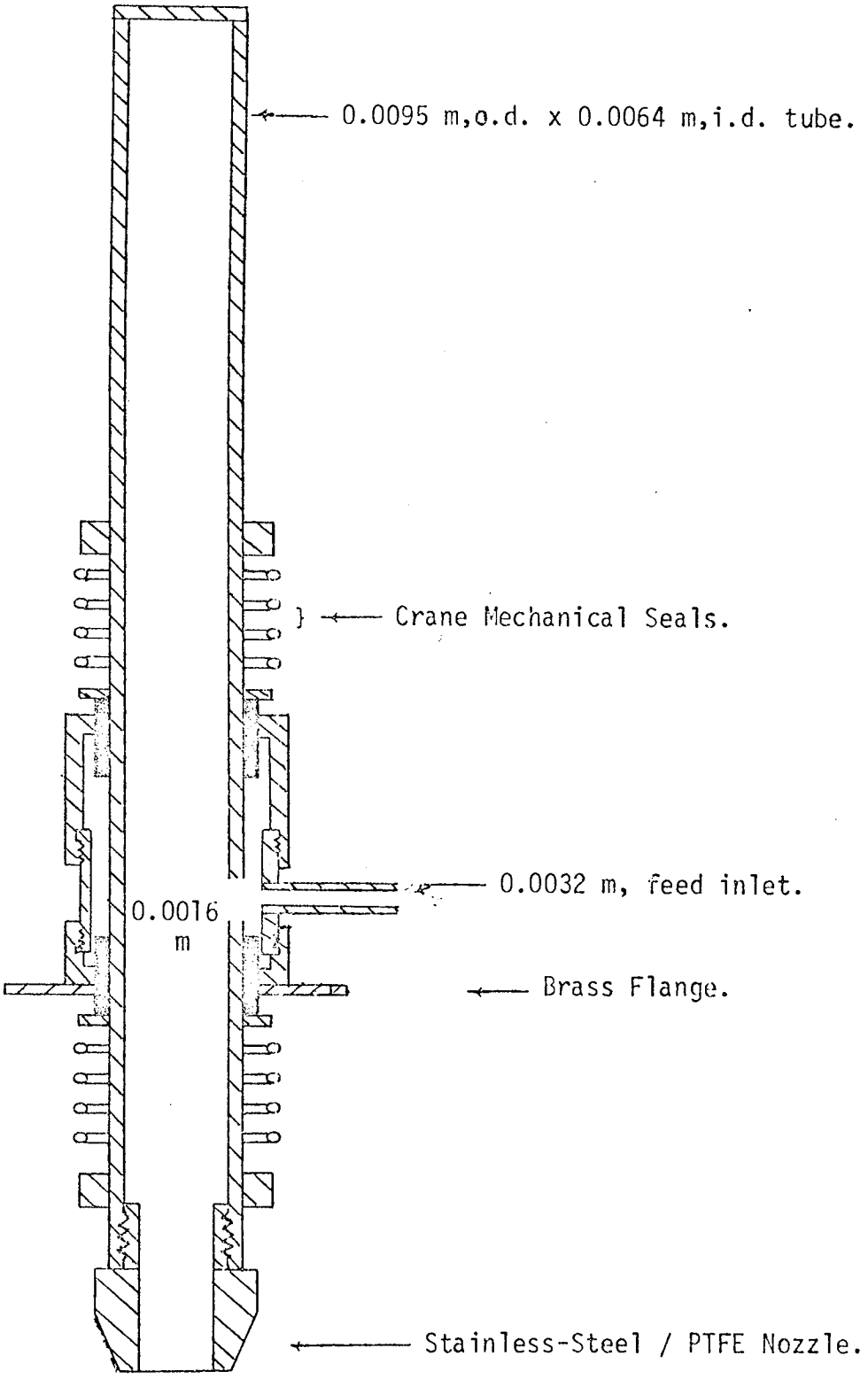

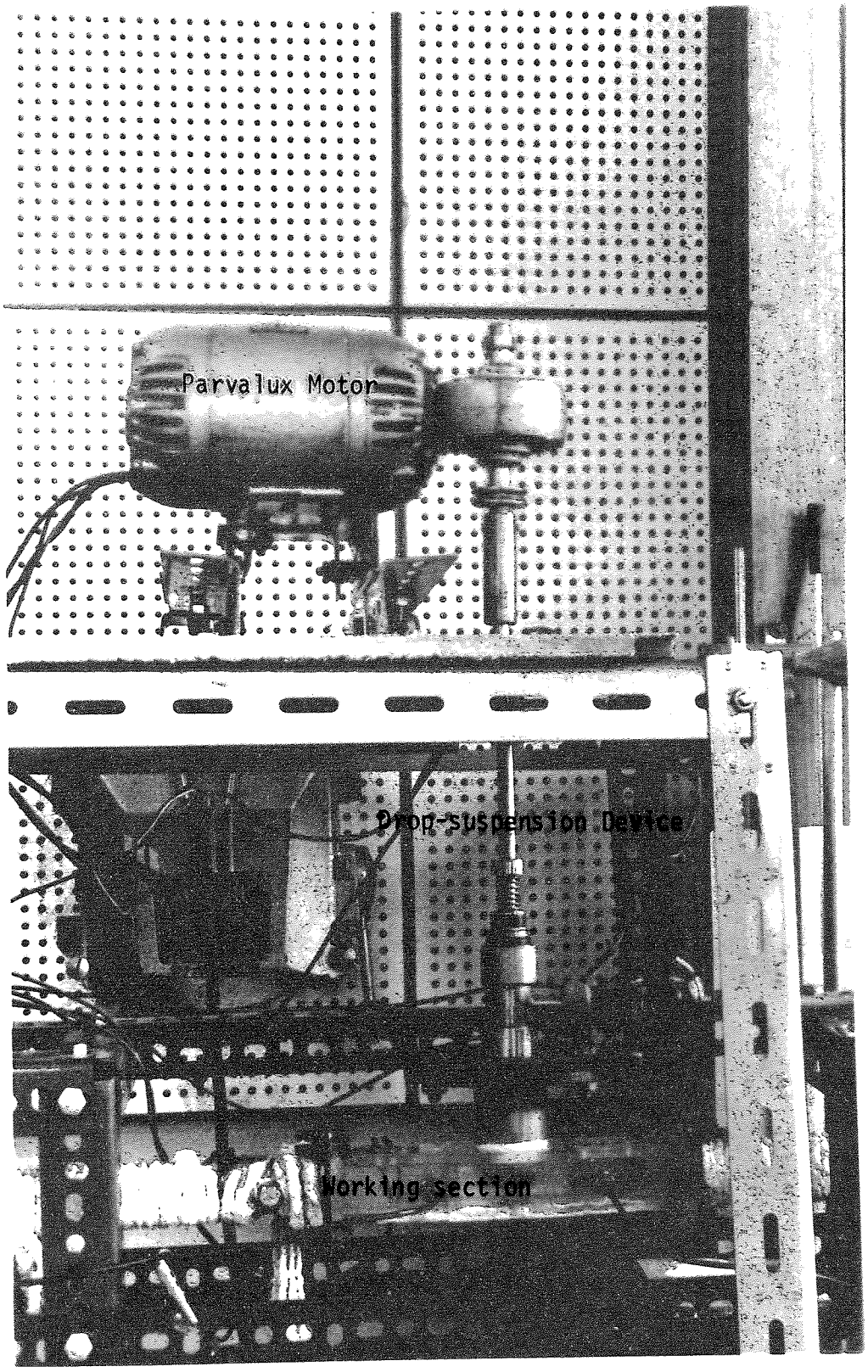

Plate 4.2

Drop Suspension Device for Less Viscous Liquids

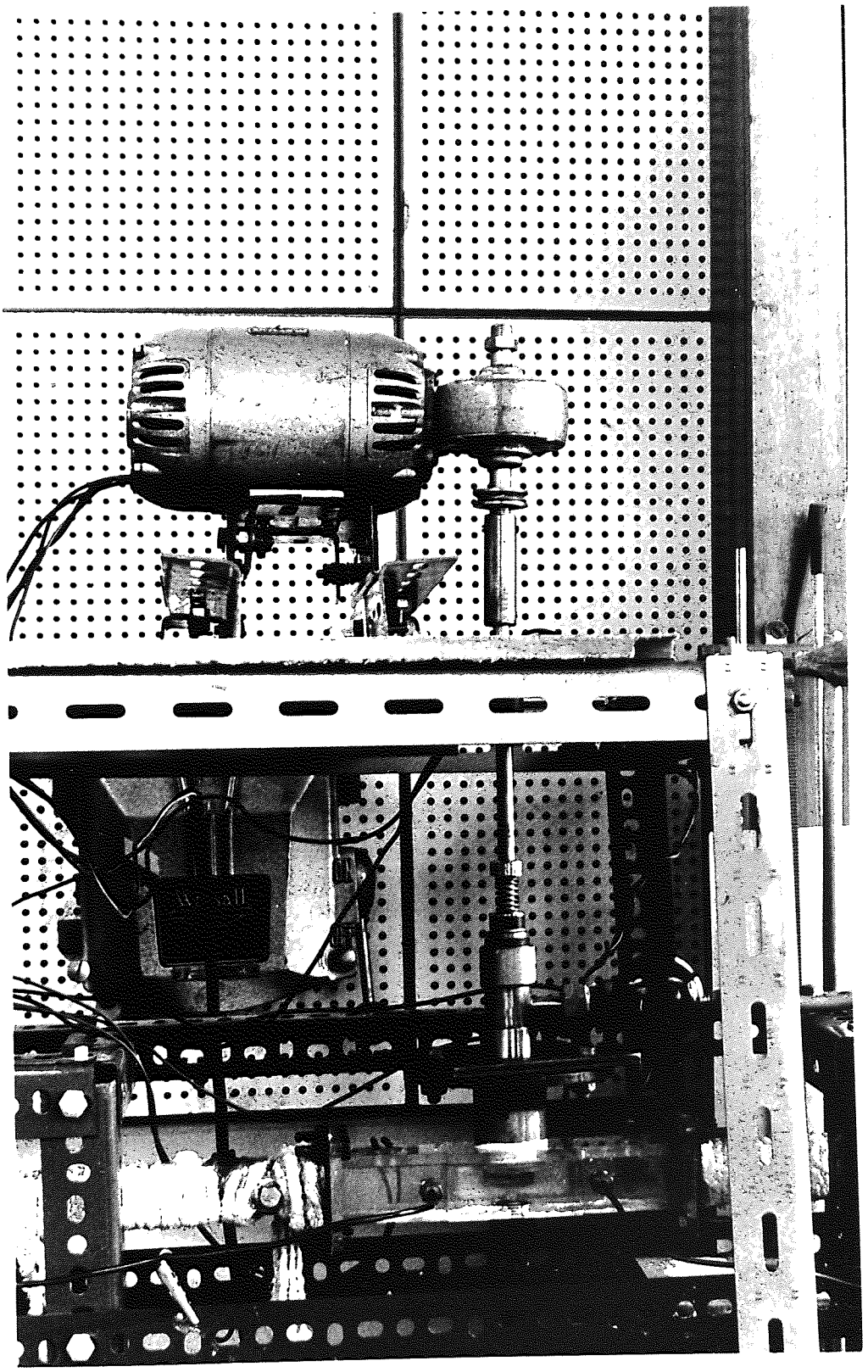

Plate 4.2

Drop Suspension Device for Less Viscous Liquids.

To counter wetting problems, the portion of the stainless steel tube below the brass plate was threaded to take a screw-on P.T.F.E. or stainless steel nipple with an internal diameter range of 0.1 cm. to 0.5 cm.

4.1.2.2 More-Viscous Slurries, (Detergent Slurries): The drop-suspension device consisted of a stainless steel piston inside a 0.95 cm. o.d. stainless steel tube. The tube was fabricated in two halves, the two being connected via a 0.64 cm. inside diameter PTFE needle valve, plate 4.3. The complete drop-suspension device was similar to a bicycle pump.

4.1.3 Feeding Device.

The feeding device, figure 4.3, was designed so that a constant drop-size was maintained during each experiment. It consisted of two glass tubes connected together via a quick-fit Rotaflo valve, type TF 2/13 supplied by Fisons Scientific Apparatus Limited. A precision glass piston was inserted at the upper arm of the larger-bore tube to prevent any oscillations of the drop. A length of 0.7 cm. i.d. rubber tubing linked the downward leg of the larger-bore tube to the cylinder T-piece.

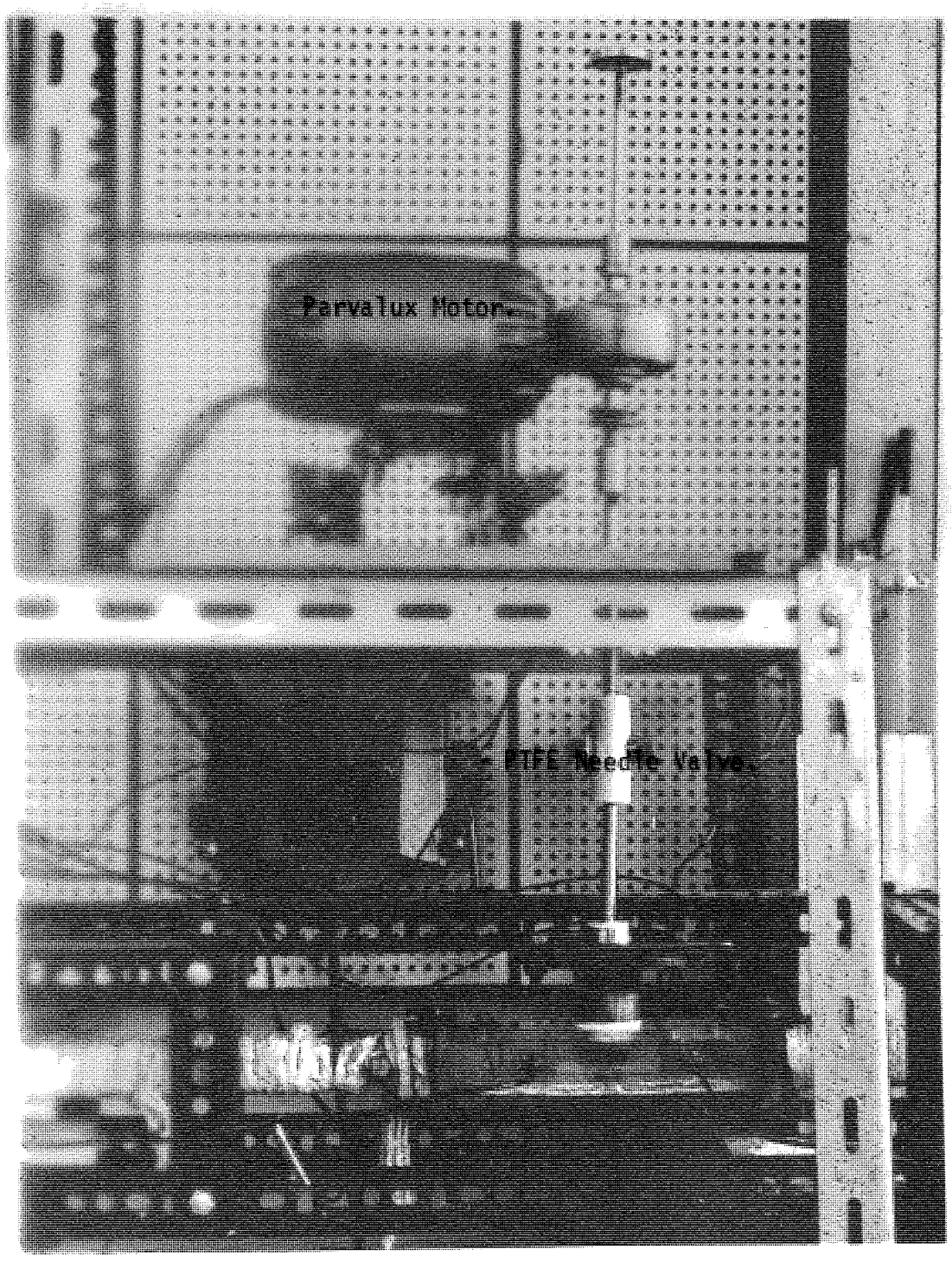

Plate 4.3

Drop Suspension Device for More Viscous Slurries.

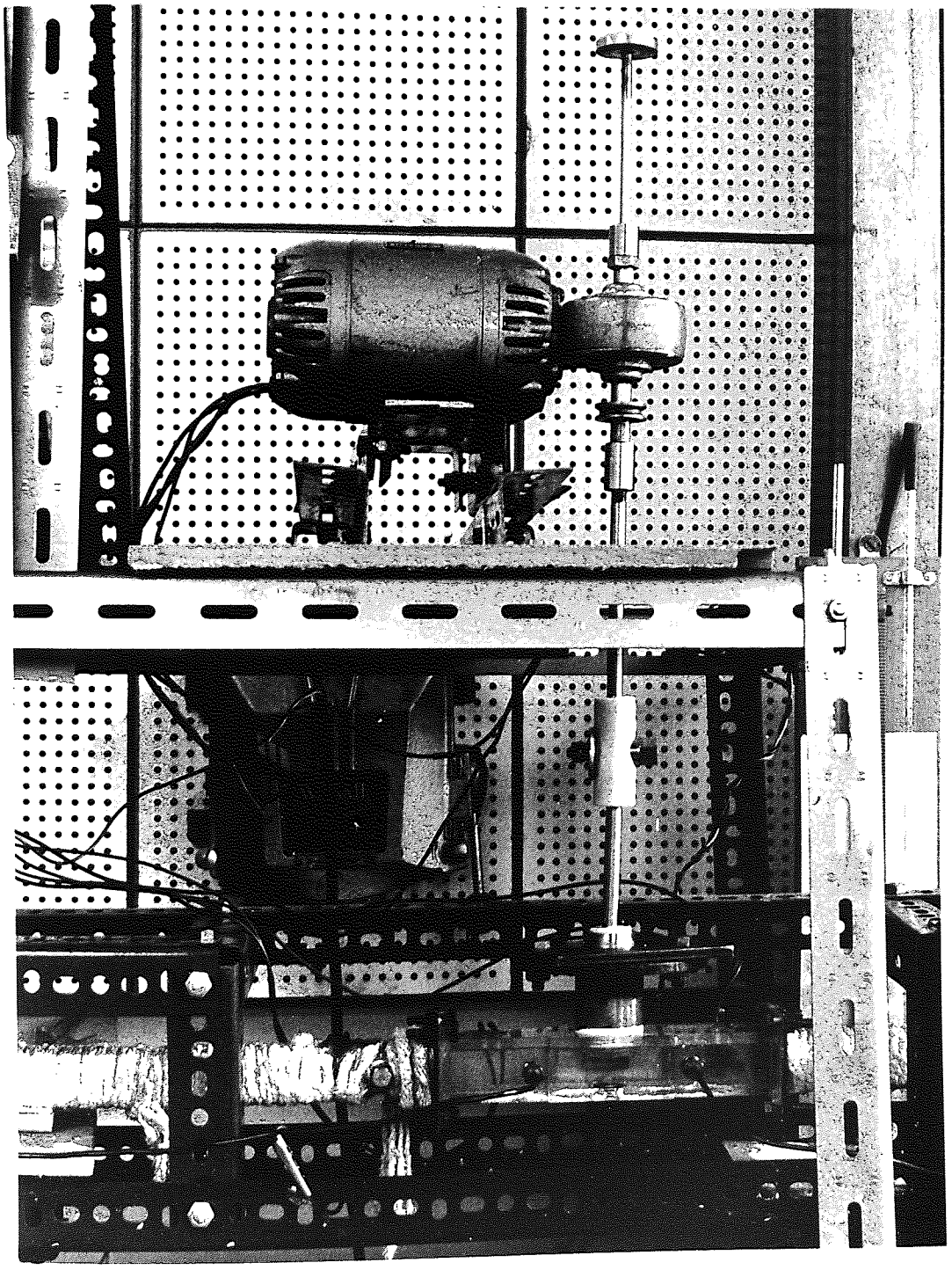

Plate 4.3

Drop Suspension Device for More Viscous Slurries.

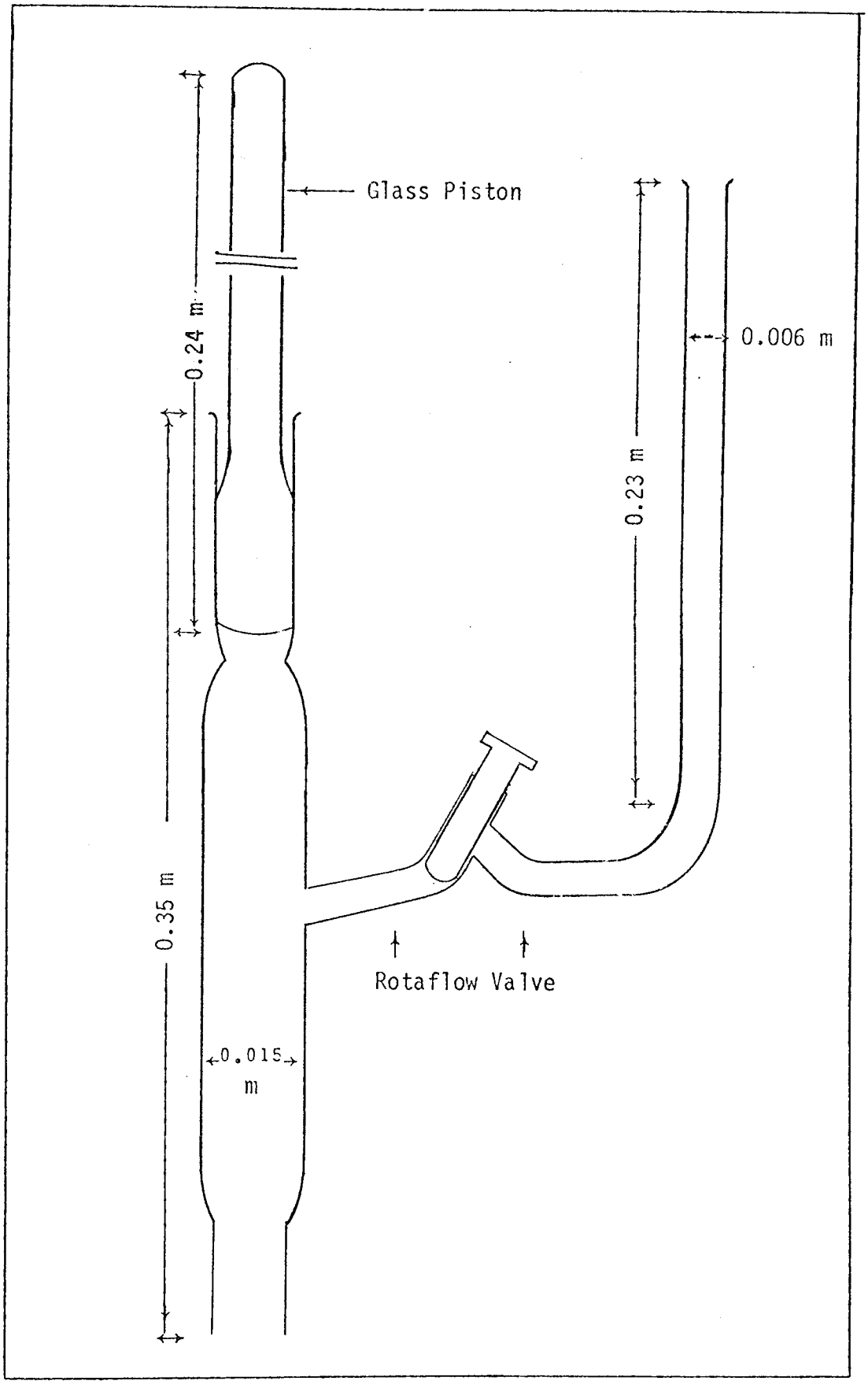

Figure 4.3 Feeding Device.

4.1.4 Shaw Hygrometry.

This instrument for humidity measurement consisted of a dew-point meter, two sensing elements, two constant temperature units, two sample pumps, three coaxial cables and a dipole valve.

The coaxial cables were connected via the dipole valve to the two sensing elements, which were screwed into the constant temperature units, and the dew point meter.

Approximately 0.5 dm^3/min of air was drawn through each constant temperature unit by means of the sample pumps to provide contact of any water vapour in the air with the sensing elements.

4.1.4.1 Sensing Elements.

Each sensing element consisted of a coaxial socket and was 15.4 cm. long. It was an idealised hygroscopic system only a few microns thick, in which a dynamic equilibrium existed between the liquid water contained in the pores, and the water vapour present outside - plate 4.4 which also shows a Hygrometer.

Plate 4.4

Hygrometer and Sensing Element.

4.1.4.2 Constant Temperature Unit.

The constant temperature unit consisted of a brass container into which the element (section 4.1.4.1.) was screwed. A sensitive thermostat maintained a constant temperature, by switching the 30-W heater, on or off, at a particular dial setting. It was supplied with fittings for 0.32 cm. outside diameter piping.

The element holder was of a heavy Brass construction and Chrome plated and was connected to the gas supply by means of 0.32 cm. outside diameter copper piping. A constant flow of air was allowed for by connecting a sample pump to the outlet valve of the element holder - plate 4.3.

4.1.4.3 The Hygrometer.

It consisted of a dial with two scales: one scale reads dew-point from $-80^{o}C$ to $-20^{o}C$ and the other scale reads 1 to 1000 parts per million of water vapour by volume - plate 4.4, which also shows a sensing element.

4.1.5 Ancillary Equipment.

The Stereoscan

The stereoscan which is essentially a scanning electron microscope produces three-dimensional pictures when the microscope specimen is scanned with a fine electron beam synchronized with the electron beam of a cathode ray picture tube. It is capable of a range of magnifications that overlaps the range of the light microscope or hand magnifying glass at the low end and the range of the transmission microscope at the high end. The scanning electron microscope is useful over a magnification range from approximately 15 diameters to about 100,000 diameters, although the image begins to get blurred above 20,000 diameters. This broad magnification range, together with the ease of changing magnification, makes it easy to zoom from a gross image of the object to an image showing fine details.

Thus structural analysis of specimens is more easily achieved.

4.2 Experimental Procedure.

4.2.1 Instrument Calibration.

4.2.1.1. Rotameter: The flow rate indicated by the rotameter float was calibrated against the volume of dry gas recorded on the counter of a Parkinson gas meter over a time interval, and a graph of float position against flow rate was plotted.

4.2.1.2 Dew Point Meter: The air from the Birlec dryer was passed through a previously-weighed bed of alumina for a definite period of time and meanwhile the humidity recorded on the meter was noted. At the end of the experiment, the moisture content of the air was computed from the difference between the final and initial weight of the bed. Both results were then compared.

4.2.2 Experiments.

The following systems were investigated:

(a) Air-Water, to compare results of the present investigation with previous work (39, 40, 54);

(b) Sodium sulphate-Water-Air, to test the model, equation ((3.15)), for predicting crust thicknesses. Sodium sulphate decahydrate was chosen because some investigators (44, 45) had successfully dried drops of sodium sulphate solution in a current of hot air; and,

(c) Detergent-Water-Air system, to provide data for mass transfer correlation that could be applied to spray drying towers.

Initially the tunnel was allowed to reach steady state at the desired air flow rate and temperature.

4.2.2.1 Air-Water System.

After steady state had been achieved, some distilled water was introduced to the feeding device, and by a careful adjustment of the rotaflow valve, a drop was formed at the tip of the nozzle of the drop suspension device. The drop was sustained by a head difference. The drop size was measured with a cathetometer which also allowed visual observation of the drop. To ensure uniform evaporation of the moisture from the drop, the drop was rotated by starting the motor driving the drop-suspension device.

The air flow rate, temperature and humidities upstream and downstream of the drop, as well as the drop diameter, were recorded at 5-minute intervals during each experiment, until the head difference could no longer sustain the drop.

4.2.2.2 Sodium sulphate-Water-Air System.

Initially the sodium sulphate decahydrate was dissolved in warm distilled water to the required moisture content per unit volume of solution. As in section 4.2.2.1, a drop was suspended from the tip of the nozzle and the upstream and downstream humidities of the air were recorded at 1-minute intervals.

For experiments involving crust thickness measurements, the air humidities were not recorded. Instead, after drying for the first 5 minutes, the drop, which had already formed a crust, was sliced off the nozzle by a guillotine device, shown in plate 4.5, which was mounted directly below the nozzle so that the crust was cut off, flush with the nozzle tip, and retained on a Number 42 Whartman filter paper at the inlet to a Buckner-type funnel. Excess solution in the hollow shell of the crust was absorbed, leaving an almost dry, but rigid, hollow crust.

A new drop was then formed on the nozzle and dried for 10 minutes and subsequently sliced off. The

[illegible] Section showing Drop-suspension Device and Guillotine

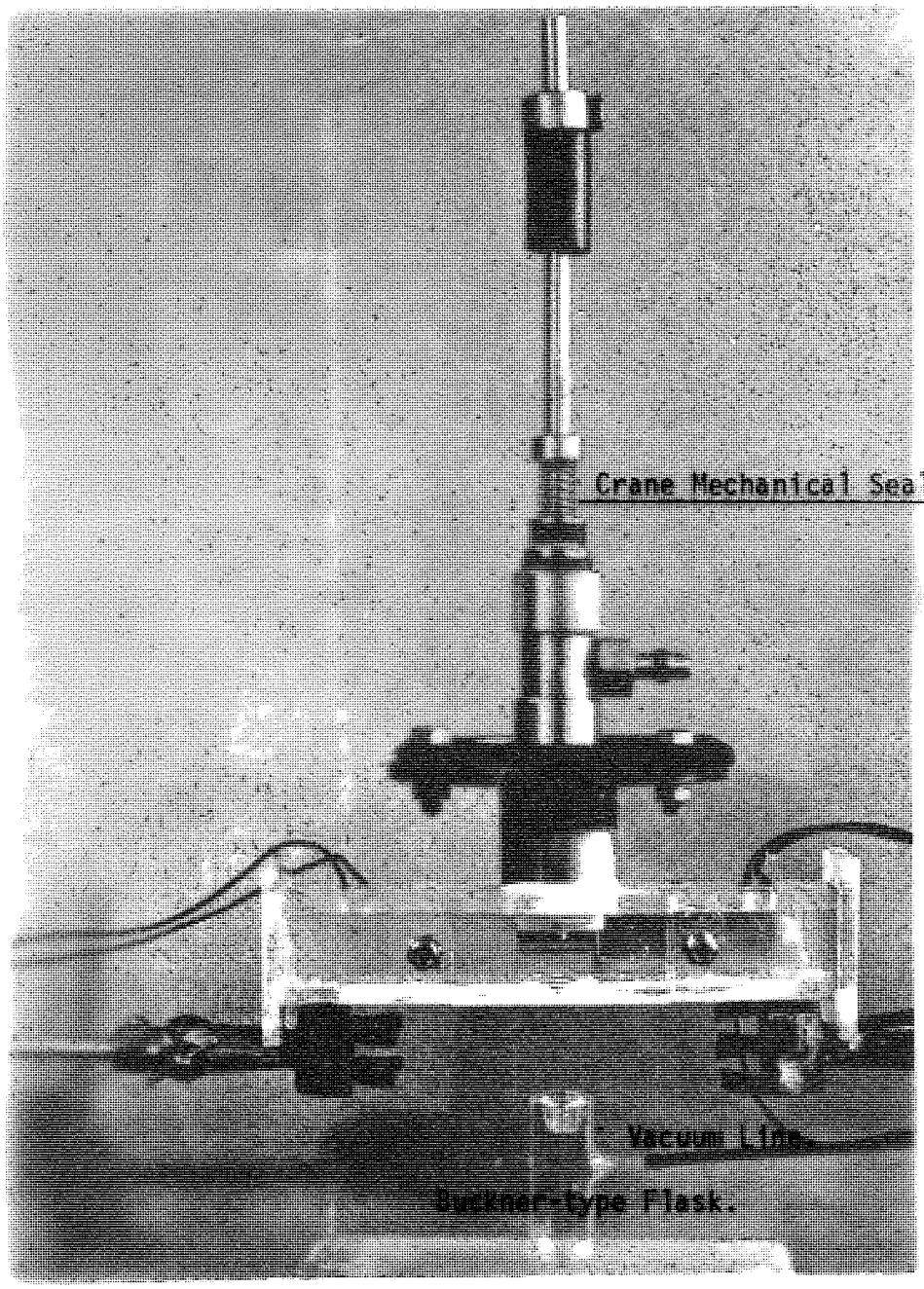

Rear View of Guillotine.

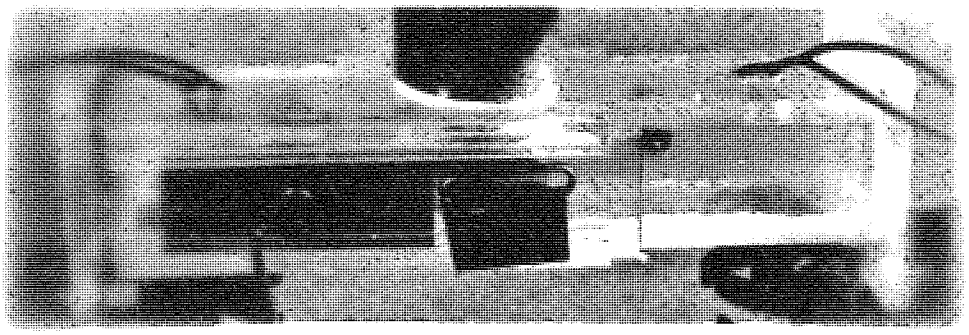

Plate 4.5 Working Section showing Drop-suspension Device and Guillotine.

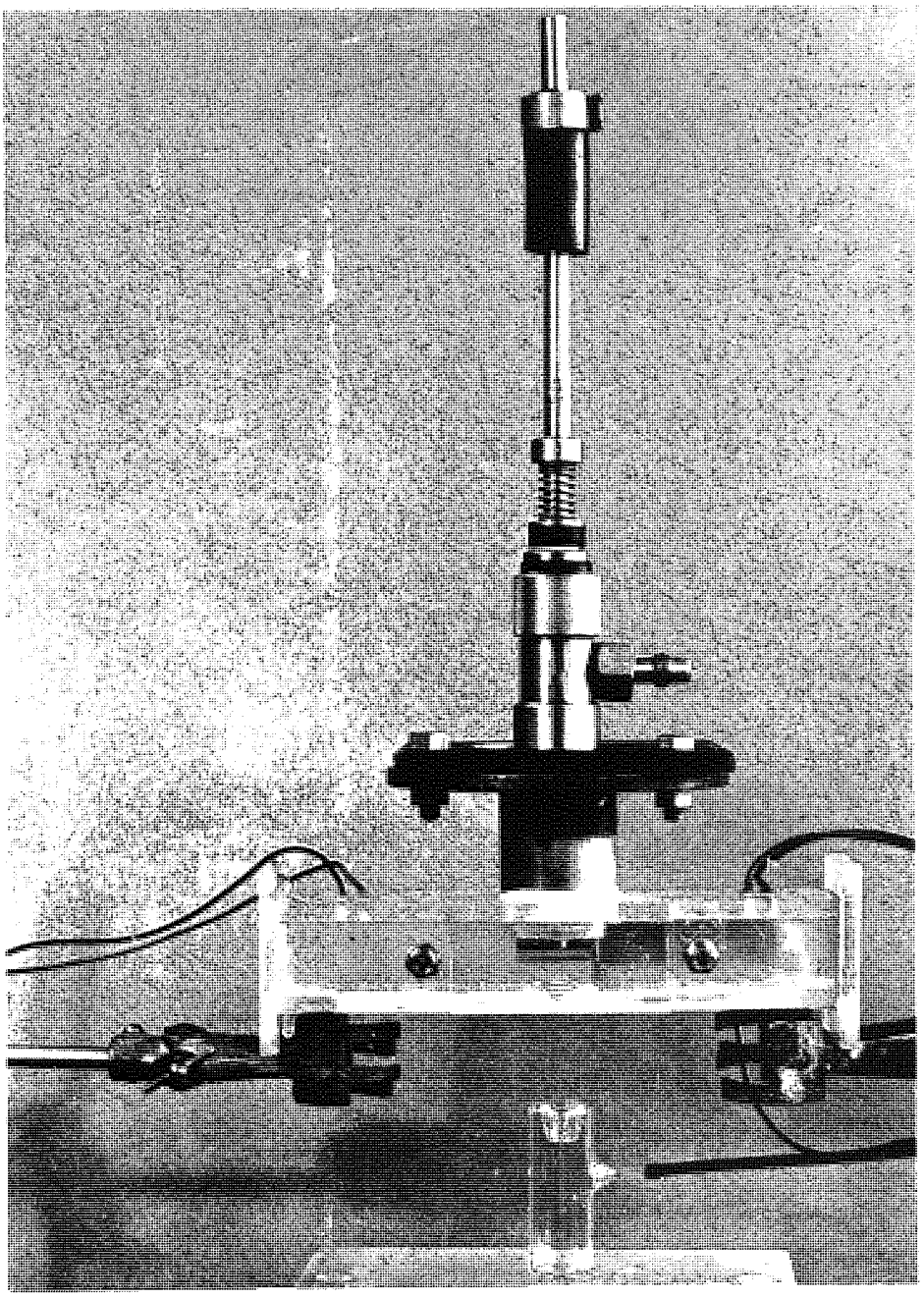

Rear View of Guillotine.

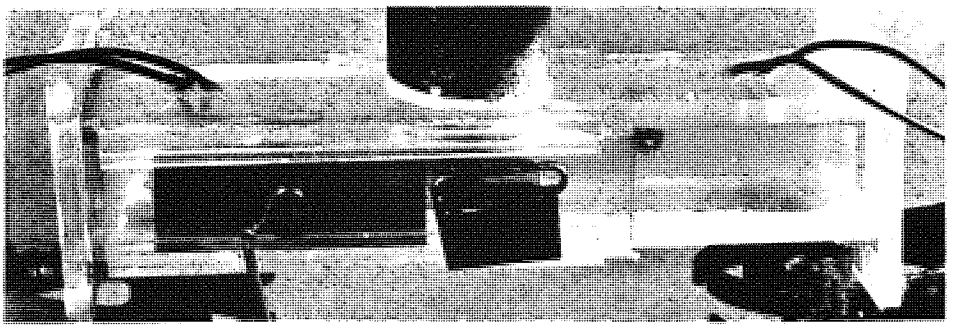

procedure was repeated for drying times of 15, 20, 25 and 30 minutes at the end of which a total of six crusts was obtained for thickness and structural analyses on the stereoscan.

4.2.2.3 Crust Thickness Measurements.

The hemispherical sodium sulphate crusts were glued with araldite to metallic studs, and when the araldite had set and the crusts were firmly secured to the studs, a thin layer of gold-palladium was evaporated onto each to hold the surface of the crust at a constant electric potential. The coating thickness was about 50 angstroms, thin enough not to obscure any fine details such as pores or cracks which might be present.

Each specimen was then introduced into the specimen chamber of the scanning microscope and photomicrographs were recorded on a 35 mm film.

Some of the specimens were mounted with the hollow facing upwards, away from the stud, before coating with gold-palladium, to permit crust thickness measurements and internal structural analysis; or vice-versa to permit analysis of the external structure.

Owing to the 3-dimensional nature of stereoscan micrographs, before crust thickness examination, it was necessary to dye the rim of the crust with Indian ink to differentiate the thickness from the inside walls of the crust.

4.2.2.4 Detergent-Water-Air System.

Nine detergent slurry formulations were investigated. The shaft of the drop-suspension device, plate 4.3, was charged with one slurry formulation at a time, after removing the piston. Meanwhile the PTFE needle valve was only slightly open. The piston was replaced and the needle valve was opened further until a drop formed at the nozzle tip. The shaft drive was started to prevent drying occurring unevenly on one side of the slurry drop, and the readings were recorded as explained in Section 4.2.2.2.

However, it was observed that when the experiment was performed with a continuous feed system, the drop grew in many directions resulting in blow holes. Consequently this system was operated as a batch process.

The moisture content of the slurry formulation was reduced to increase the viscosity. A drop was then formed by injecting it carefully from a syringe onto the nozzle tip.

As drying progressed, the nozzle with the drop was unscrewed at 5-minute intervals and weighed on an analytical balance and returned to the wind tunnel immediately. At the end of each experiment the specimens were mounted for stereoscan examination.

Experiments for crust thickness measurements, as explained in Section 4.2.2.2, were carried out as well as the pressure drop through the crust.

4.2.2.5 Pressure Drop Test for Determining Porosity, ε, of the Crust.

Kozeny's (34) technique, for correlating pressure drop and mean velocity for flow through packed beds in terms of porosity and specific surface area of the bed, was adopted to estimate the porosity of the crust.

The pressure drop test was performed in the apparatus schematically shown in figure 4.4. The test involved passing air, reduced to atmospheric pressure, through the crust and recording the pressure drop across it with an inclined-tube manometer, for a given air velocity.

Figure 4.4 Schematic Diagram of Pressure-Drop Apparatus.

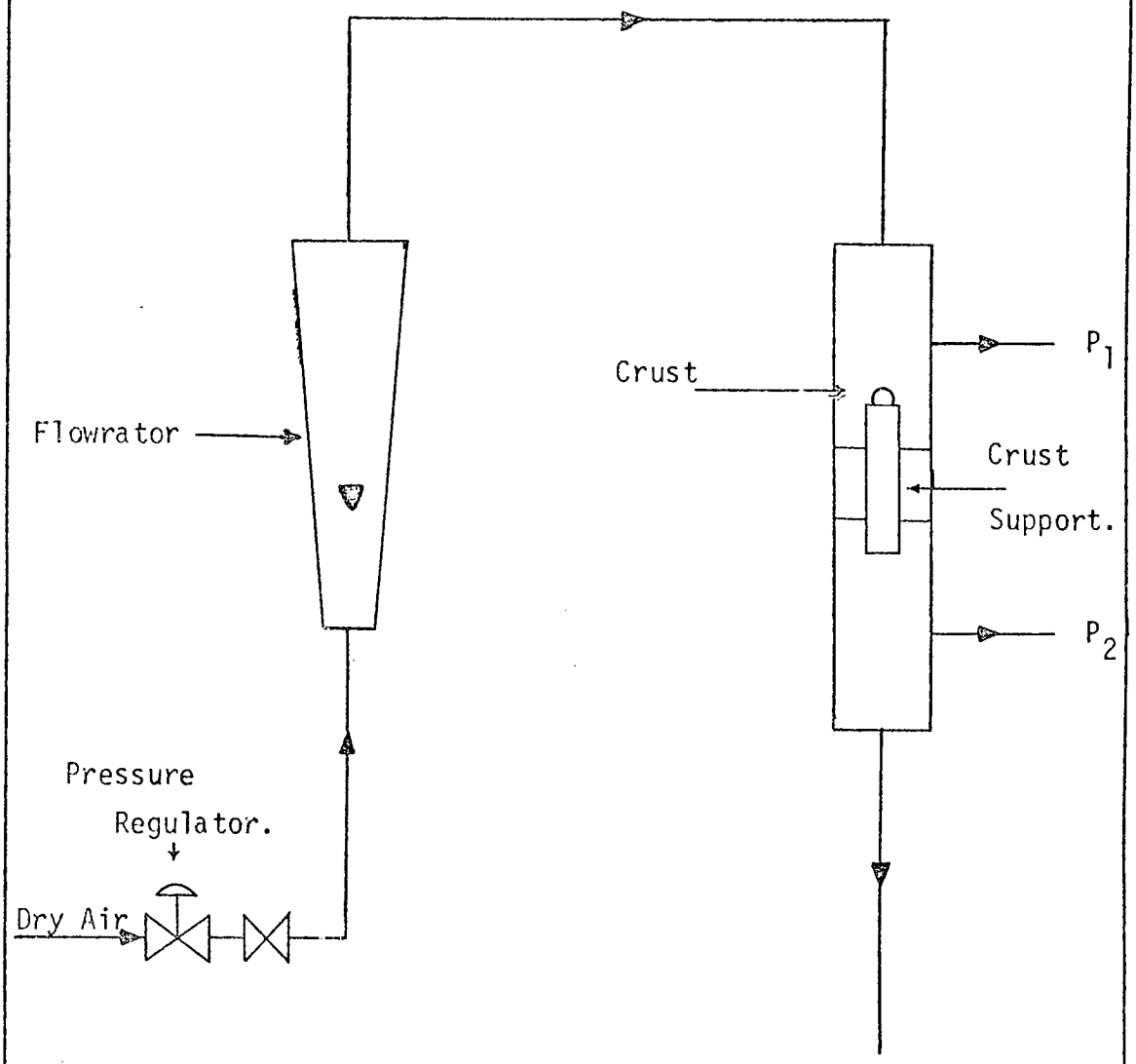

Section Five

Presentation and Analysis of Results.

Chapter 5.1 Pure Water Drops.

Chapter 5.2 Aqueous Sodium Sulphate Drops

Chapter 5.3 Detergent Slurry Drops.

5. Presentation and Analysis of Results.

The experimental results for pure water drops, aqueous sodium sulphate drops and detergent slurry drops have been presented graphically, and where applicable a correlation has been proposed. Observations from the stereoscan micrographs are also presented.

5.1 Pure Water Drops.

The mass transfer rates were calculated from equation ((3.2)), and the mass transfer coefficients from equation ((3.9)).

The separate effects of air temperature and drop diameter on the mass transfer coefficient and on the rate of mass transfer are discussed.

5.1.1 Effect of Air temperature.

5.1.1.1 Mass Transfer Coefficient: In figure 5.1 is plotted the mass transfer coefficient as a function of the air flow rate. The figure shows that mass transfer coefficient increases with rise in air temperature, thus indicating an increase in mass transfer rate.

5.1.1.2 Mass Transfer Rate: Mass transfer rate increases to a greater extent than the mass transfer coefficient with rise in temperature. This has been shown in figures 5.2 and 5.3.

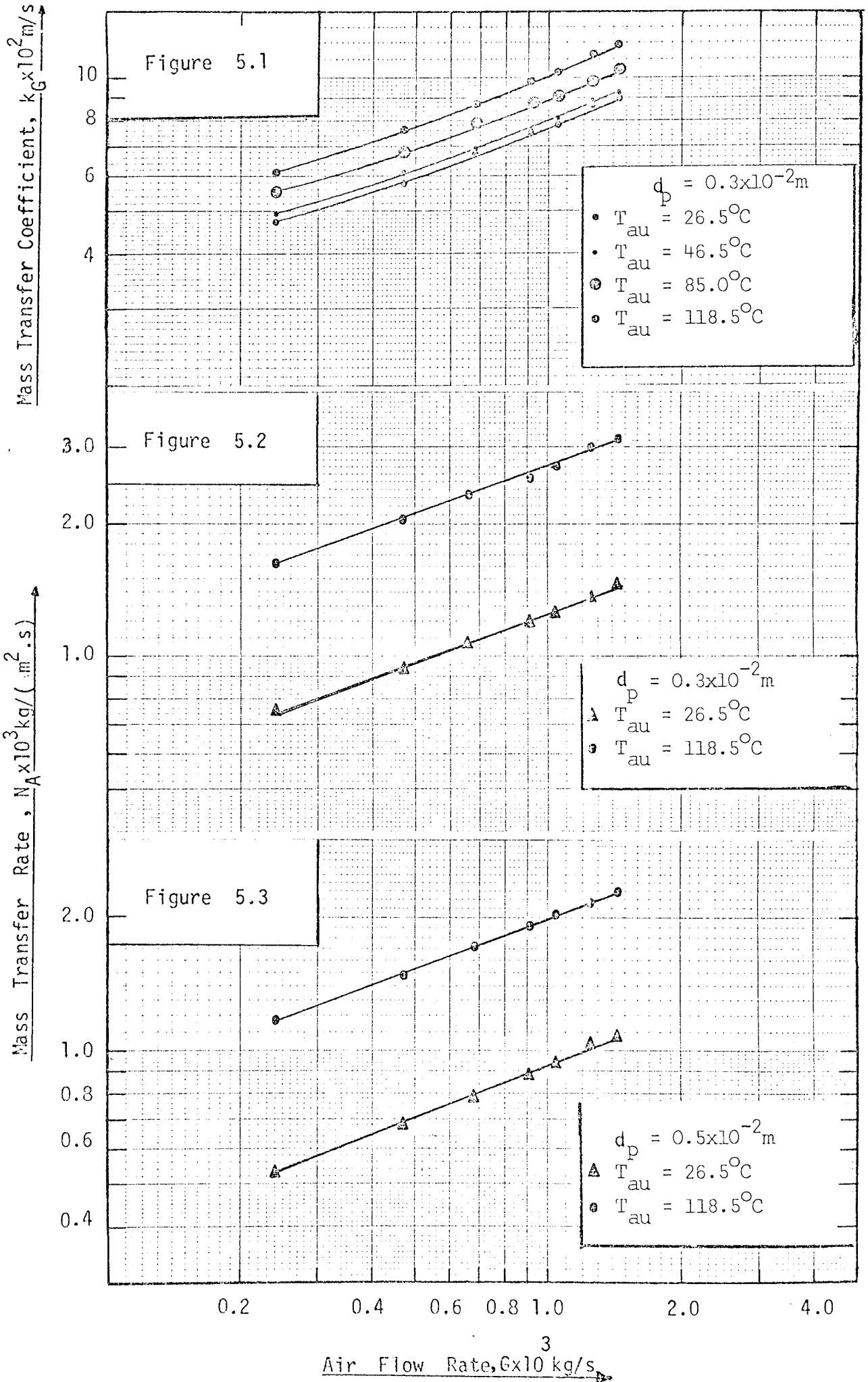
Figure 5.1
Mass Transfer Coefficient, $k_G \times 10^2$ m/s
10
8
6
4
$d_p = 0.3 \times 10^{-2}$ m
$T_{au} = 26.5^oC$
$T_{au} = 46.5^oC$
$T_{au} = 85.0^oC$
$T_{au} = 118.5^oC$
Figure 5.2
3.0
2.0
1.0
$d_p = 0.3 \times 10^{-2}$ m
$T_{au} = 26.5^oC$
$T_{au} = 118.5^oC$
Figure 5.3
Mass Transfer Rate, $N_A \times 10^3$ kg/(m^2.s)
2.0
1.0
0.8
0.6
0.4
$d_p = 0.5 \times 10^{-2}$ m
$T_{au} = 26.5^oC$
$T_{au} = 118.5^oC$
0.2
0.4
0.6
0.8
1.0
2.0
4.0
Air Flow Rate, $G \times 10^3$ kg/s

TABLE 5.1

	Reynolds Number	Instantaneous Mass Transfer Rate	Instantaneous Mass Trans. Coeff.	Schmidt Number	Sherwood Number	$Re^{\frac{1}{2}}Sc^{1/3}$
		$N_A \times 10^4$ g/(cm^{2}S.)	k_G cm/s	Sc	Sh	
$d_p = 0.10$ cm.	51.53	1.94	12.06	0.603	4.77	6.19
	74.55	2.25	13.96	0.603	5.52	7.45
	99.77	2.49	15.45	0.603	6.11	8.61
	115.1	2.54	15.75	0.603	6.23	9.25
	138.1	2.72	16.92	0.603	6.69	10.14
	157.9	2.84	17.63	0.603	6.97	10.84
$d_p = 0.30$ cm.	78.9	0.76	4.71	0.603	5.59	7.66
	154.6	0.94	5.81	0.603	6.90	10.72
	223.7	1.08	6.71	0.603	7.97	12.90
	299.3	1.21	7.51	0.603	8.91	14.92
	345.4	1.26	7.83	0.603	9.29	16.03
	414.4	1.38	8.57	0.603	10.17	17.56
	473.6	1.46	9.03	0.603	10.72	18.77
$d_p = 0.50$ cm.	131.6	0.53	3.31	0.603	6.55	9.89
	257.7	0.68	4.22	0.603	8.36	13.84
	372.8	0.79	4.88	0.603	9.64	16.65
	498.9	0.89	5.52	0.603	10.92	19.26
	575.6	0.94	5.80	0.603	11.48	20.69
	690.7	1.02	6.33	0.603	12.52	22.67
	789.4	1.08	6.71	0.603	13.27	24.23

TABLE 5.2

	Reynolds Number	Instantaneous Mass Transfer Rate	Instantaneous Mass Trans. Coeff.	Schmidt Number	Sherwood Number	$Re^{\frac{1}{2}}Sc^{1/3}$
	Re	$N_A \times 10^4$ g/(cm^{2}s)	k_G cm/s	Sc	Sh	
d_p = 0.10 cm.	24.93	3.55	10.89	0.615	3.92	4.25
	48.82	4.29	13.16	0.615	4.73	5.94
	70.63	4.77	14.63	0.615	5.26	7.15
	94.52	5.04	15.44	0.615	5.56	8.27
	109.1	5.40	16.59	0.615	5.97	8.88
	130.9	5.65	17.35	0.615	6.24	9.73
	149.6	6.23	19.14	0.615	6.88	10.40
d_p = 0.30 cm.	74.79	1.59	4.87	0.615	5.25	7.34
	146.5	1.98	6.07	0.615	6.55	10.30
	211.9	2.23	6.85	0.615	7.39	12.38
	283.6	2.48	7.59	0.615	8.19	14.33
	327.2	2.62	8.05	0.615	8.68	15.39
	392.6	2.87	8.82	0.615	9.52	16.86
	448.7	3.01	9.23	0.615	9.96	18.02
d_p = 0.50 cm.	124.6	1.12	3.44	0.615	6.18	9.50
	244.1	1.42	4.37	0.615	7.86	13.29
	353.2	1.63	5.00	0.615	8.99	15.99
	472.6	1.81	5.57	0.615	10.01	18.49
	545.3	1.96	6.03	0.615	10.84	19.87
	654.4	2.09	6.42	0.615	11.55	21.76
	747.8	2.08	6.38	0.615	11.48	23.27

TABLE 5.3

	Reynolds Number	Instantaneous Mass Transfer Rate	Instantaneous Mass Trans. Coeff.	Schmidt Number	Sherwood Number	$Re^{\frac{1}{2}}Sc^{1/3}$
	Re	$N_A \times 10^4$ g/(cm^{2}s)	k_G cm/s	Sc	Sh	
$d_p = 0.10$ cm.	22.55	3.60	12.39	0.835	3.76	3.95
	44.17	4.28	14.71	0.835	4.46	5.52
	63.90	4.63	15.93	0.835	4.83	6.64
	85.52	5.10	17.53	0.835	5.31	7.68
	98.67	5.28	18.16	0.835	5.50	8.25
	118.4	5.93	20.42	0.835	6.19	9.04
	135.3	6.23	21.44	0.835	6.50	9.66
$d_p = 0.30$ cm.	67.66	1.59	5.47	0.835	4.98	6.83
	132.5	1.97	6.78	0.835	6.16	9.56
	191.7	2.27	7.79	0.835	7.08	11.5
	256.6	2.53	8.70	0.835	7.91	13.3
	296.0	2.62	9.01	0.835	8.20	14.3
	355.2	2.83	9.75	0.835	8.86	15.7
	406.0	2.98	10.26	0.835	9.33	16.7
$d_p = 0.50$ cm.	112.8	1.12	3.85	0.835	5.83	8.82
	220.8	1.42	4.89	0.835	7.41	12.3
	319.5	1.64	5.62	0.835	8.52	14.8
	427.6	1.82	6.25	0.835	9.47	17.2
	493.4	1.94	6.66	0.835	10.1	18.5
	592.0	2.09	7.19	0.835	10.9	20.2
	676.6	2.23	7.66	0.835	11.6	21.6

TABLE 5.4

	Reynolds Number	Instantaneous Mass Transfer Rate	Instantaneous Mass Trans. Coeff.	Schmidt Number	Sherwood Number	$Re^{\frac{1}{2}}Sc^{1/3}$
	Re	$N_A \times 10^4$ g/(cm^{2}s)	cm/s	Sc		
$d_p = 0.10$ cm.	22.03	3.71	13.95	0.915	3.69	3.76
	43.14	4.40	16.53	0.915	4.37	5.26
	62.42	4.85	18.22	0.915	4.82	6.32
	83.53	5.33	20.03	0.915	5.30	7.31
	96.38	5.61	21.10	0.915	5.58	7.86
	115.7	5.93	22.31	0.915	5.90	8.61
	132.2	5.96	22.41	0.915	5.93	9.20
$d_p = 0.30$ cm.	66.09	1.63	6.13	0.915	4.87	6.51
	129.4	2.03	7.63	0.915	6.06	9.10
	187.3	2.32	8.71	0.915	6.92	10.95
	250.6	2.57	9.65	0.915	7.66	12.67
	289.1	2.71	10.19	0.915	8.09	13.61
	347.0	2.99	11.26	0.915	8.93	14.91
	396.5	3.13	11.76	0.915	9.33	15.94
$d_p = 0.50$ cm.	110.1	1.18	4.42	0.915	5.85	8.40
	215.7	1.49	5.58	0.915	7.38	11.75
	312.1	1.71	6.43	0.915	8.50	14.14
	417.6	1.91	7.18	0.915	9.50	16.35
	481.9	2.04	7.67	0.915	10.15	17.57
	578.3	2.18	8.22	0.915	10.87	19.24
	660.9	2.29	8.61	0.915	11.38	20.57

5.1.2 Effect of Drop Diameter.

5.1.2.1. Mass Transfer Coefficient: The mass transfer coefficient decreases with increase in drop diameter as shown in figure 5.4. This is discussed in page 153.

5.1.2.2. Mass Transfer Rate: As expected, mass transfer rate also decreases with increase in diameter - figure 5.5.

5.1.3. Correlations.

The following correlations were deduced from the mass transfer coefficients in Tables 5.1 - 5.4 by a least-squares curve-fitting technique described in Appendix A.

The primary objective of this exercise was to determine the value of the constant, Ψ , in a modified form of equation ((2.13)) shown here as:

$$Sh = 2.0 + \Psi\, Re^{0.5} Sc^{0.33} \qquad ((5.1))$$

The correlations are shown in Table 5.5 below:

TABLE 5.5

CORRELATIONS for Pure Water Drops

Air Temperature T_{au} °C	Correlation	Correlation Coefficient	Figure
26.5	$Sh=2.0+0.473Re^{\frac{1}{2}}Sc^{1/3}$	0.9996	5.6
46.5	$Sh=2.0+0.438Re^{\frac{1}{2}}Sc^{1/3}$	0.9965	5.7
85.0	$Sh=2.0+0.39Re^{\frac{1}{2}}Sc^{1/3}$	0.9990	5.8
118.5	$Sh=2.0+0.38Re^{\frac{1}{2}}Sc^{1/3}$	0.99	5.9

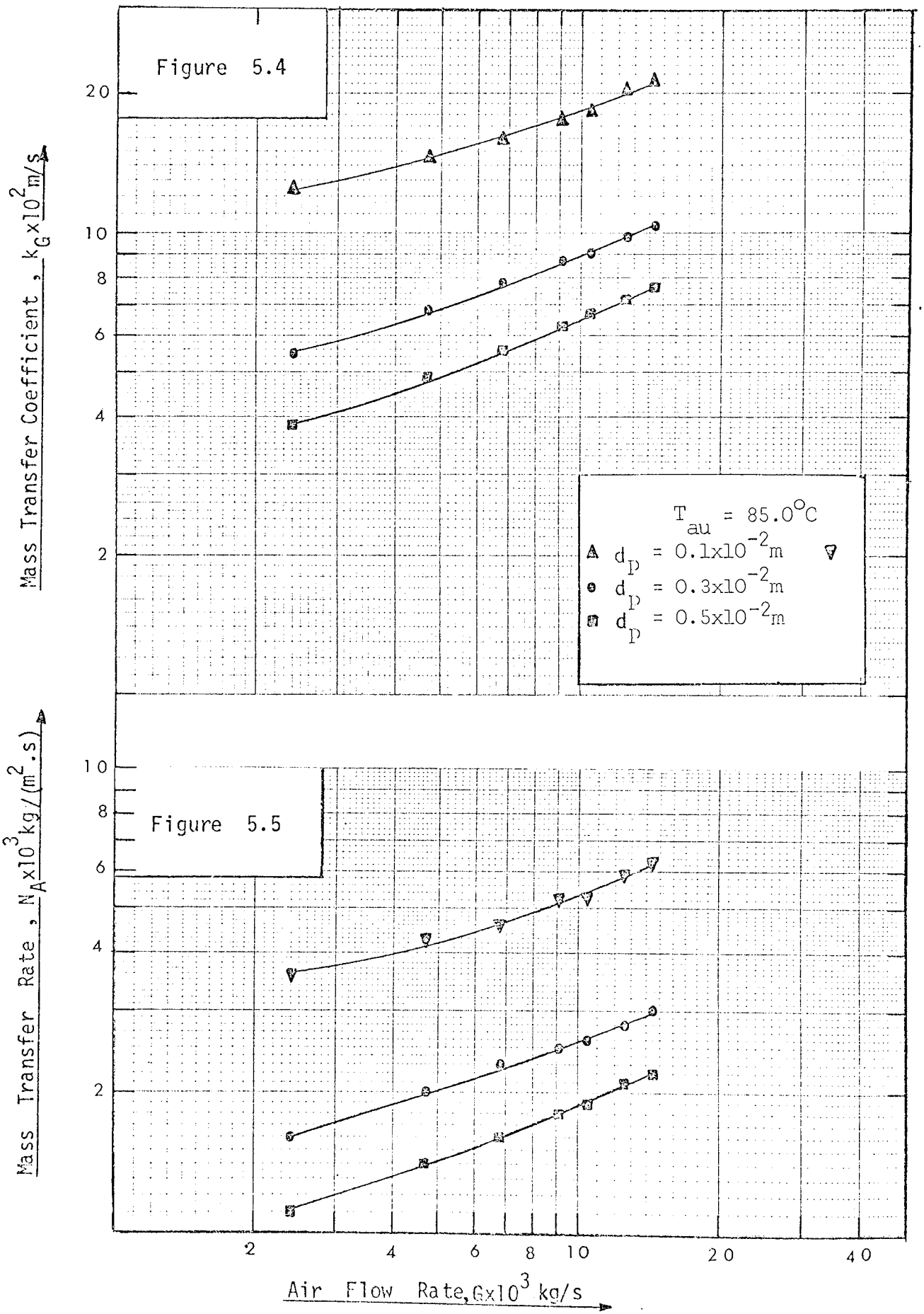
Figure 5.4
Figure 5.5
Mass Transfer Coefficient , $k_G \times 10^2$ m/s
Mass Transfer Rate , $N_A \times 10^3$ kg/(m^2.s)
Air Flow Rate, $G \times 10^3$ kg/s
T_{au} = 85.0°C
d_p = 0.1×10^{-2} m
d_p = 0.3×10^{-2} m
d_p = 0.5×10^{-2} m
20
10
8
6
4
2
10
8
6
4
2
2
4
6
8
10
20
40

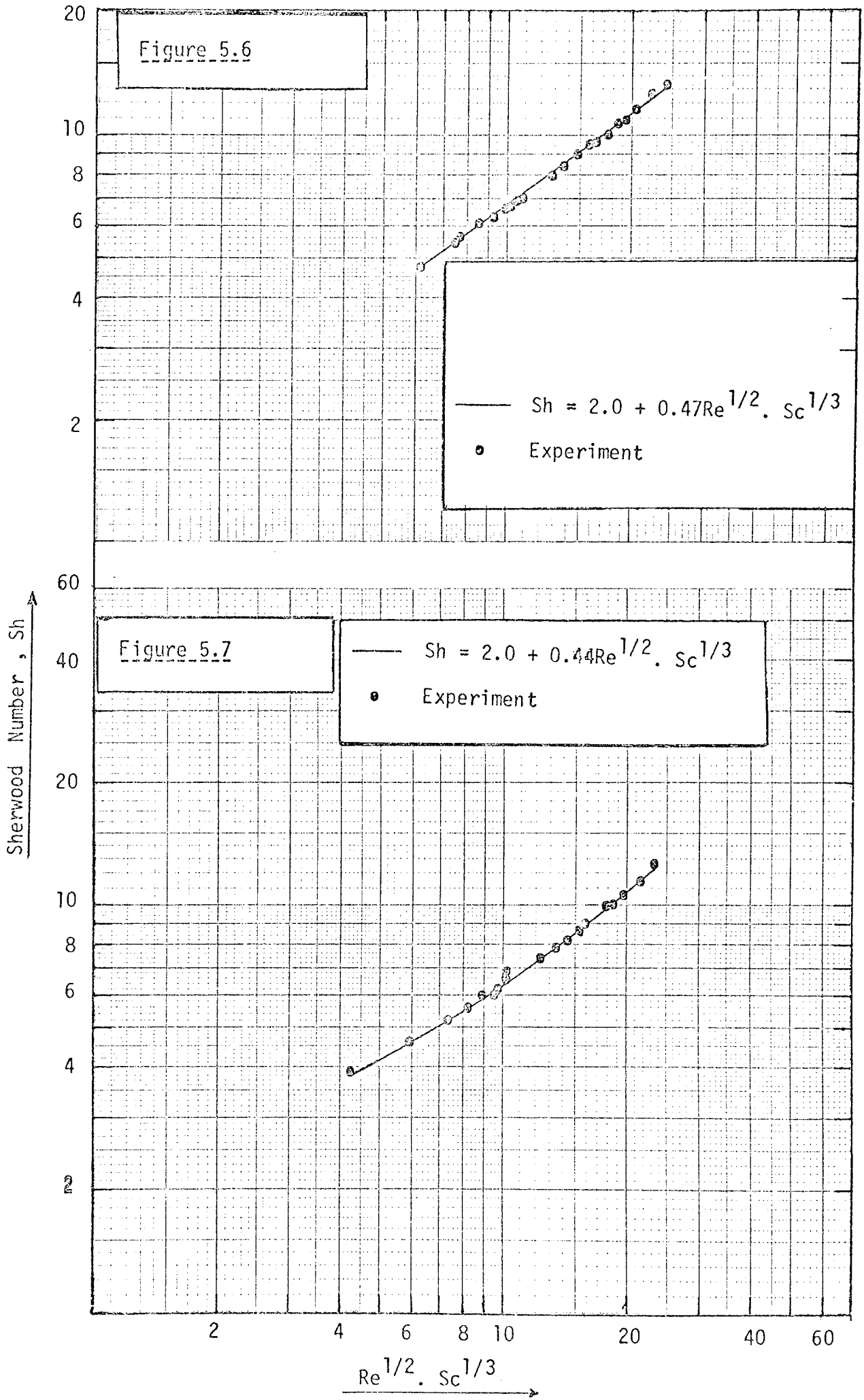
Figure 5.6
Sh = 2.0 + 0.47Re^1/2 . Sc^1/3
Experiment
Figure 5.7
Sh = 2.0 + 0.44Re^1/2 . Sc^1/3
Experiment
Sherwood Number , Sh
Re^1/2 . Sc^1/3
20
10
8
6
4
2
60
40
20
10
8
6
4
2
2
4
6
8
10
20
40
60

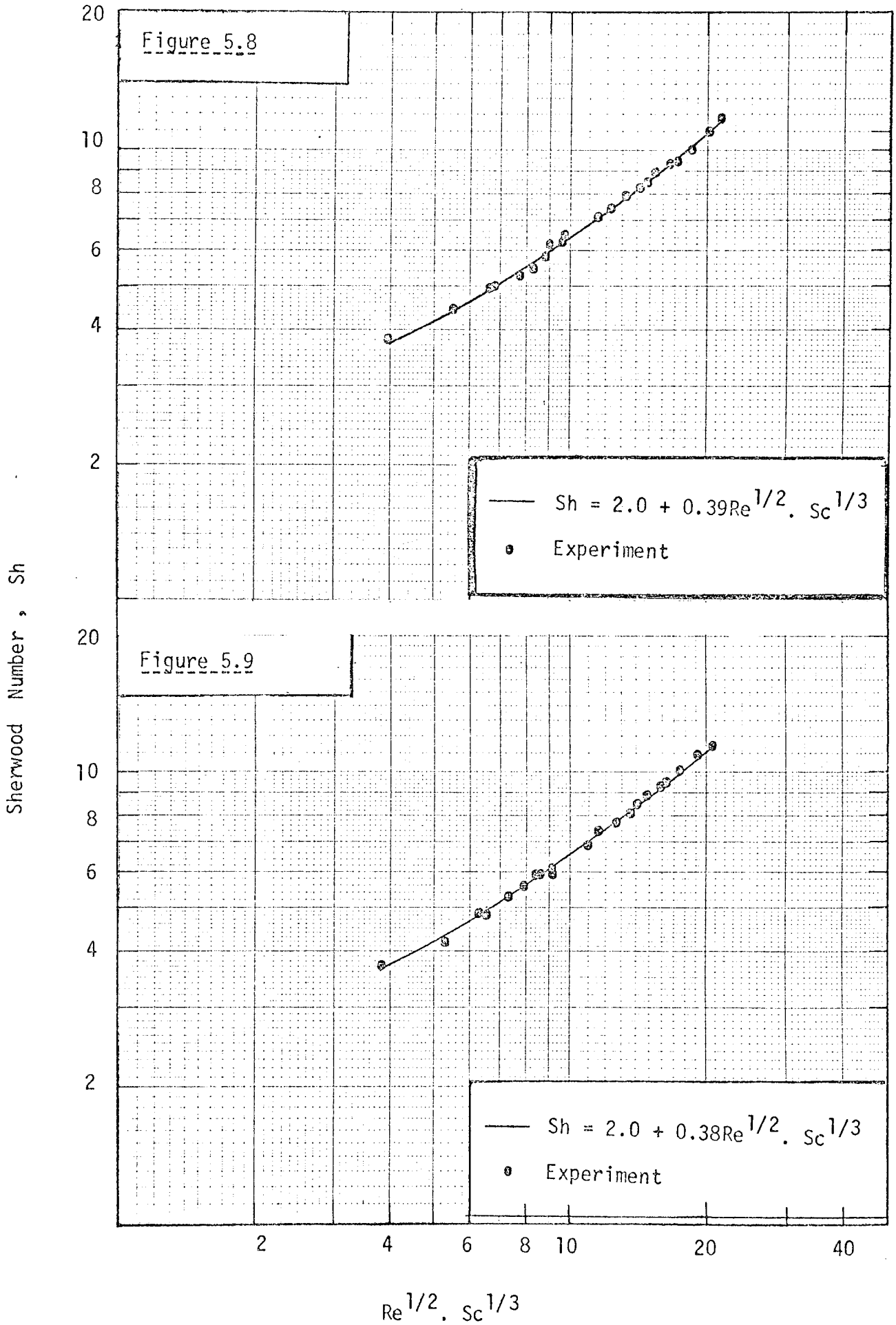
Figure 5.8
Sh = 2.0 + 0.39Re^1/2 . Sc^1/3
Experiment
Figure 5.9
Sh = 2.0 + 0.38Re^1/2 . Sc^1/3
Experiment
Sherwood Number , Sh
Re^1/2 . Sc^1/3
20
10
8
6
4
2
2
4
6
8
10
20
40

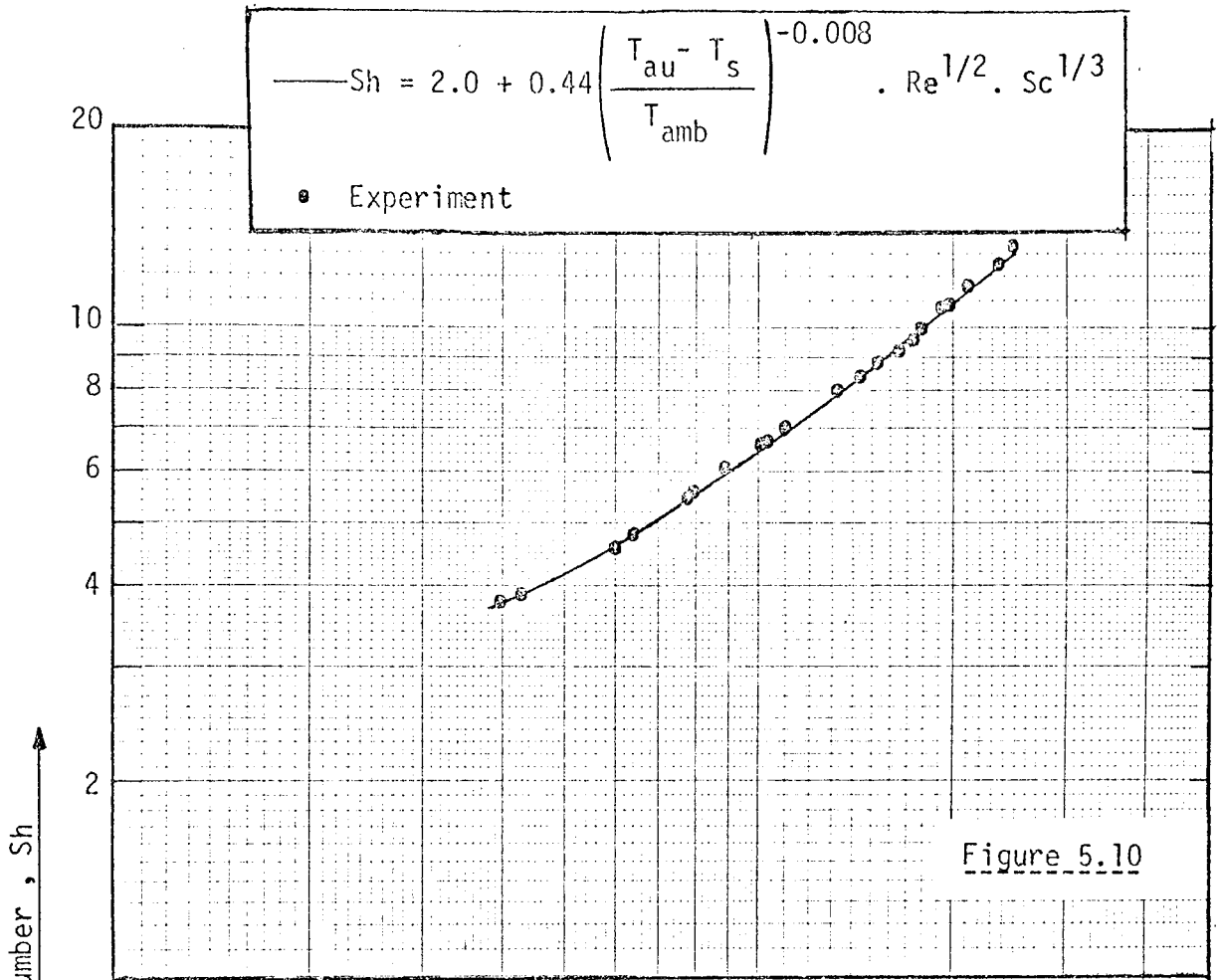

Figure 5.10

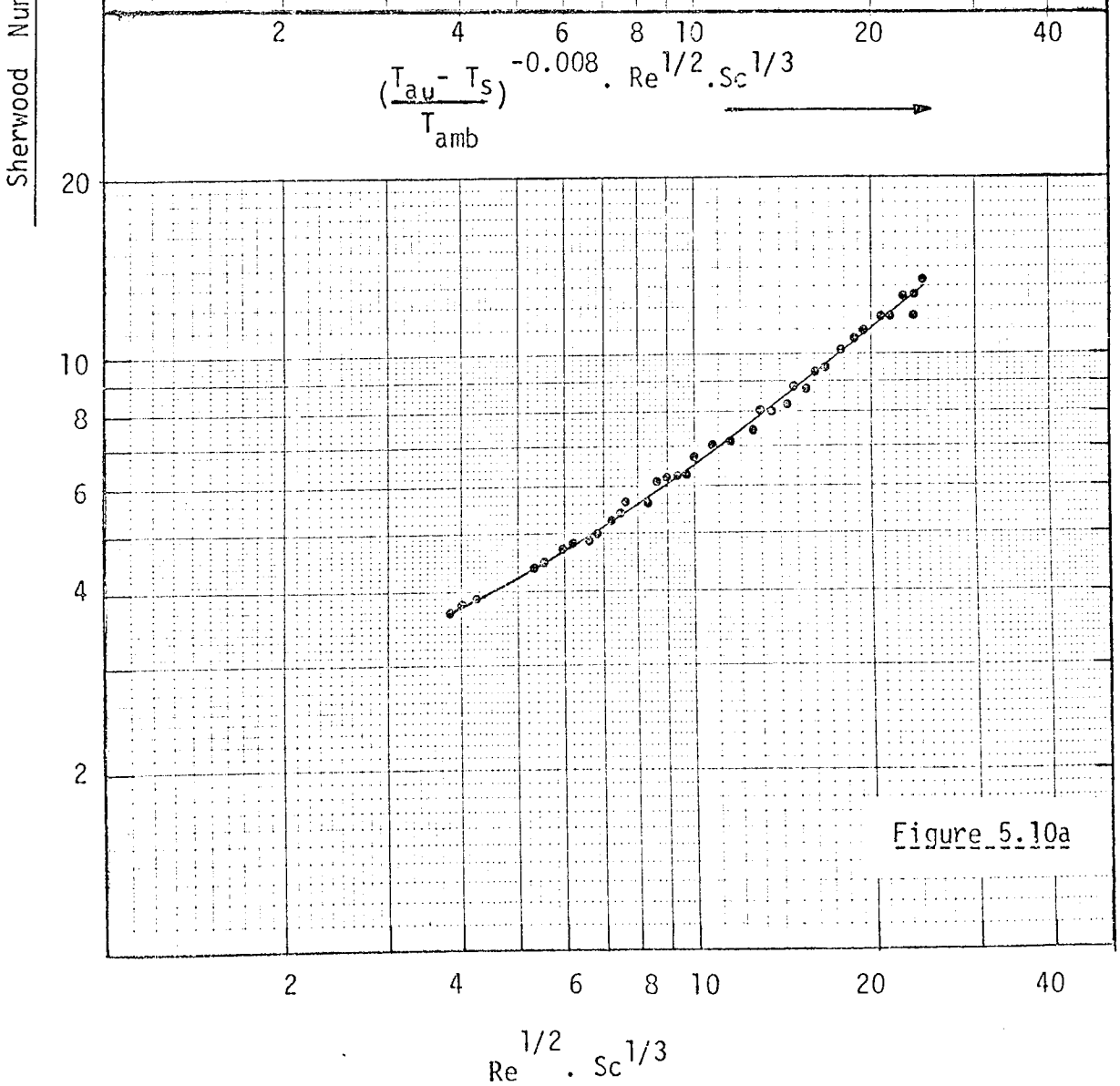

Figure 5.10a

The value of Ψ appears to vary with air temperature and within the range $0.38 \leqslant \Psi \leqslant 0.47$.

As a result of the above range of Ψ, all the data were correlated by taking the sensible heat into account. Thus the data were fitted to equation ((5.2))

$$Sh = 2.0 + \delta \left(\frac{T_{au} - T_s}{T_{amb}}\right)^{\eta} . Re^{0.5} . Sc^{0.33} \qquad ((5.2))$$

The resulting correlation was,

$$Sh = 2.0 + 0.44 \left(\frac{T_{au} - T_s}{T_{amb}}\right)^{-0.008} Re^{0.5} Sc^{0.33} \qquad ((5.3))$$

where T_{au} = air temperature (deg K)

T_s = drop temperature (deg K)

T_{amb} = ambient temperature (293.16K)

The standard deviation of the experimental points from the correlation given by equation ((5.3)) was found to be 2.3, and the coefficient of correlation was 0.998. The graph of Sherwood Number versus $((T_{au}-T_s)/T_{amb})^{-0.008} Re^{0.5} Sc^{0.33}$ is shown in figure 5.10.

5.2 Sodium Sulphate Decahydrate Drops.

The theoretical results were obtained from equations ((3.14)), for the crust thickness rate, ((3.16)) for the overall mass transfer coefficient, and ((3.24)) for the driving force for transfer. Experimental crust thicknesses were obtained from the stereoscan micrographs shown in plates 5.1 and 5.2.

PLATE 5.1

Experimental Measurement of Sodium Sulphate Crust Thickness. Stereoscan Photographs with Magnification = 550

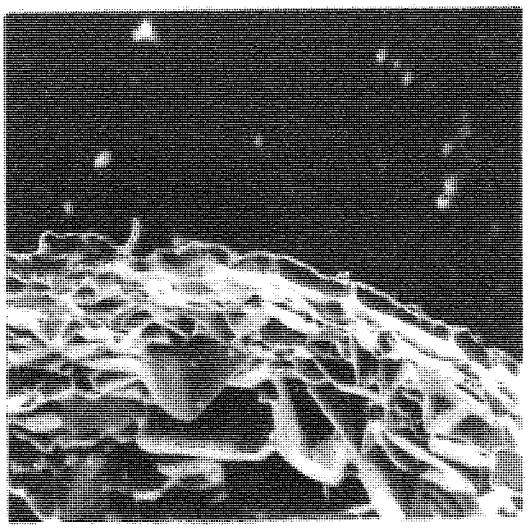

Drying Time = 300 s.

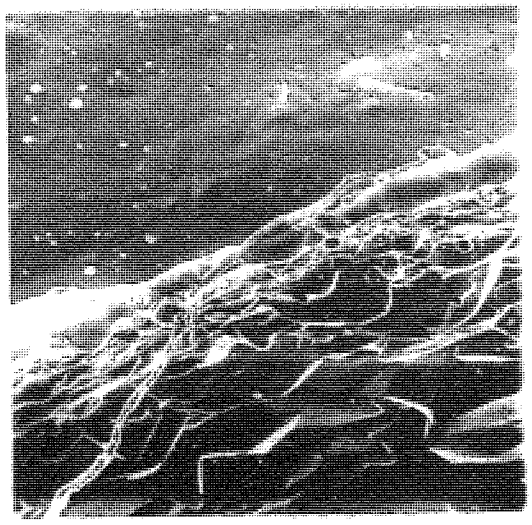

Drying Time = 600 s.

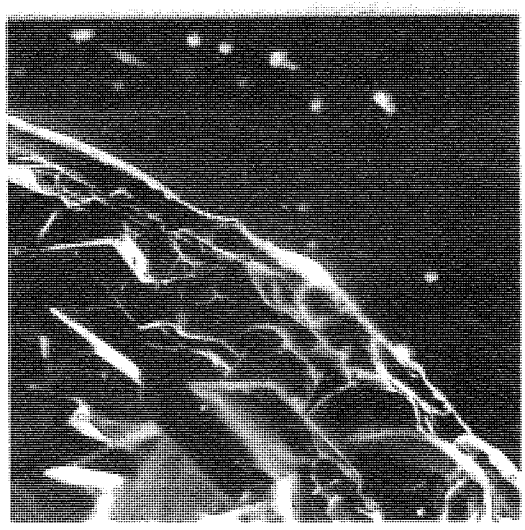

Drying Time = 900 s.

PLATE 5.2

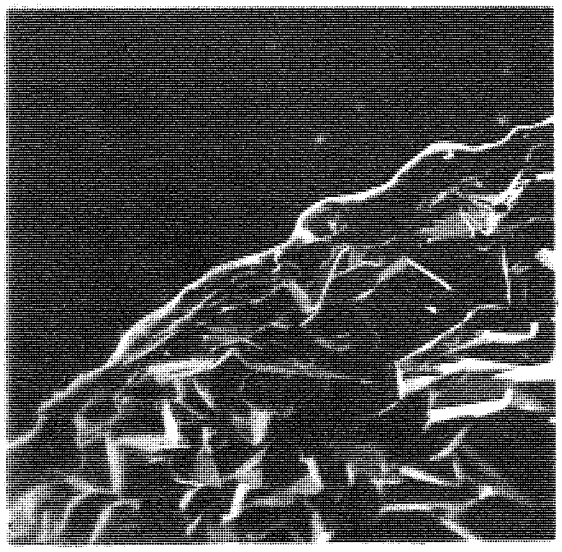

Drying Time =1200 s.

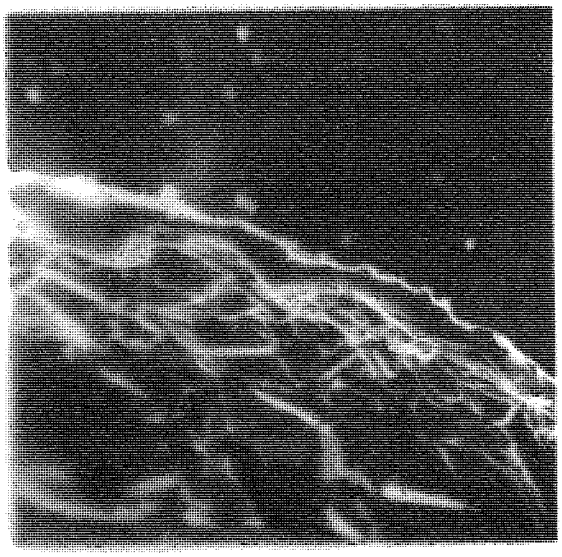

Drying Time =1500 s.

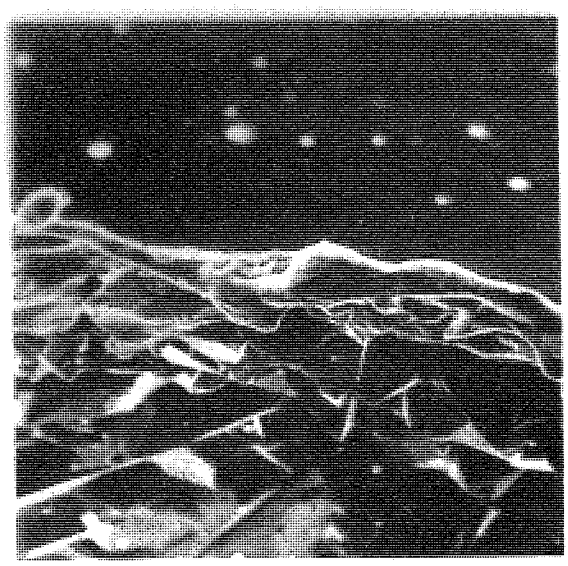

Drying Time =1800 s.

The effects of (i) air flow rate,

(ii) different initial drop radius,

(iii) air temperature, and

(iv) initial moisture content,

on the crust thickness rate, overall mass transfer coefficient, and the driving force were considered.

5.2.1 Effect of Air flow rate.

5.2.1.1 Crust Thickness Rate: Figure 5.11 indicates that the crust thickness rate increases with increase in air flow rate. This suggests that, as drying progresses, the overall mass transfer coefficient, and hence the drying rate, will be reduced as the crust becomes thicker.

5.2.1.2. Overall Mass Transfer Coefficient: As expected, the overall mass transfer coefficient decreases with increase in crust thickness. This is shown in figure 5.12. However, the overall mass transfer coefficient increases with increase in air flow rate; consequently the drying rate increases.

5.2.1.3. Driving Force: The driving force tends to increase with increase in air flow rate as shown in figure 5.13, hence the drying rate will increase.

5.2.2 Effect of Initial Drop Radius.

5.2.2.1. Crust Thickness Rate: The crust thickness rate increases with decrease in the drop radius because the crust forms over a smaller area. This effect is shown in figures 5.14, 5.15, and 5.16.

Figure 5.11

Effect of Air flow Rate , G

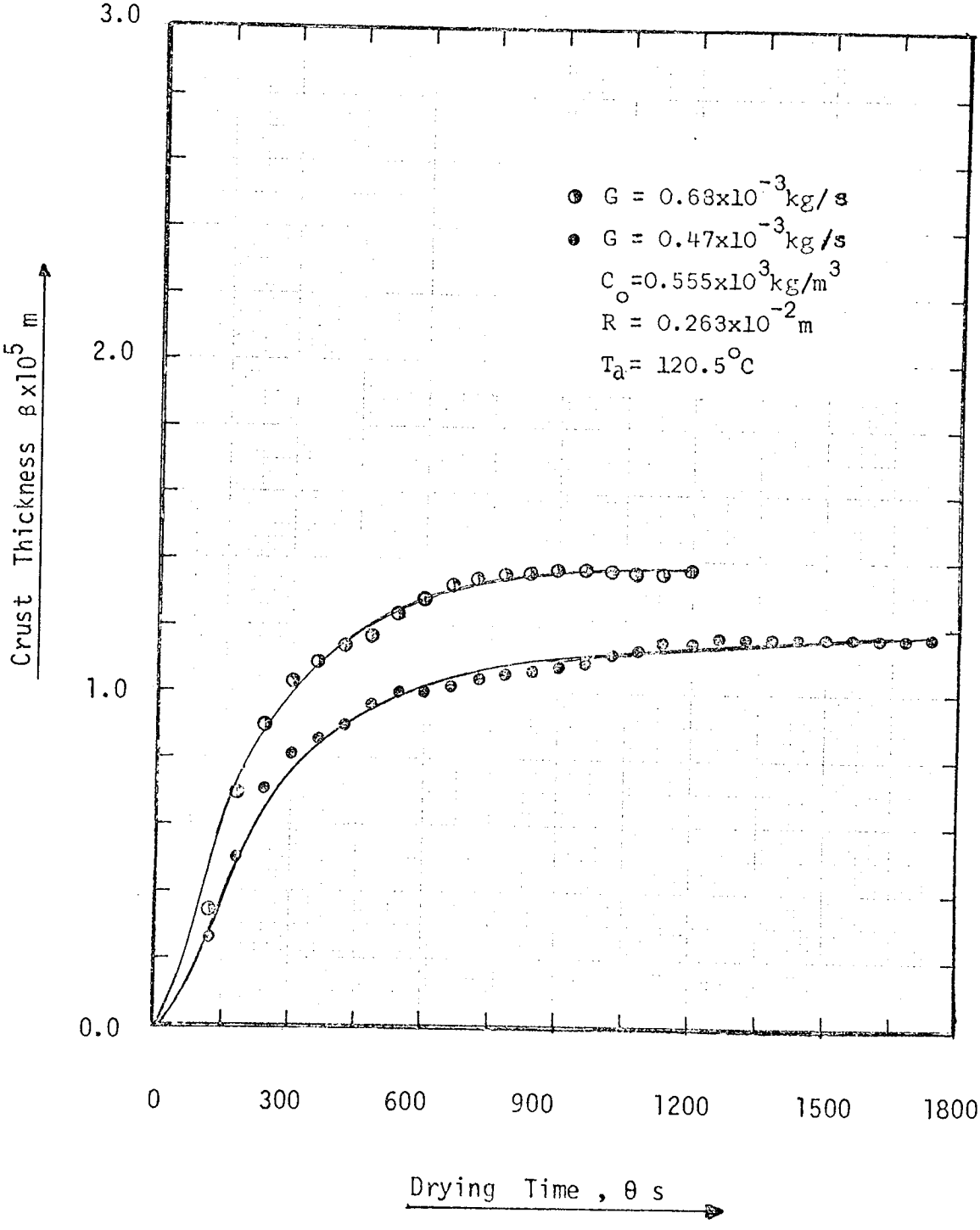

Figure 5.12

Effect of Air Flow Rate, G

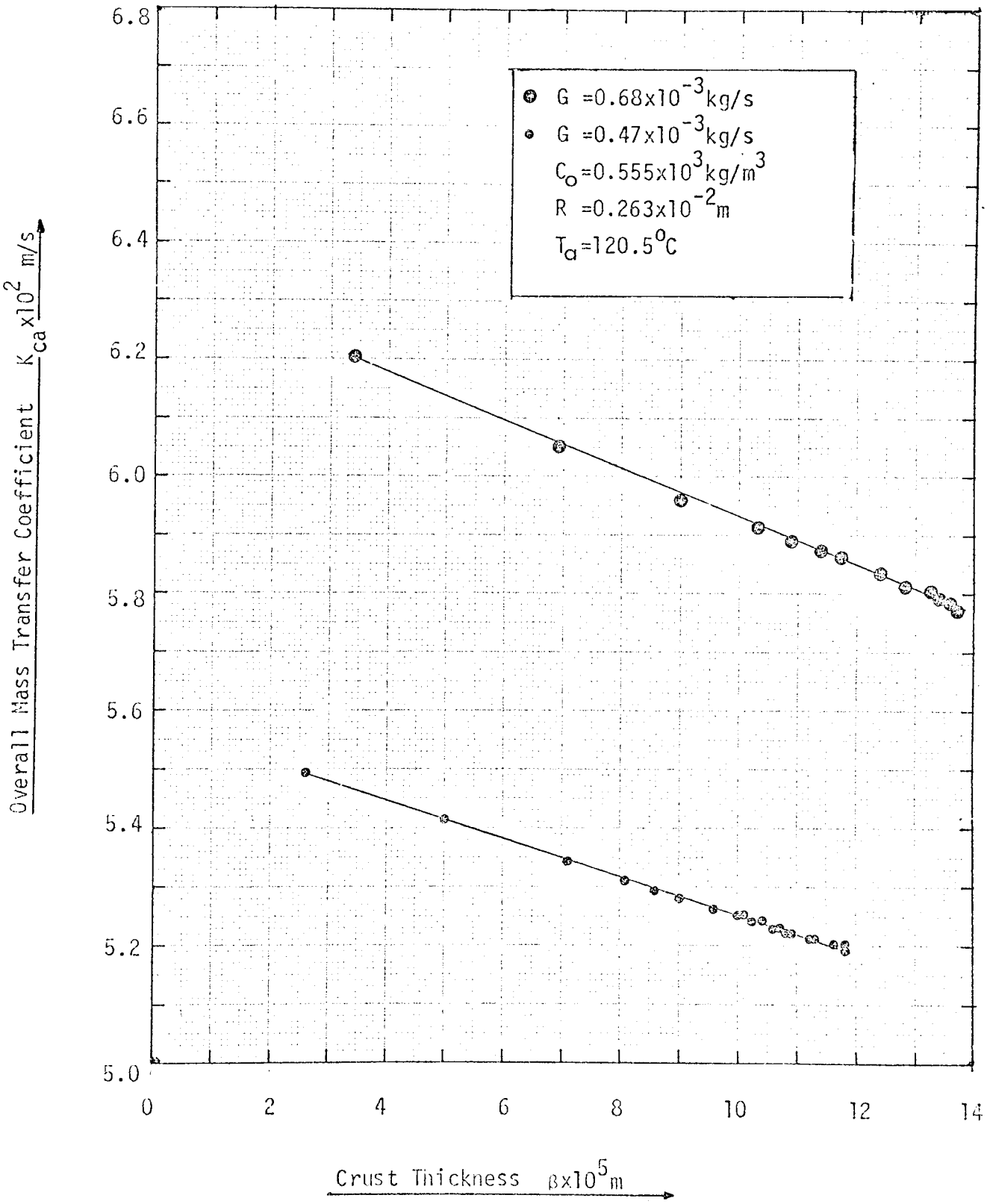

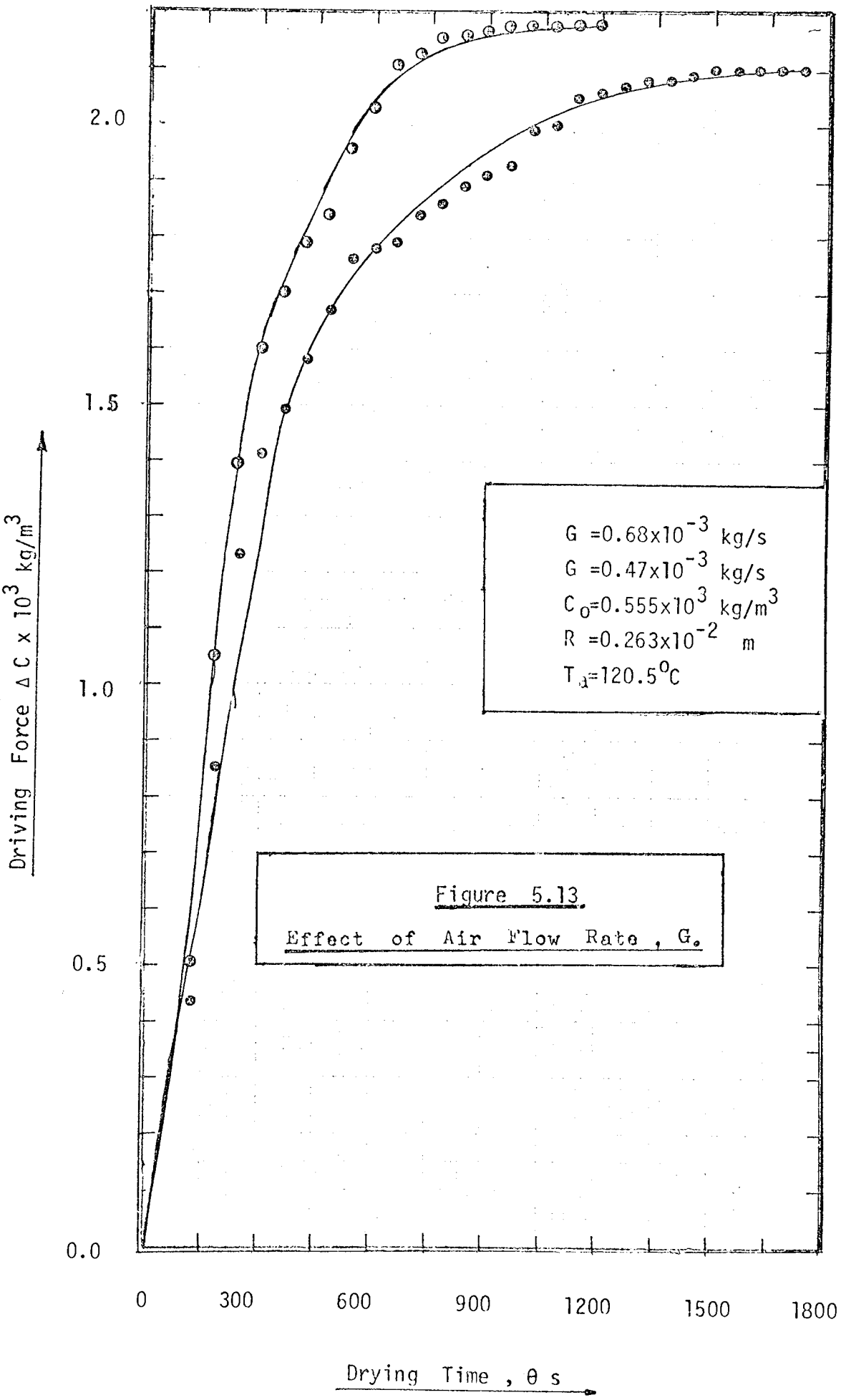

Figure 5.13

Effect of Air Flow Rate , G.

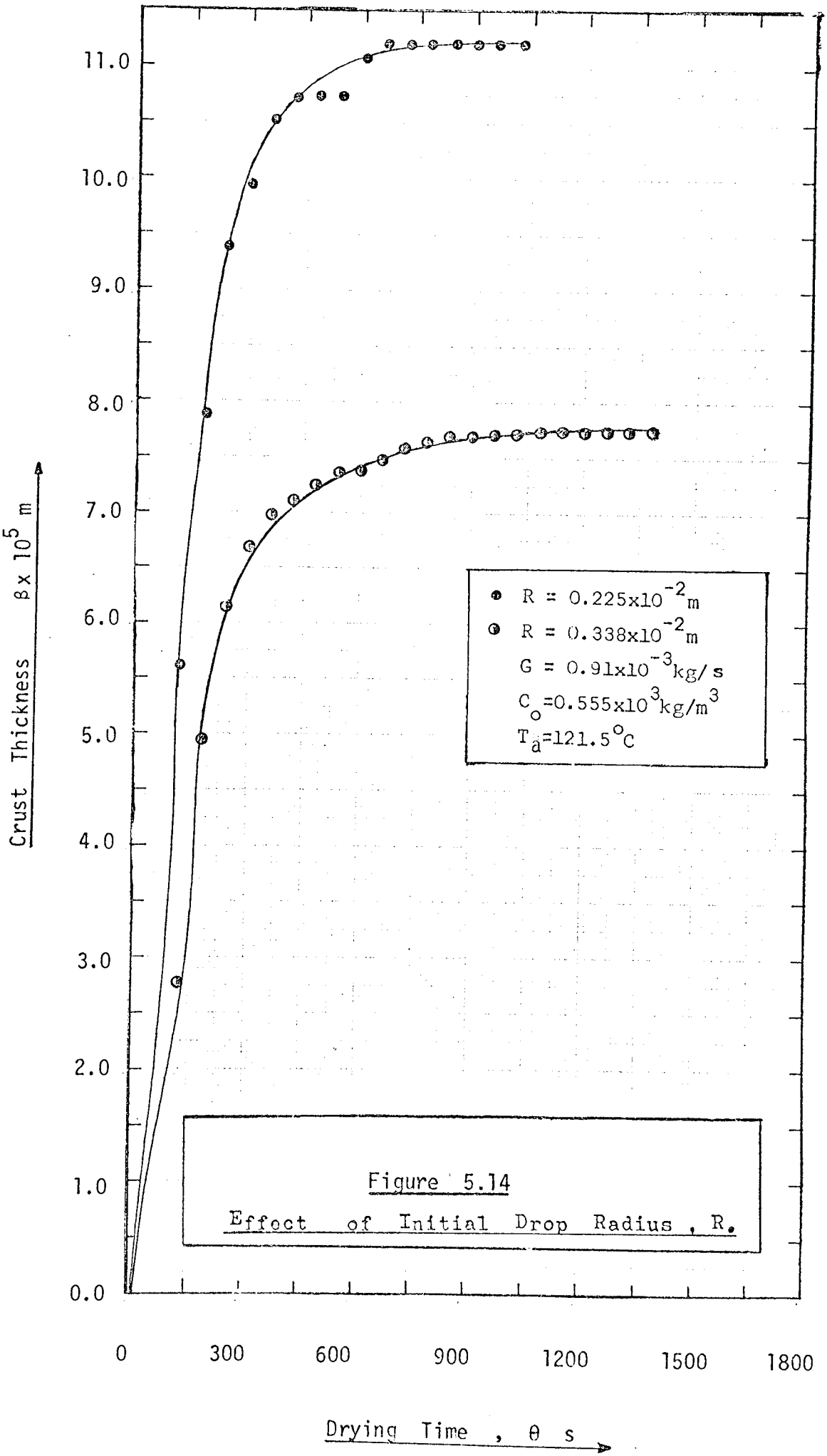

Figure 5.14

Effect of Initial Drop Radius , R.

Figure 5.15

Effect of Initial Drop Radius , R

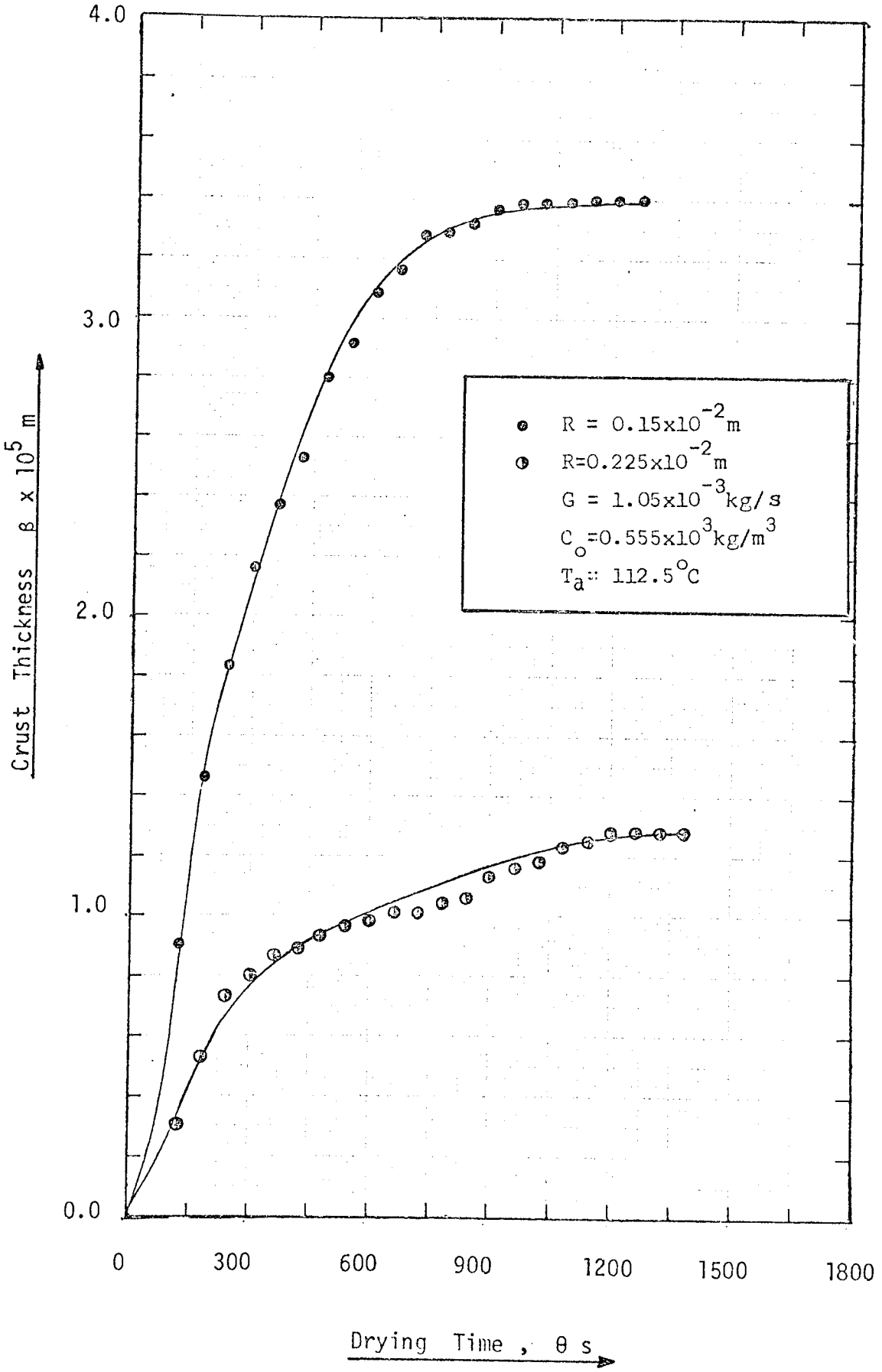

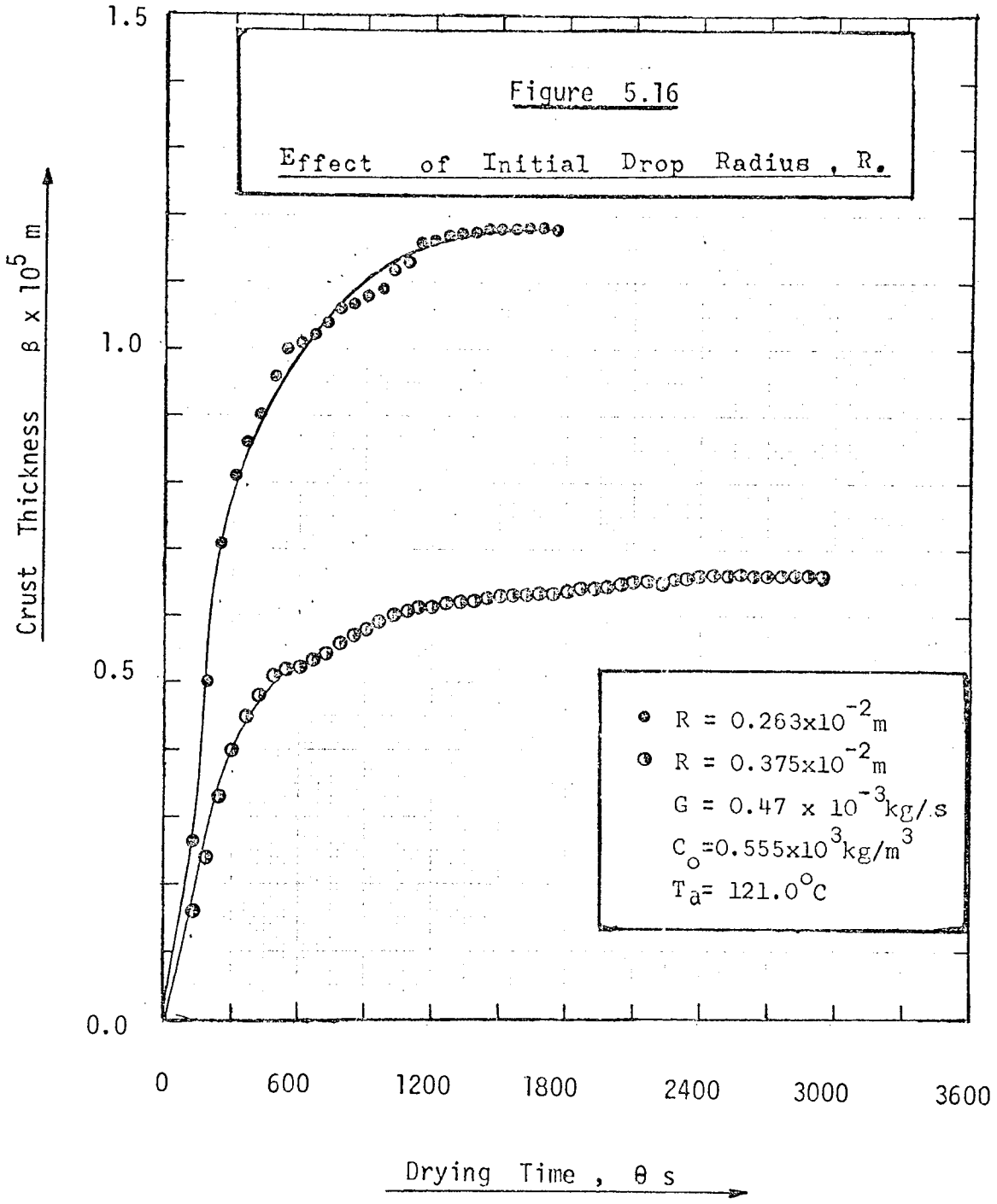
Figure 5.16
Effect of Initial Drop Radius , R.
Crust Thickness β x 10^5 m
1.5
1.0
0.5
0.0
0
600
1200
1800
2400
3000
3600
Drying Time , θ s
R = 0.263x10^-2 m
R = 0.375x10^-2 m
G = 0.47 x 10^-3 kg/.s
C_o=0.555x10^3 kg/m^3
T_a= 121.0°C

5.2.2.2 Overall Mass Transfer Coefficient: Figures 5.17 and 5.18, show conclusively that the overall mass transfer coefficient, and hence the rate of drying, increases for a decrease in the drop radius.

5.2.2.3 Driving Force: The driving force increases to about $1.09 \times 10^{-3} kg/m^3$ above the highest value of ΔC for $R = 0.225 \times 10^{-2} m$ for an increase of $0.038 \times 10^{-2} m$ in the drop radius, as shown in figure 5.19.

5.2.3. Effect of Air Temperature.

5.2.3.1 Crust Thickness Rate: It is apparent from figure 5.20 that the crust thickness rate is affected by the air temperature because a temperature difference of only $2.5^{o}C$ resulted in an increase of $0.72 \times 10^{-5} m$. in the crust thickness rate.

5.2.3.2 Overall Mass Transfer Coefficient: The mass transfer coefficient is affected to a lesser degree by the air temperature leading to a rise of about 0.03×10^{-2} m/sec for a temperature drop of $2.5^{o}C$ as shown in figure 5.21. This finding is in fair agreement with the negative power of the temperature correction factor in the correlation of pure water drops obtained in section 5.1.3.

5.2.3.3 Driving Force: Figure 5.22 indicates an increase of 2.0×10^{-3} kg/m^3 in the driving force for an increase of $2.5^{o}C$ in the air temperature.

Figure 5.17

Effect of Initial Drop Radius , R

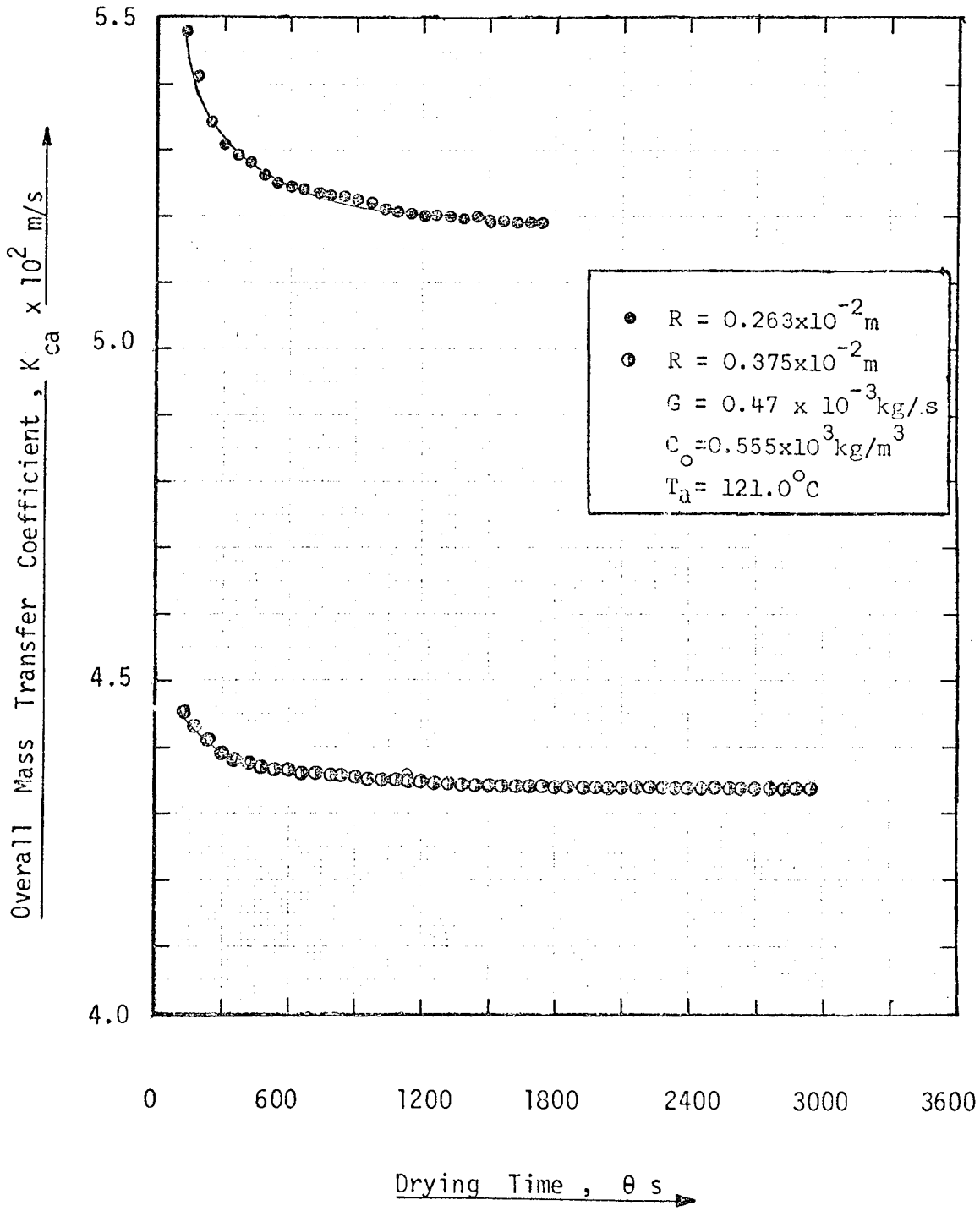

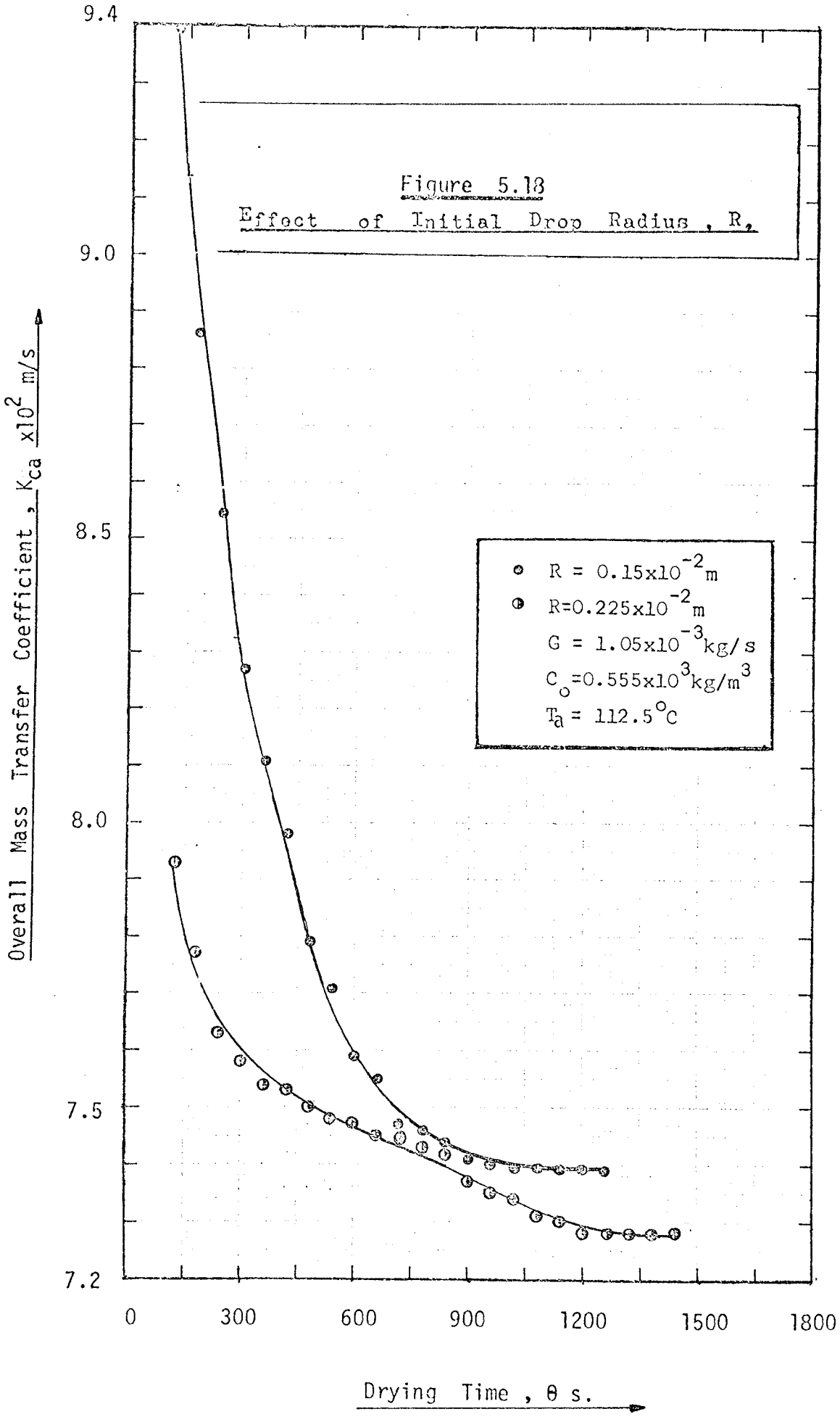
Figure 5.18
Effect of Initial Drop Radius , R,
R = 0.15x10^-2 m
R=0.225x10^-2 m
G = 1.05x10^-3 kg/s
C_o=0.555x10^3 kg/m^3
T_a = 112.5°C
Overall Mass Transfer Coefficient , K_ca x10^2 m/s
9.4
9.0
8.5
8.0
7.5
7.2
0
300
600
900
1200
1500
1800
Drying Time , θ s.

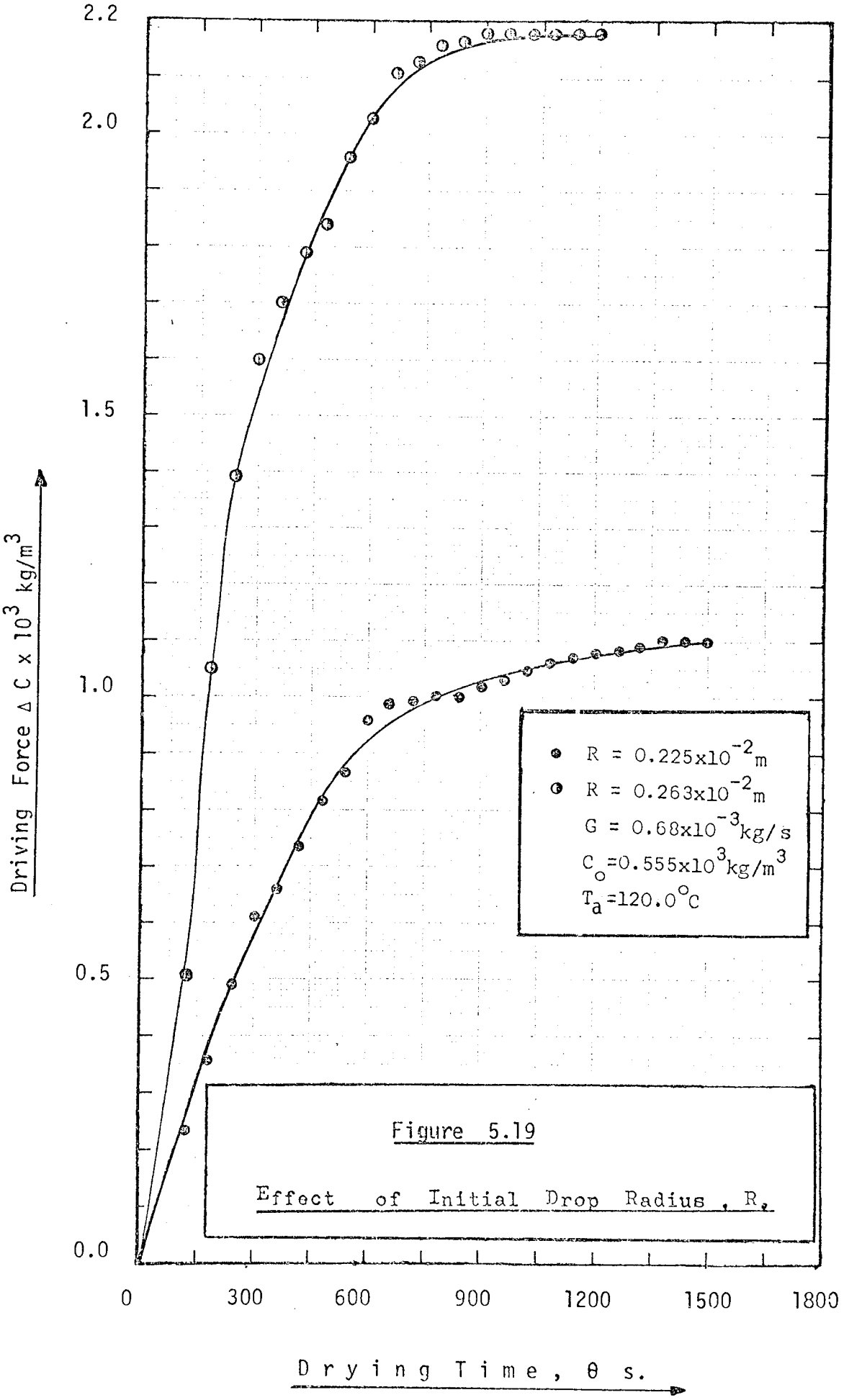

Figure 5.19

Effect of Initial Drop Radius, R.

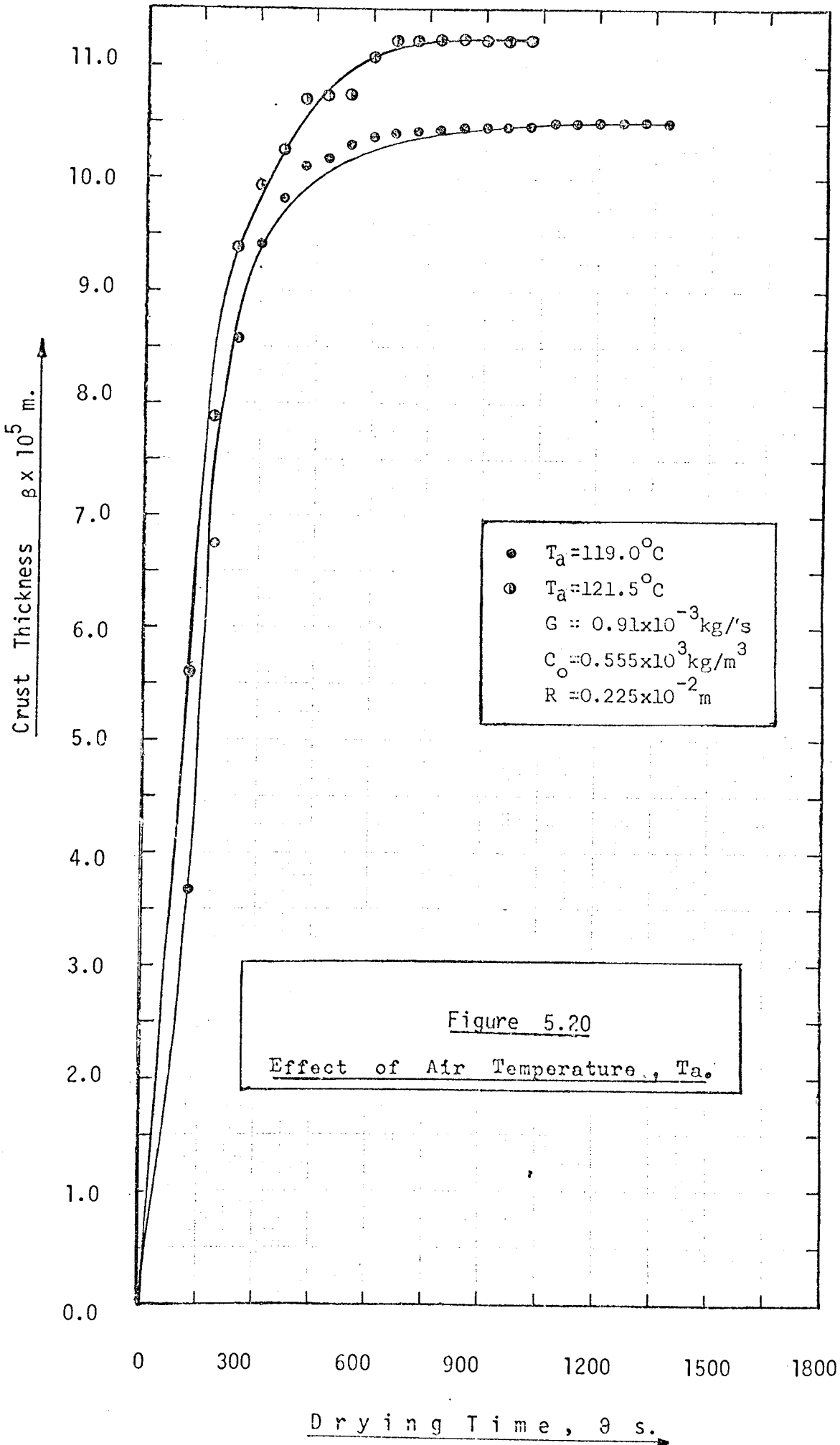

Figure 5.20

Effect of Air Temperature, Ta.

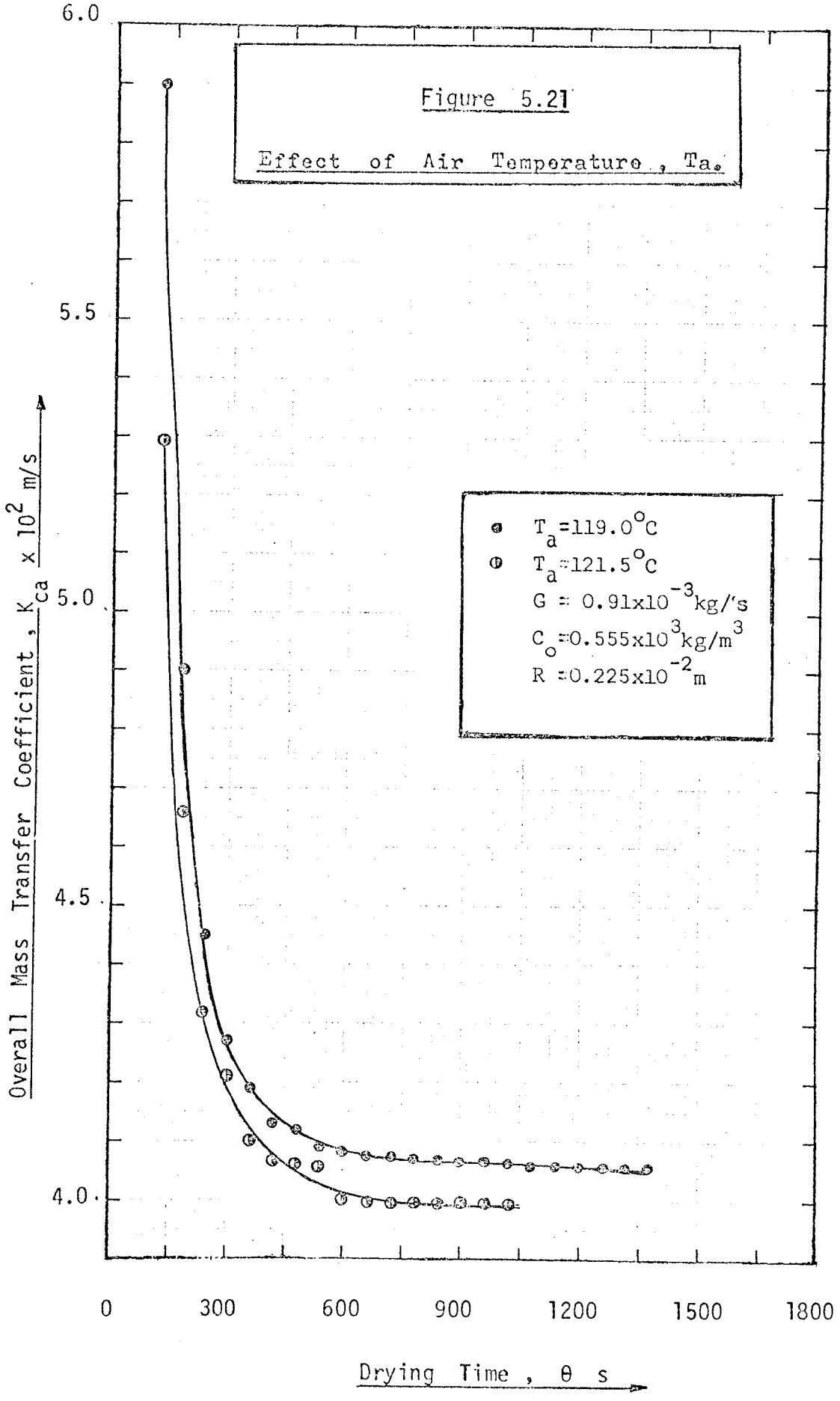
Figure 5.21
Effect of Air Temperature , Ta.
T_a=119.0°C
T_a=121.5°C
G = 0.91x10^{-3}kg/'s
C_o=0.555x10^{3}kg/m^3
R =0.225x10^{-2}m
Overall Mass Transfer Coefficient , K_{Ca} x 10^2 m/s
6.0
5.5
5.0
4.5
4.0
0
300
600
900
1200
1500
1800
Drying Time , θ s

Figure 5.22

Effect of Air Temperature , T_a

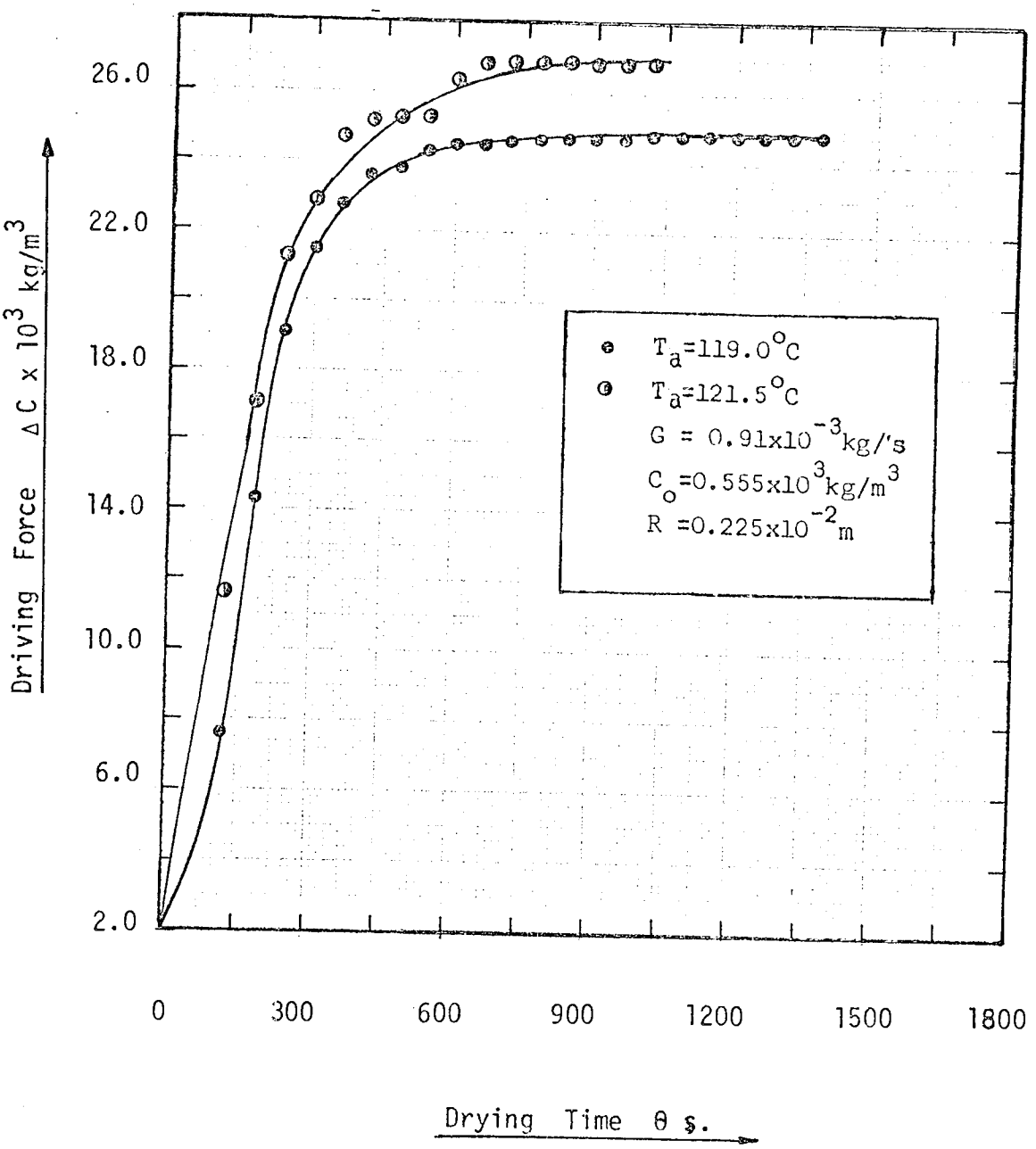

5.2.4. Effect of Initial Moisture Content.

5.2.4.1 Crust Thickness Rate: The crust thickness rate increases with increase in the initial moisture content as shown in figure 5.23.

5.2.4.2 Overall Mass Transfer Coefficient: Figure 5.24 shows that the higher the initial moisture content, the lower the overall mass transfer coefficient, hence the lower the drying rate.

5.2.4.3 Driving Force: It appears that for longer drying times, the driving force is only slightly affected by the initial moisture content - figure 5.25.

5.2.5 Comparison of Predicted with Experimental Crust Thickness.

From figure 5.26, the experimental crust thicknesses obtained from the stereoscan micrographs agree very well with thicknesses predicted from equation ((3.14)). The standard deviation of the experimental points from the prediction was found to be 0.15×10^{-5}.

5.2.6 Sodium Sulphate Micrographs.

Plates 5.1 and 5.2 are stereoscan micrographs from which the experimental crust thicknesses were evaluated.

Plates 5.3 and 5.4 show the internal and external structures of dried sodium sulphate crusts. The crusts appear to be smoother on the external than in the internal surface. This supports the findings of Charlesworth and

Figure 5.23

Effect of Initial Moisture Content , Co

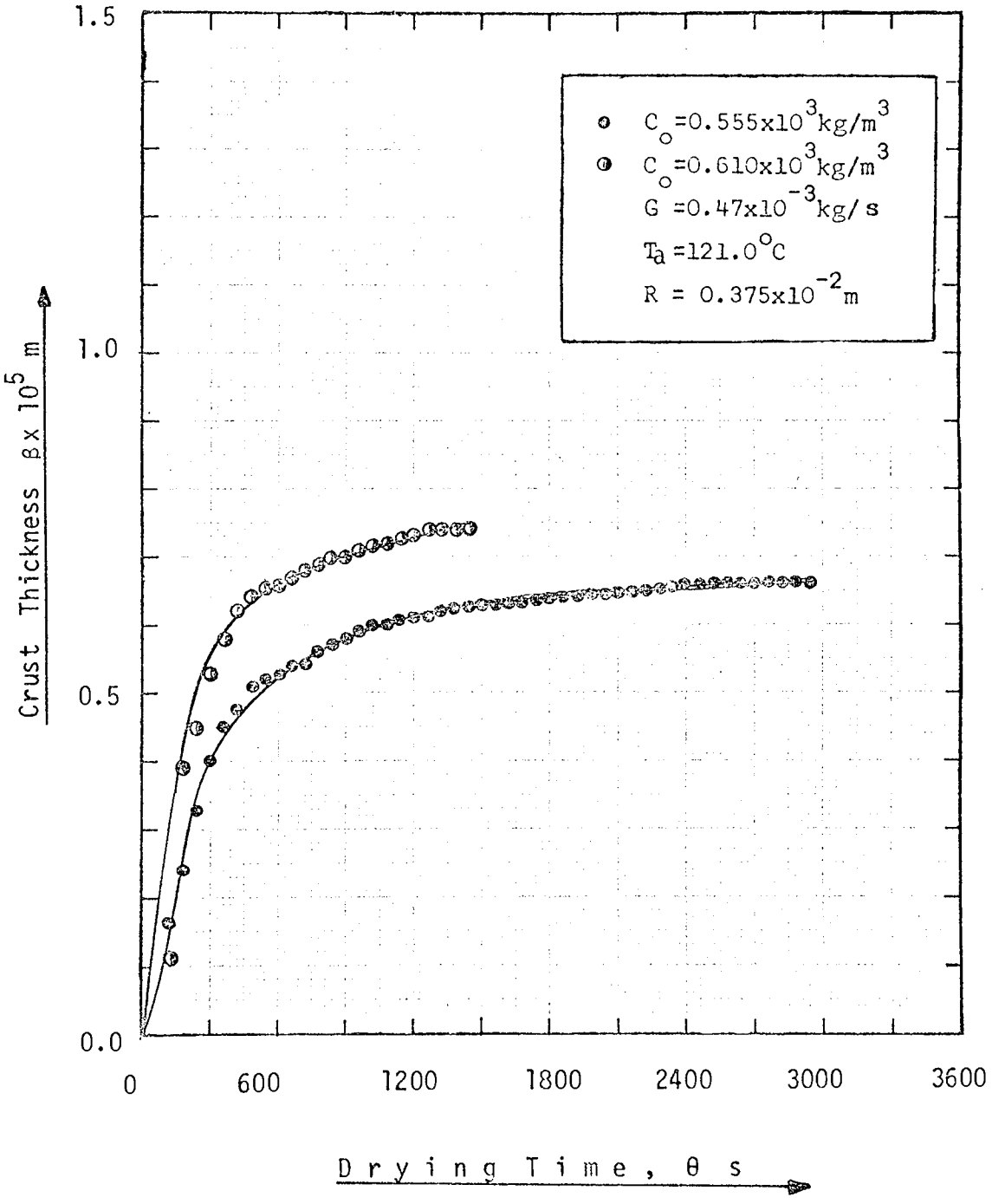

Figure 5.24

Effect of Initial Moisture Content , Co

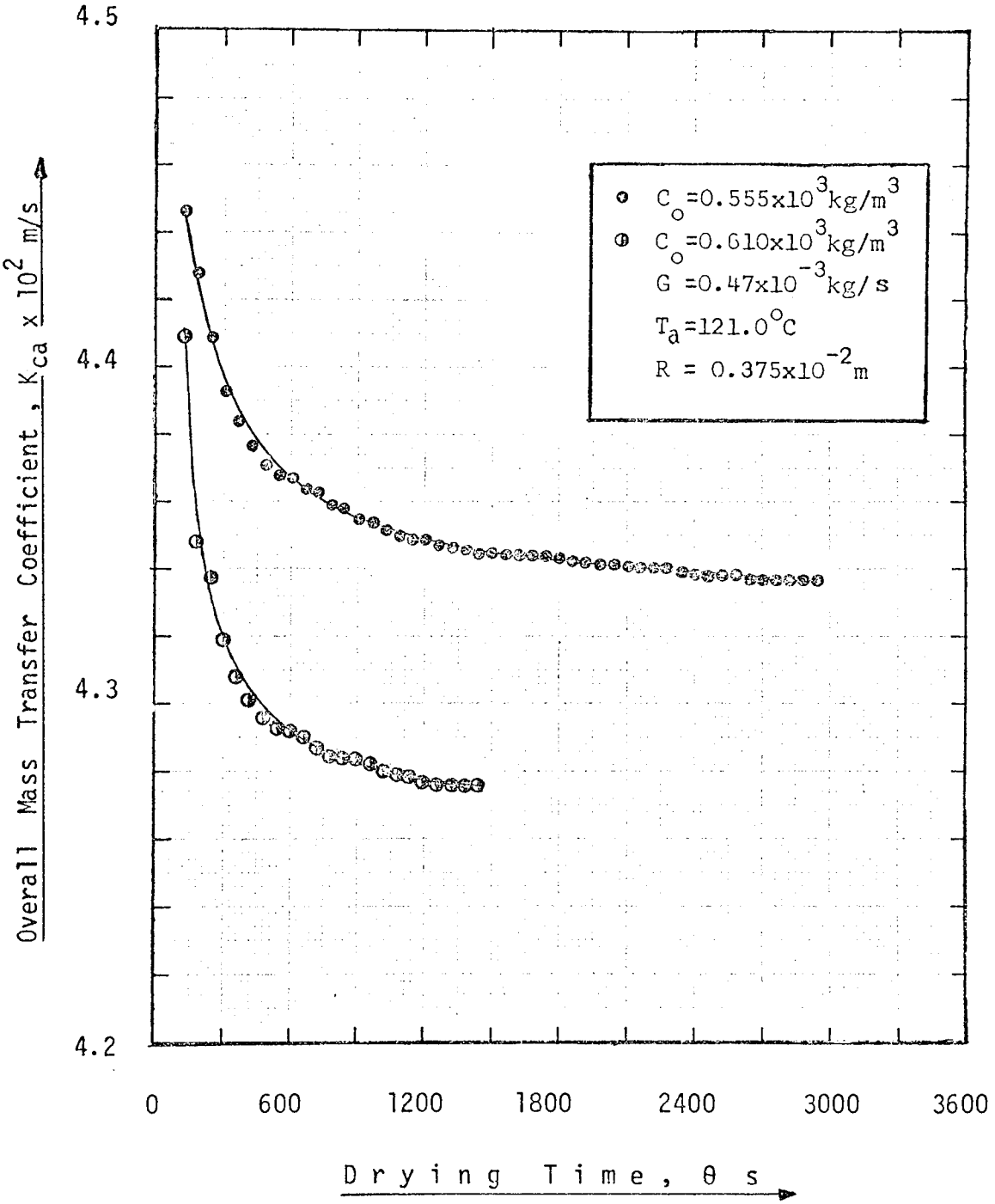

Figure 5.25

Effect of Initial Moisture Content, Co

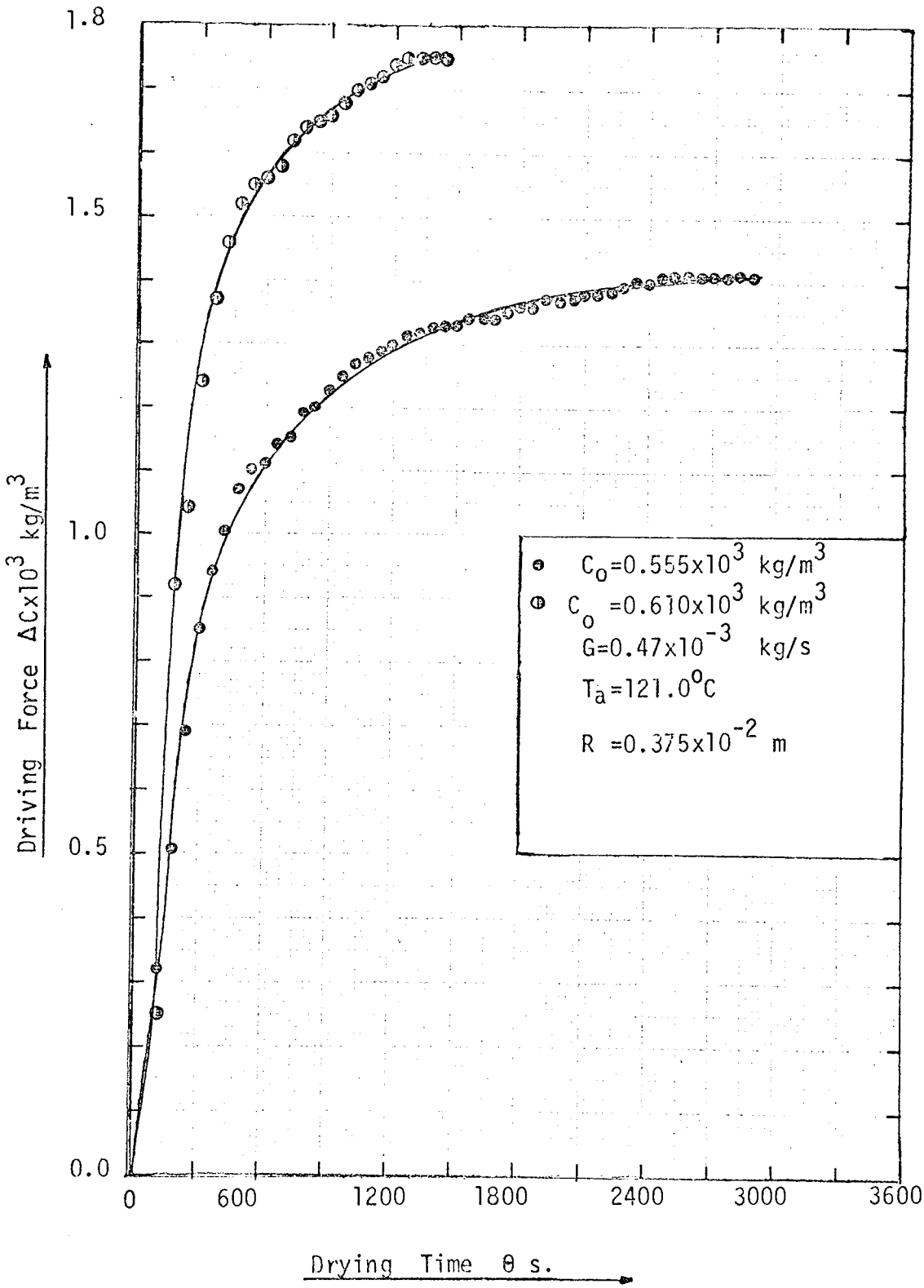

Figure 5.26

Comparison of Predicted Crust Thickness with Experimental Crust Thickness.

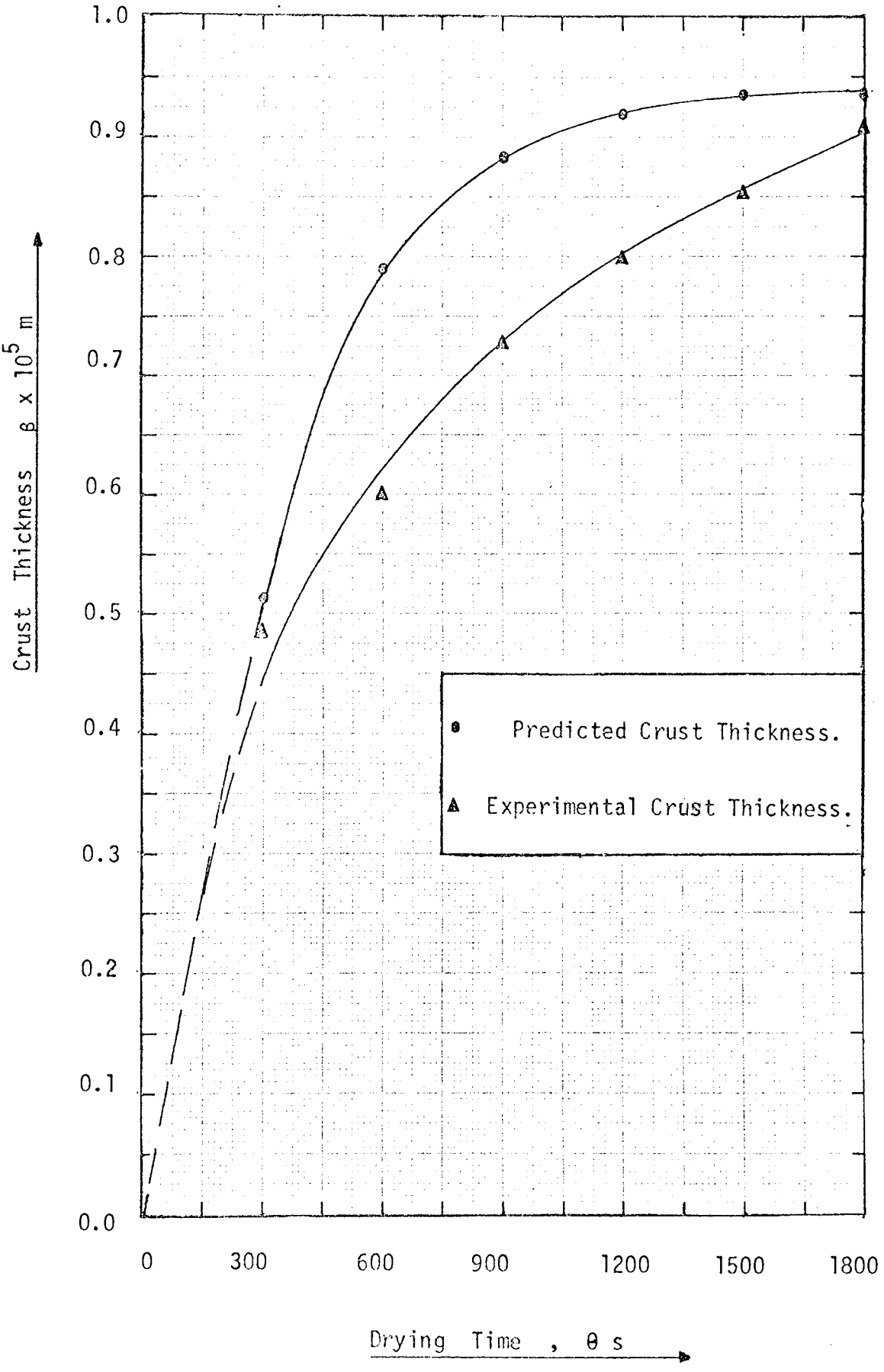

PLATE 5.3

Sodium Sulphate Crust
Magnification = 25×

Internal Structure

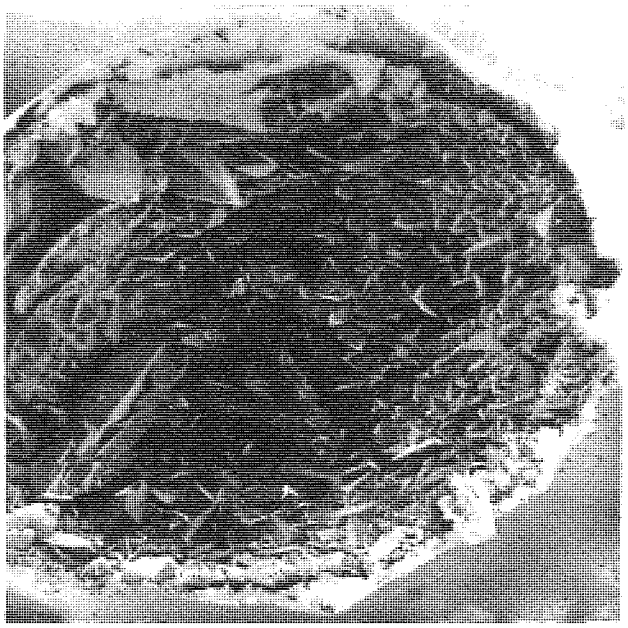

External Structure

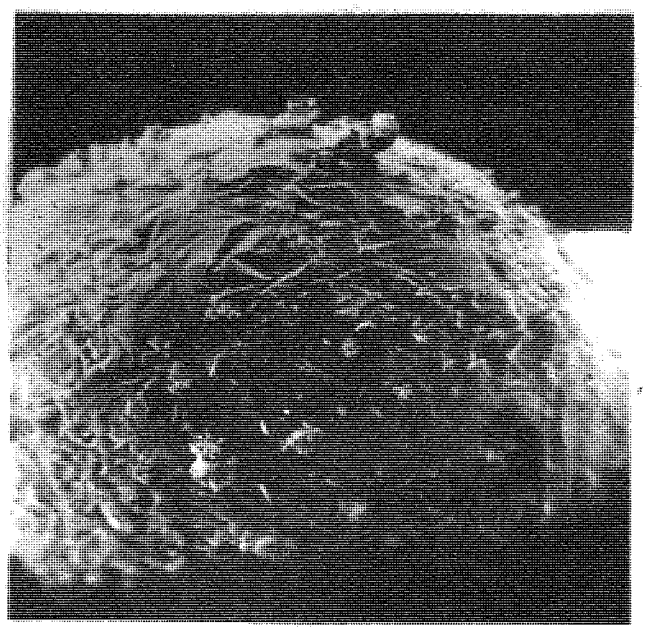

PLATE 5.4

Sodium Sulphate Crust
Magnification = 340 x

Internal Structure

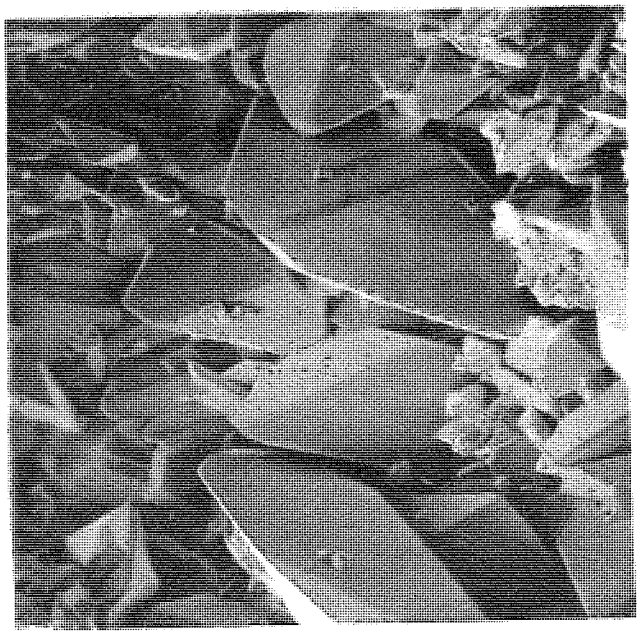

External Structure

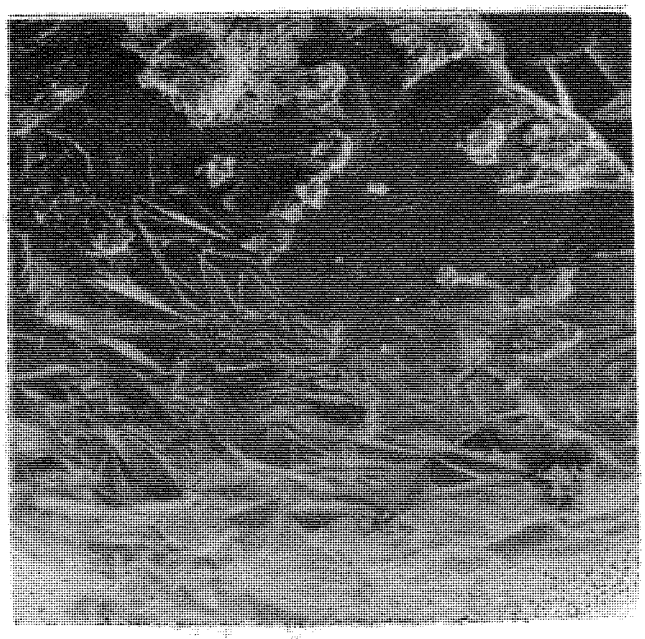

PLATE 5.5

Sodium Sulphate Crust showing Cracks and Holes

Magnification
= 25 x

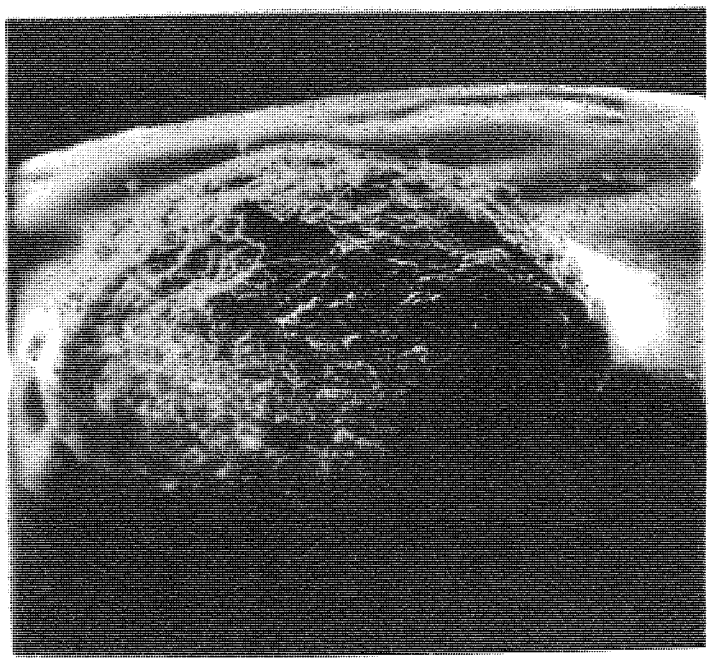

Magnification
= 220 x

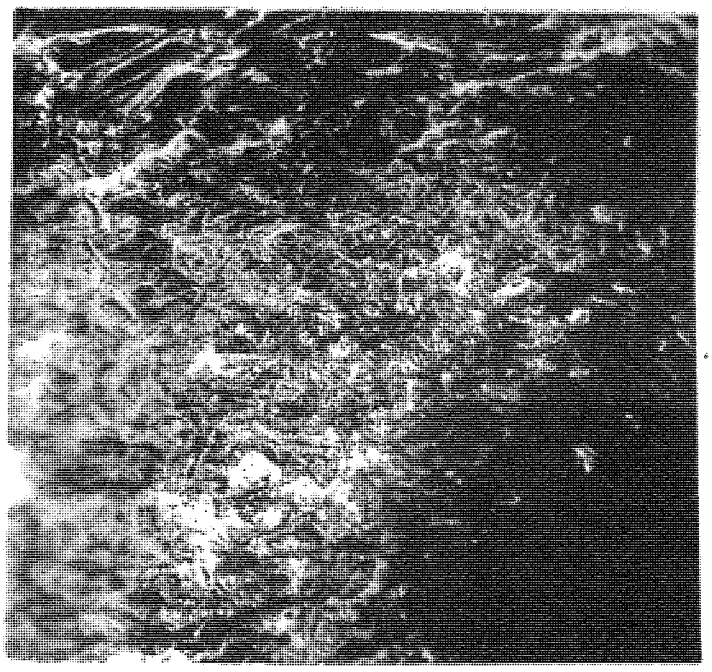

PLATE 5.6

Effect of Initial Moisture Content on Porosity of Sodium Sulphate Crust

Magnification = 6000 ×

$C_o = 0 \cdot 385 \times 10^3 kg/m^3$

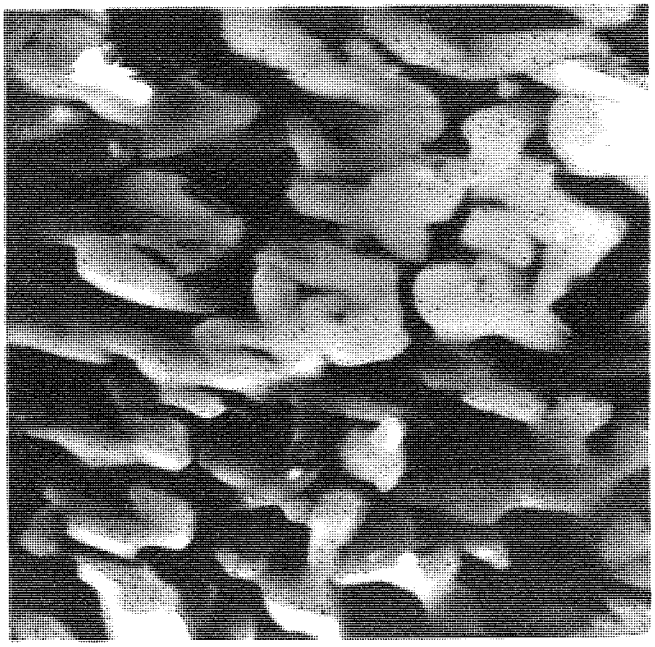

$C_o = 0 \cdot 555 \times 10^3 kg/m^3$

PLATE 5.7

Effect of Initial Moisture Content on Porosity of Sodium Sulphate Crust
Magnification = 6000 ×

$C_o = 0{\cdot}385 \times 10^3 kg/m^3$

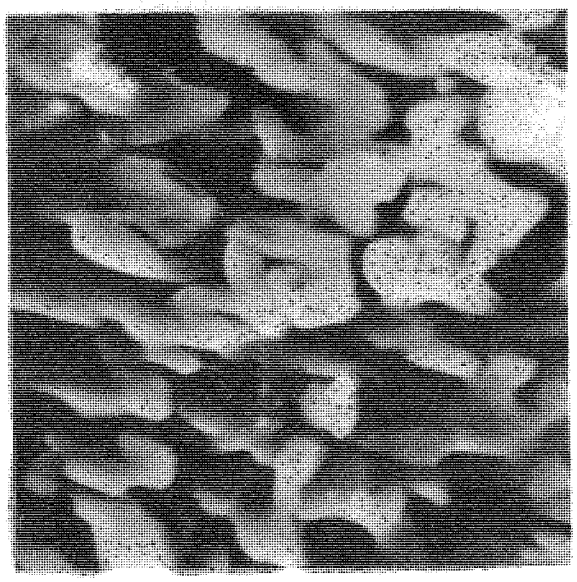

$C_o = 0{\cdot}555 \times 10^3 kg/m^3$

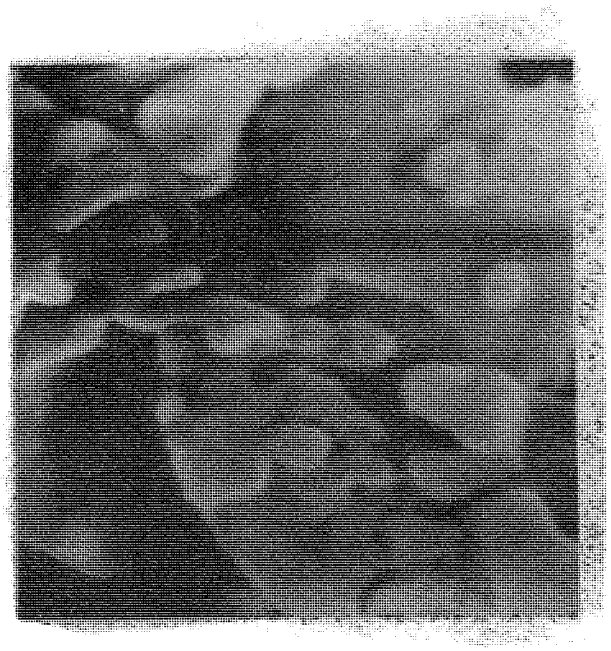

Marshall (45). The lower micrograph on plate 5.3 depicts the hemispherical symmetry of the crust. At a higher magnification, plate 5.4 reveals the crystal structure associated with sodium sulphate, and hence it can be concluded that free moisture was the only material expelled from the drop as drying progressed, and no structural degradation or transformation has occurred.

Charlesworth and Marshall (45), and Trommelen and Crosby (55) observed fracturing of the crust in their investigations with aqueous sodium sulphate drops. Plate 5.5 clearly displays this fracture. This is due (65) to the generation of steam in the centre of the drop. The crust cracks to release the internal pressure.

It was assumed that pore diffusion was a likely mechanism of moisture movement within the crust. (see Section 3.2). Plate 5.6, which also shows the effect of the initial moisture content on porosity of sodium sulphate crust, reveals the presence of the pores in the crust.

Plate 5.7 is a transparency of plate 5.6. This transparency was scanned on the Quantimet for porosity, ε.

5.3 Detergent Slurry Drops.

The rate of drying of detergent slurry drops increases with the increase in porosity, ε, and decreases with increase in crust thickness, β. As would be expected mathematically, the above is presented as:

$$N_A = f\left(\frac{\varepsilon}{\beta}\right) \qquad ((5.4))$$

The porosity, ε, was determined by application of a modified form of Kozeny's (34) equation - shown below.

$$\varepsilon = \left(\frac{5GS_b^2}{2\pi R^2} \cdot \nu \frac{\beta}{\Delta P}\right)^{0.33} \qquad ((5.5))$$

where S_b	=	specific surface area of bed	(cm^{-1})
ν	=	kinematic viscosity of fluid	(cm^2/s)
β	=	crust thickness	(cm)
G	=	air mass flow rate	(g/s)
R	=	external radius of crust	(cm)
ΔP	=	pressure drop through crust	($g.cm^{-1}.s^{-2}$)
π	=	constant	(-)
ε	=	porosity of crust	(-)

5.3.1 Determination of Specific surface area, S_b of bed.

One possibility was the use of the adsorption isotherms due to Brunauer, Emmet and Teller (66). Adsorption accounts for the existence of a higher concentration of a particular substance at the surface of a liquid or solid than is present in the bulk of the medium.

5.3.1.1. The B.E.T. Method: Branauer, Emmet and Teller (66) derived an expression, known as the B-E-T equation for calculating the surface area of the adsorbent when a single molecular layer of a gas, such as nitrogen or argon, was adsorbed by at least 10 g. of adsorbent. The B-E-T equation is given by,

$$\frac{p}{V(p_o-p)} = \frac{1}{V_m F} + \frac{F-1}{V_m F}\frac{p}{p_o} \qquad ((5.6))$$

where V = volume of gas adsorbed at the pressure p, and V_m is the volume adsorbed when the surface of the adsorbent is covered with a single layer of molecules; F is a constant, approximately equal to $\exp((E_1-E_L)/R_cT)$ where E_1 is the heat of adsorption of the first layer of molecules and E_L is the heat of condensation of the gas to liquid.

When equation ((5.6)) is plotted as $p/(V(p_o-p))$ versus p/po, the volume of gas, V_m required to form a single molecular layer on the adsorbent, can be obtained from the slope, $(F-1)/(V_mF)$, and the intercept, $1/(V_mF)$

The surface area can then be calculated from the known molecular diameter if close packing in the unimolecular layer was assumed.

However, owing to the limitation that a minimum of 10 grams of adsorbent was required,when actually the weight of the crust is 0.3 gram, the B.E.T. method could not be adopted.

5.3.1.2 The Geometric Method: The technique which was used in this investigation is explained with the aid of the diagram in figure 5.27.

Figure 5.27

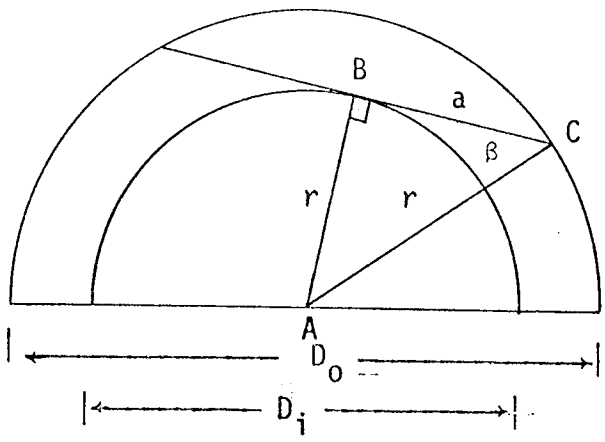

It can be shown, from the properties of triangle ABC, that

$$a^2 + r^2 = (r + \beta)^2 \qquad ((5.7))$$

which, on expanding the terms in parenthesis, becomes:

$$a^2 = \beta(2r + \beta) \qquad ((5.8))$$

but $2r = D_i = D_o - 2\beta$

$\therefore \quad a^2 = \beta(D_o - \beta)$

or $\quad a = (\beta(D_o - \beta))^{0.5} \qquad ((5.9))$

If the pores were straight the longest cylindrical pore would be equal to a, and the shortest pore is assumed equal to the thickness, β, of the crust. However, since the pores are tortuous, with a tortuosity, τ, the length of the longest pore is τa, and the shortest will be $\tau\beta$.

Hence the mean pore length, τL, becomes:

$$\tau L = \frac{\tau}{2}(\beta + (\beta(D_o - \beta))^{0.5}) \qquad ((5.10))$$

As explained in section 3.2.3.1, the tortuosity factor, takes into account the fact that pores can be of any orientation, and τ is the mean value for the crust.

The tortuosity factor is not easily obtained from first principles. However, from the predictions of Knudsen and Deryaguin (42), τ can be estimated as follows.

From the work with fine capillaries, Knudsen predicted the flux of molecules through capillaries in terms of a model which was based on the assumption that molecules, upon collision with the tube wall, were briefly adsorbed and lost their momentum. For a capillary which was very long relative to its diameter, Knudsen proposed the following expression for the diffusivity:

$$D_K = \frac{4}{3} r \sqrt{\{\frac{2}{\pi} R_c \frac{T}{M}\}} \qquad ((5.11))$$

where D_K = Knudsen diffusivity

r = capillary radius

R_c = gas constant

T = absolute temperature

M = molecular weight of the transported species.

Equation ((5.11)) is used after substituting the equivalent radius r_e of the capillary for r. On that basis, the

Knudsen diffusivity is given by,

$$D_K = \frac{8\varepsilon_p}{3S_m\rho_p} \sqrt{\left\{ \frac{2R_cT}{\pi M} \right\}} \qquad ((5.12))$$

where ε_p = porosity of a catalyst pellet

ρ_p = apparent density of a catalyst pellet, and

S_m = surface area per unit mass of catalyst.

Deryaguin (42) based his approach to Knudsen diffusion upon a model in which the porous medium was considered as completely random in nature. He considered elastic and inelastic collisions between a molecule and the wall. The results of his analysis were summerised by two equations. The first, for elastic collisions, was exactly the same expression, equation (5.12)), obtained by Knudsen, and the second, for inelastic collisions, a more realistic model of the diffusion process, is shown below:

$$D_K = \frac{24}{13} \frac{\varepsilon_p}{S_m\rho_p} \sqrt{\left\{ \frac{2R_cT}{\pi M} \right\}} \qquad ((5.13))$$

It has been shown that the equivalent diffusivity D_e can be obtained from equation (5.12)) by multiplying D_K by ε_p/τ while Deryaguin's formula, equation ((5.13)), need only be corrected for the porosity, ε_p.

Thus from equation ((5.12))

$$De = D_K \frac{\varepsilon_p}{\tau} = \frac{8\varepsilon_p^2}{3\tau S_m\rho_p} \sqrt{\left\{ \frac{2R_cT}{\pi M} \right\}} \qquad ((5.14))$$

and from equation ((5.13))

$$D_e = D_K \varepsilon_p = \frac{24\varepsilon_p^2}{13 S_m \rho_p} \sqrt{\left\{ \frac{2R_c T}{\pi M} \right\}} \qquad ((5.15))$$

Equating the two expressions, ((5.14)) and ((5.15)) gives,

$$\frac{8}{3\tau} = \frac{24}{13}$$

$$\therefore \quad \tau = 1.44 \qquad ((5.16))$$

The result compares very well with previous values of τ which have been shown (42) to be in the range $1.41 \leqslant \tau \leqslant 1.58$.

Thus the mean pore length corrected for the tortuosity becomes:

$$L' = \frac{1.44}{2} \left(\beta + (\beta(D_o - \beta))^{0.5}\right) \qquad ((5.17))$$

The specific surface area of the pores, assumed to be cylindrical, is given by,

$$S_p = \frac{\text{Total surface of pores}}{\text{Volume of the hemispherical crust}}$$

$$= \frac{N_p \times 2\pi R_p L'}{\frac{\pi}{12}\left(D_o^3 - (D_o - 2\beta)^3\right)}$$

$$= \frac{24 N_p R_p L'}{D_o^3 - (D_o - 2\beta)^3} \qquad ((5.18))$$

where N_p = total number of pores

R_p = radius of pores

N_p and R_p were estimated from stereoscan micrographs, plates 5.8 - 5.16.

If the crust is considered as a solid mass with no pores present, the specific surface area of the crust, S_c is given by,

$$S_c = \frac{\frac{\pi D_o^2}{2}}{\frac{\pi}{12}(D_o^3 - (D_o - 2\beta)^3)}$$

or

$$Sc = \frac{6\ D_o^2}{D_o^3 - (D_o - 2\beta)^3}$$

The specific surface area of the bed of particles constituting the crust is obtained from the sum of equations ((5.18)), for S_p, and ((5.19)), for S_c. That is,

$$S_b = S_p + S_c$$

$$= \frac{24N_pR_pL'}{D_o^3 - (D_o - 2\beta)^3} + \frac{6Do^2}{D_o^3 - (D_o - 2\beta)^3}$$

$$S_b = \frac{24N_pR_pL' + 6Do^2}{D_o^3 - (D_o - 2\beta)^3} \qquad ((5.20))$$

The porosity was then calculated from equation ((5.5)) after substituting values for S_b, ν , β , R and ΔP.

5.3.2 Analysis of Mass Transfer Characteristics.

The mass transferred per unit area, W_c, and the drying rate were computed and listed in Tables 5.6 and 5.7. Figures 5.28a and 5.28b are presented together in figure 5.28, to facilitate the comparison of the drying characteristics of formulations used. Table 5.8, for { ε/β } values, and figure 5.28 are inside the pocket at the rear cover of this thesis.

As was stated earlier on, the rate of drying is proportional to the ratio, { ε/β }. Thus the higher this ratio, the higher the rate of drying.

5.3.2.1 Trends of curves for the Nine Detergent Formulations:

On the basis of the {ε/β} ratio, the order of drying, from the best to the worst should be :

(i)	Formulation	I
(ii)	Formulation	H
(iii)	Formulation	G
(iv)	Formulation	A
(v)	Formulation	D
(vi)	Formulation	B
(vii)	Formulation	F
(viii)	Formulation	C
(ix)	Formulation	E

TABLE 5.6

Mass Transferred, $W_c \times 10^2$ g/cm^2

Drying Time θs. \ Formulation	A	B	C	D	E	F	G	H	I
300	1.45	1.49	1.35	1.59	1.22	1.67	2.17	2.34	2.69
600	2.23	2.15	1.89	2.36	1.70	2.34	3.09	3.64	4.09
900	2.94	2.60	2.19	2.92	1.98	2.71	3.64	4.47	5.34
1200	3.42	3.13	2.42	3.38	2.30	3.04	4.01	4.99	6.14
1500	3.92	3.39	2.65	3.78	2.57	3.34	4.38	5.23	6.85
1800	4.40	3.62	2.85	4.09	2.76	3.62	4.71	5.36	7.34
2100	4.80	4.00	3.04	4.33	2.94	3.83	4.94	5.41	7.59
2400	5.13	4.13	3.21	4.63	3.11	4.06	5.14	5.51	7.73
2700	5.44	4.35	3.31	4.85	3.29	4.24	5.36	5.59	7.85
3000	5.68	4.57	3.43	5.03	3.45	4.47	5.54	5.63	7.90
3300	5.86	4.79	3.50	5.18	3.56	4.67	5.71	5.67	7.97
3600	6.08	4.93	3.60	5.35	3.70	4.85	5.87	5.70	7.99
3900	6.26	5.08	3.71	5.47	3.84	5.08	6.05	5.73	8.03
4200	6.34	5.22	3.77	5.58	3.95	5.23	6.18	5.74	8.06
4500	6.36	5.39	3.80	5.69	4.08	5.35	6.31	5.75	8.10
4800	6.38	5.53	3.82	5.82	4.19	5.52	6.42	5.75	8.12
5100	6.41	5.63	3.84	5.90	4.33	5.68	6.53	5.76	8.13
5400	6.42	5.86	3.85	5.94	4.43	5.82	6.67	5.76	8.14
5700	6.42	5.97	3.86	6.05	4.57	5.97	6.80	5.76	8.15

TABLE 5.7

Drying Rate $N_A \times 10^5$ g/cm^2 s

Formulation / Drying Time θs	A	B	C	D	E	F	G	H	I
300	4.83	4.96	4.49	5.32	4.08	5.57	7.23	7.80	8.95
600	3.72	3.58	3.16	3.94	2.83	3.90	5.14	6.07	6.82
900	3.26	2.89	2.44	3.25	2.20	3.01	4.05	4.96	5.93
1200	2.85	2.61	2.02	2.82	1.92	2.53	3.34	4.16	5.11
1500	2.62	2.26	1.77	2.52	1.72	2.22	2.92	3.49	4.57
1800	2.44	2.01	1.59	2.27	1.53	2.01	2.62	2.98	4.08
2100	2.28	1.91	1.45	2.06	1.40	1.82	2.35	2.58	3.61
2400	2.14	1.72	1.34	1.93	1.30	1.69	2.14	2.29	3.22
2700	2.01	1.61	1.23	1.79	1.22	1.57	1.99	2.07	2.91
3000	1.89	1.52	1.14	1.68	1.15	1.49	1.85	1.88	2.63
3300	1.78	1.45	1.06	1.57	1.08	1.42	1.73	1.72	2.41
3600	1.69	1.37	1.00	1.49	1.03	1.35	1.63	1.58	2.22
3900	1.61	1.30	0.95	1.40	0.99	1.30	1.55	1.47	2.06
4200	1.51	1.24	0.90	1.33	0.94	1.24	1.47	1.37	1.92
4500	1.41	1.20	0.84	1.26	0.91	1.19	1.40	1.28	1.80
4800	1.33	1.15	0.80	1.21	0.87	1.15	1.34	1.20	1.69
5100	1.26	1.10	0.75	1.16	0.85	1.11	1.28	1.13	1.59
5400	1.19	1.08	0.71	1.10	0.82	1.08	1.23	1.07	1.51
5700	1.13	1.05	0.68	1.06	0.80	1.05	1.19	1.01	1.43

The trend is, in fact, obeyed. The controlled sudser, I, has the highest rate of evaporation, and formulation E evaporates least. Although, upto a drying time of about 3000 seconds, formulation C has a higher rate of drying than formulation E, and appears to dry to a lower final moisture content, formulation E dries least because it continues to dry.

5.3.2.2 Effect of Additives on Drying Rate.

i) Formulations A and B; E and F : From the { ε/β } criterion, A dries better than B. Consequently it appears that the addition of sodium carboxy methyl cellulose, SCMC, reduces the drying rate. On the same basis, however, the addition of SCMC improves the drying rate in favour of formulation F compared with E. As expected, B and F behave similarly although A and E are farther apart than can be deduced from the {ε/β} ratios alone.

ii) Formulations B and C; F and G : The addition of sodium toluene sulphonate, STS, appears to inhibit the drying rate of C, compared with B. However it appears that the addition of STS improves the drying rate of G, compared with F. Thus it seems that the addition of STS cannot be treated in isolation from the other additives.

iii) Formulations C and D: The {ε/β} ratio for D is higher than that of C and thus it appears that coconut ethanol amide, CEA, improves drying.

(iv) Formulations H and I: These are complete detergent powder formulations, known as High Non Ionic and Controlled Sudser respectively. In formulation H, where the active detergent has not been added, and the concentration of sodium sulphate is very low, the rate of drying has reduced considerably, compared with I.

5.3.3 Detergent Micrographs.

An observation of the structure of the crusts presented in plates 5.8 - 5.16, suggests that unlike sodium sulphate crusts, these are micro-porous. The crusts punctured at several points on the surface revealing the hollow inside, and thus suggesting that detergent crusts are rather plastic in nature. They are rougher at the external surface than was the situation with sodium sulphate crusts, the roughness tending to increase from formulation A to I.

5.3.4 Correlation of Mass Transfer Coefficients.

Garner and Keey (67) showed that, at Reynolds numbers greater than 250, mass transfer coefficients could be correlated by equation ((5.21)):

$$Sh = gRe^{x}.\ Sc^{y} \qquad ((5.21))$$

where g, x and y are constants, evaluated by least-squares

curve-fitting technique. The computational algorithm for equation ((5.21)) has been developed in Appendix C.3.

The correlation was found to be,

$$\left(\frac{K_m \beta_m}{D_M \varepsilon^{1.5}}\right) = 0.58 \left(\frac{\rho u d_p}{\mu}\right)^{0.047} \left(\frac{\mu}{\rho D_M \varepsilon^{1.5}}\right)^{0.058} \qquad ((5.22))$$

Equation ((5.22)) has a standard deviation of 0.036 with a correlation coefficient of 0.958, indicating a good fit. The correlation is represented in figure 5.29; and the Re values are tabulated in Table 5.9.

Plate 5.8 Formulation A

Magnification = 24x

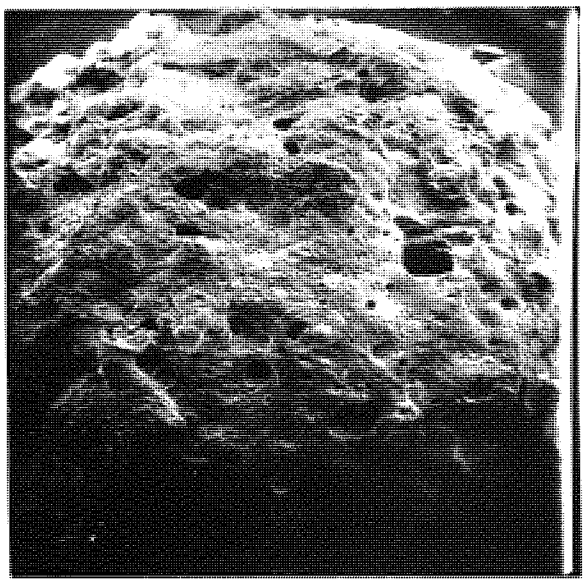

Magnification = 240x

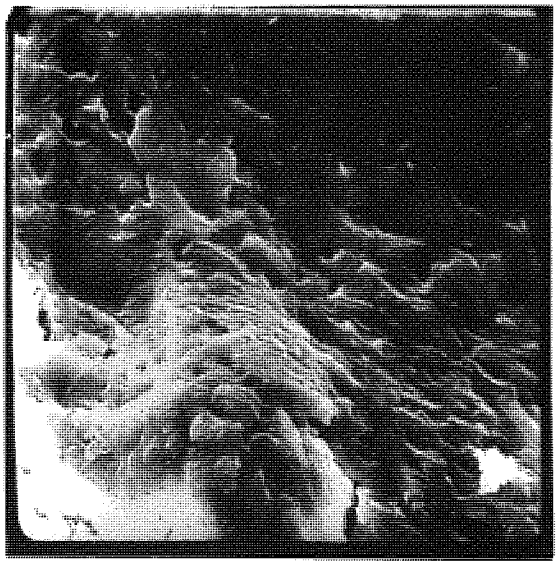

Plate 5.9 Formulation B

Magnification = 34x

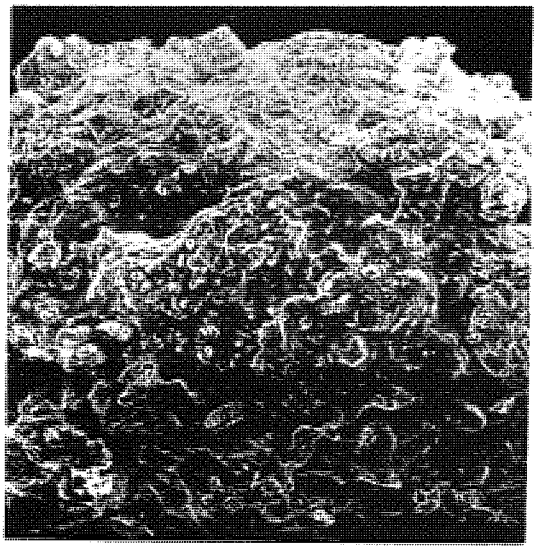

Magnification = 230x

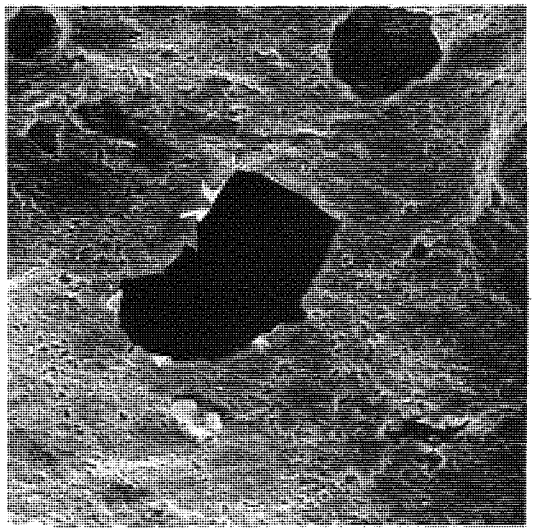

Magnification = 580x

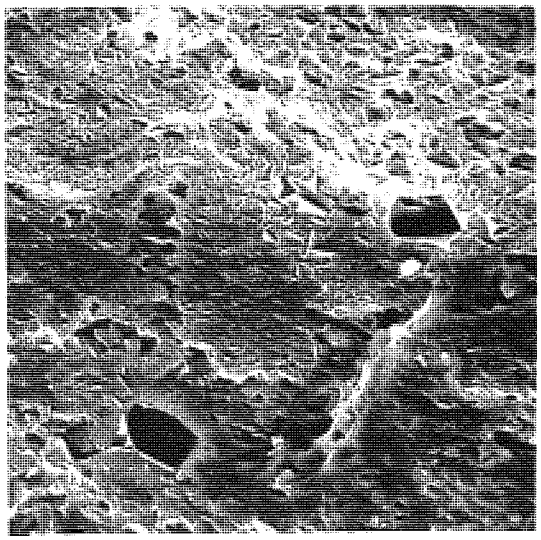

Plate 5.10 Formulation C

Magnification = 24x

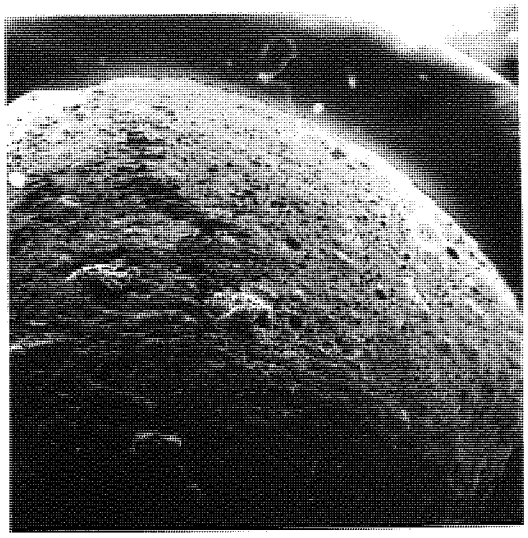

Magnification = 240x

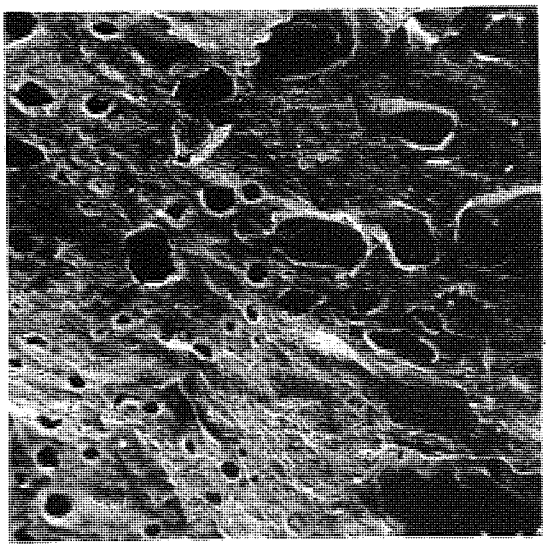

Magnification = 6000x

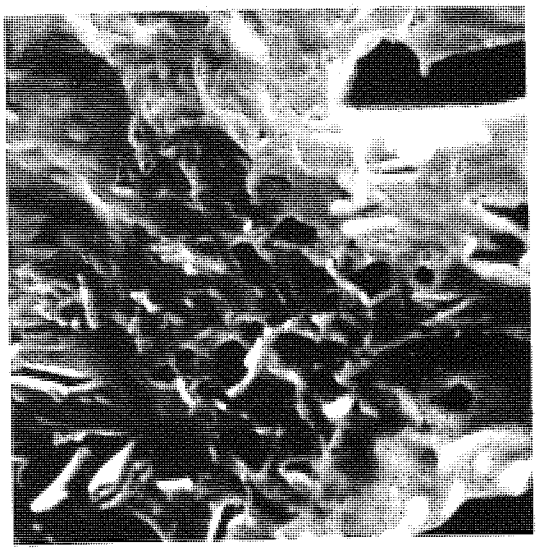

Plate 5.11 Formulation D

Magnification = 24x

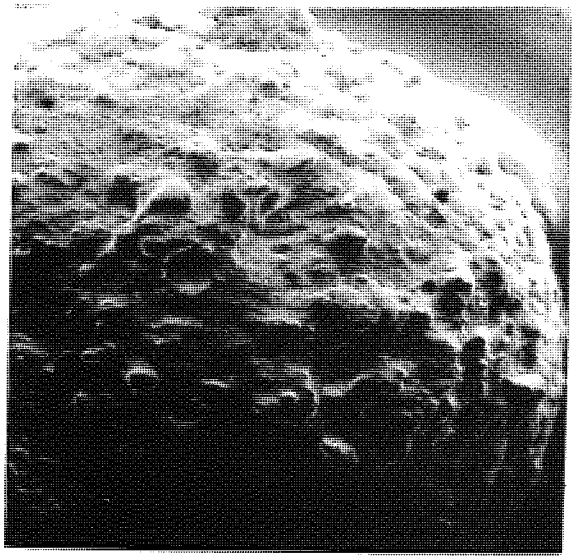

Magnification = 120x

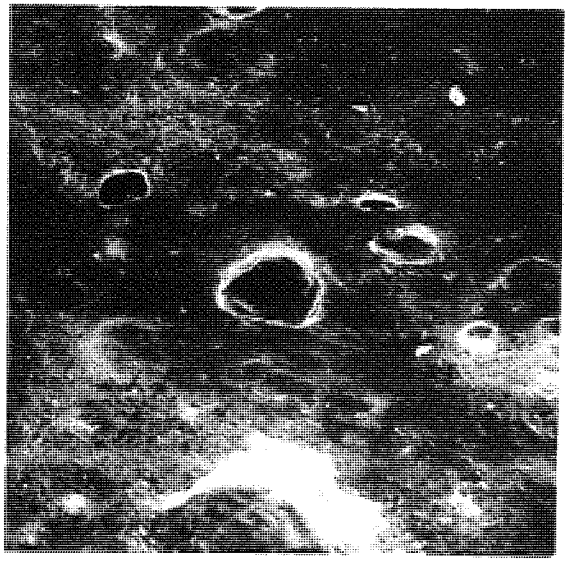

Magnification = 1200x

Plate 5.12 Formulation E

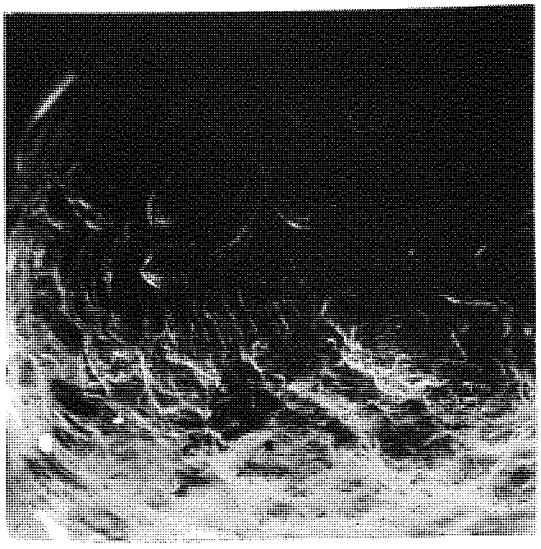

Magnification = 26x

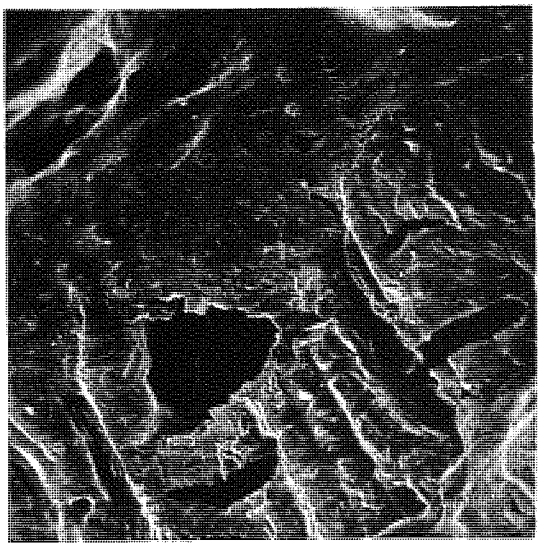

Magnification = 130x

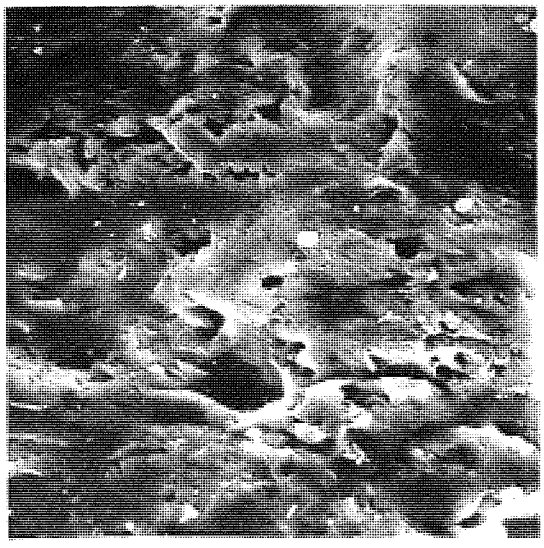

Magnification = 650x

Plate 5.13 Formulation F

Magnification = 25x

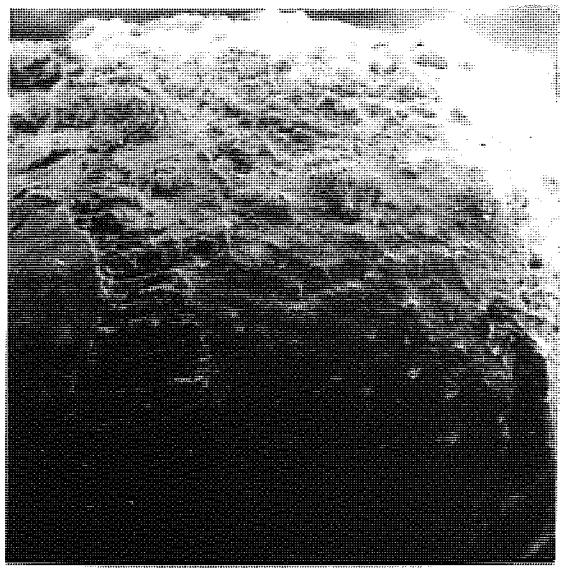

Magnification = 123x

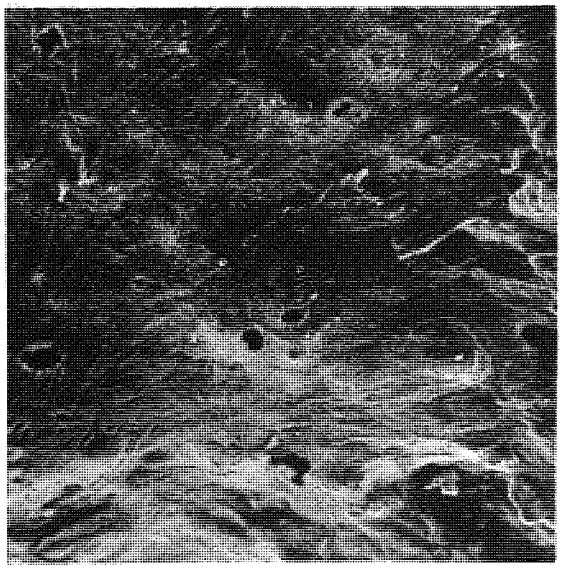

Magnification = 6100x

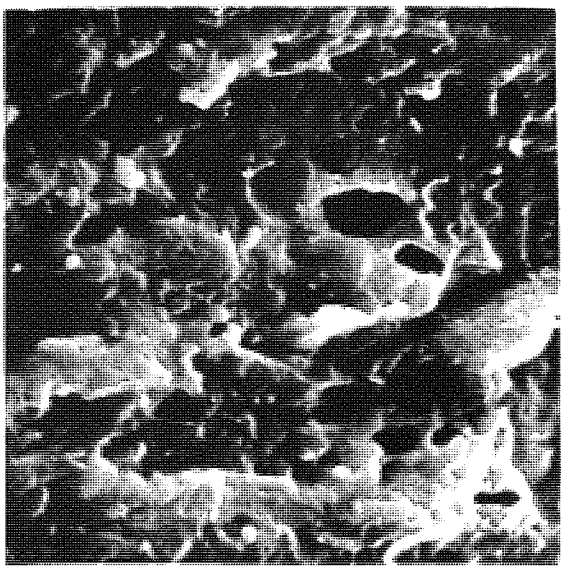

Plate 5.14 Formulation G

Magnification = 25x

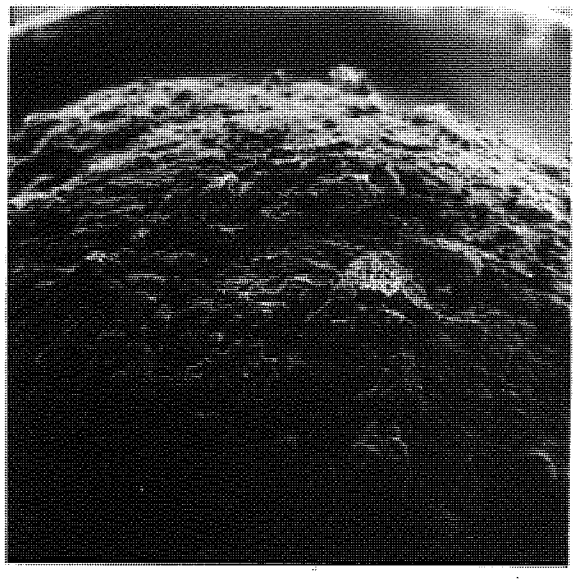

Magnification = 120x

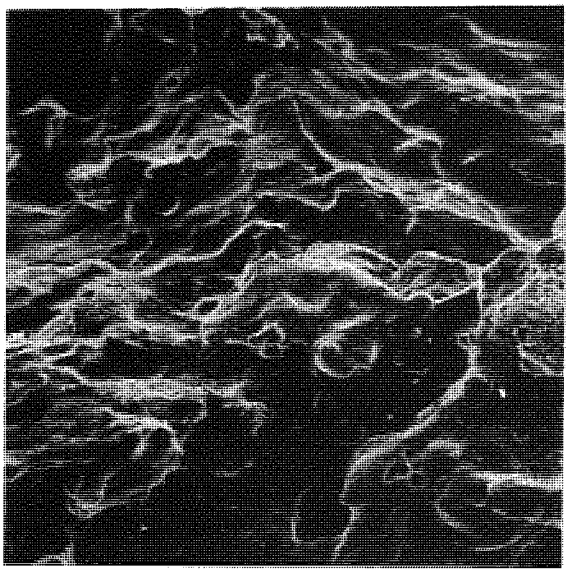

Magnification = 1200x

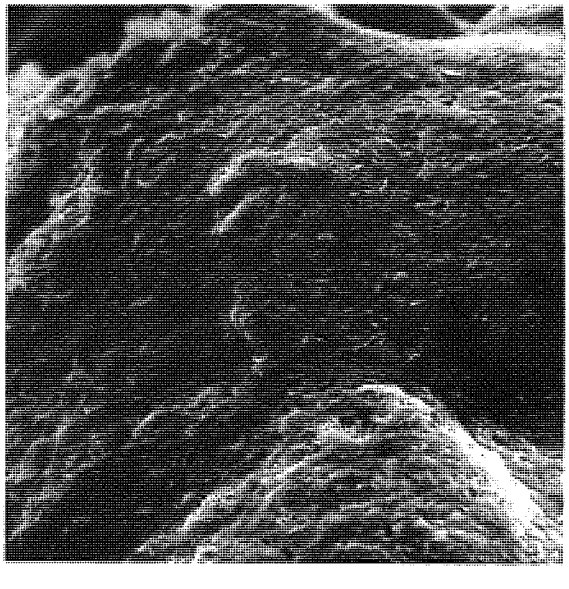

Plate 5.15 Formulation H

Magnification = 58x

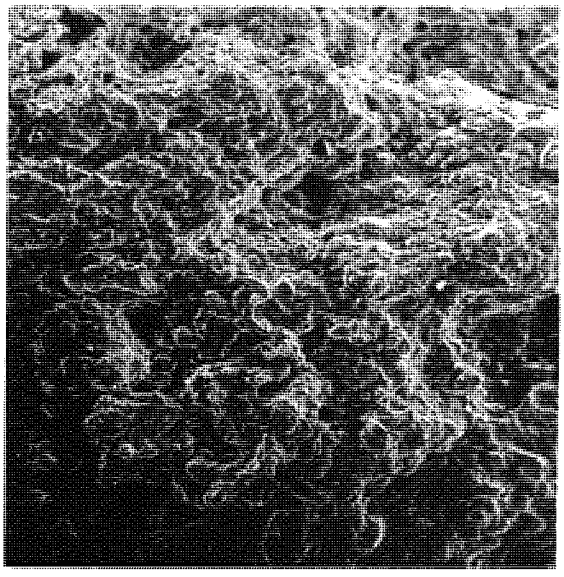

Magnification = 230x

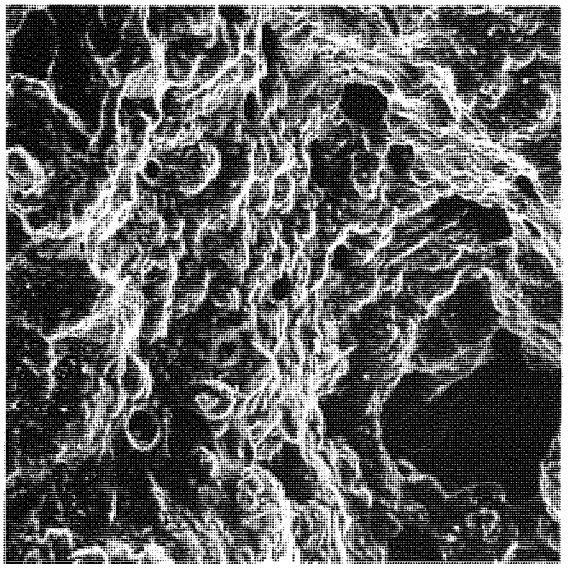

Magnification = 2300x

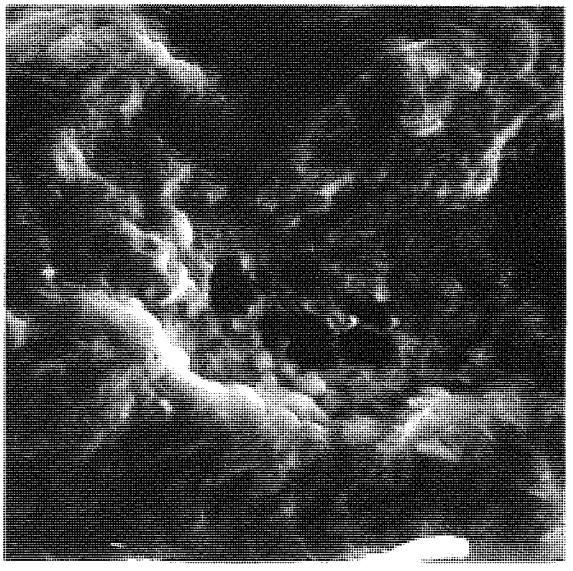

Plate 5.16 Formulation I

Magnification = 24x

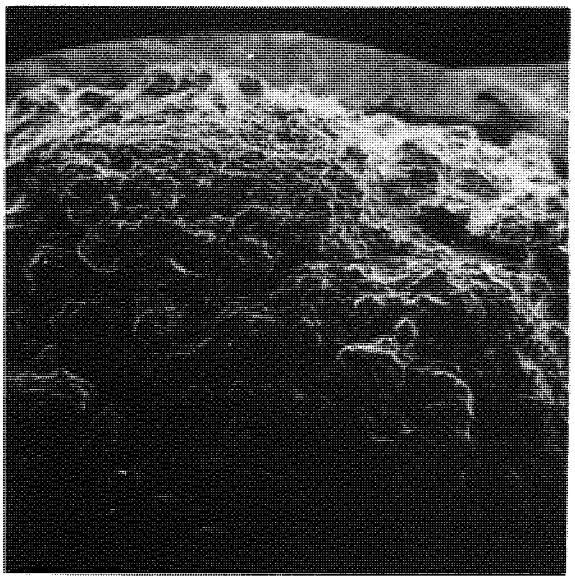

Magnification = 60x

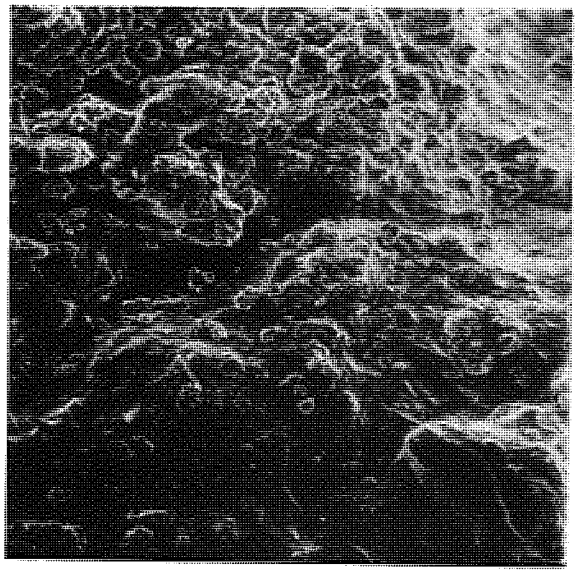

Magnification = 240x

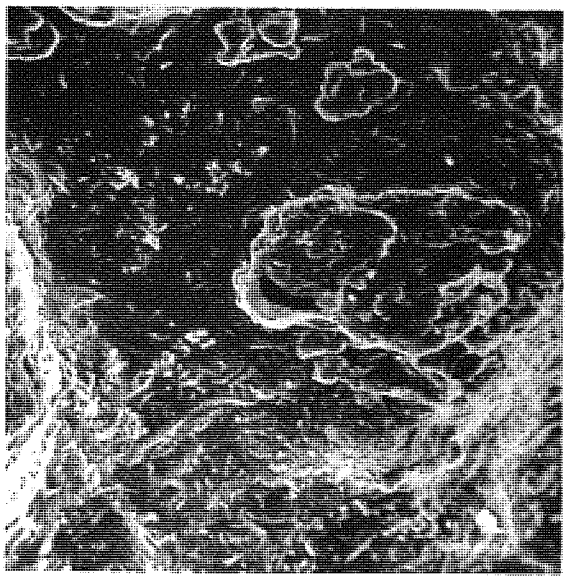

Figure 5.29.

Proposed Correlation for Particulate Slurries.

$$\frac{K_m \cdot \beta_m}{D_M \, \varepsilon^{1.5}} = 0.58(\rho u d_p/\mu)^{0.05} \cdot (\mu/\rho D_M \, \varepsilon^{1.5})^{0.06}$$

—●— Experiment

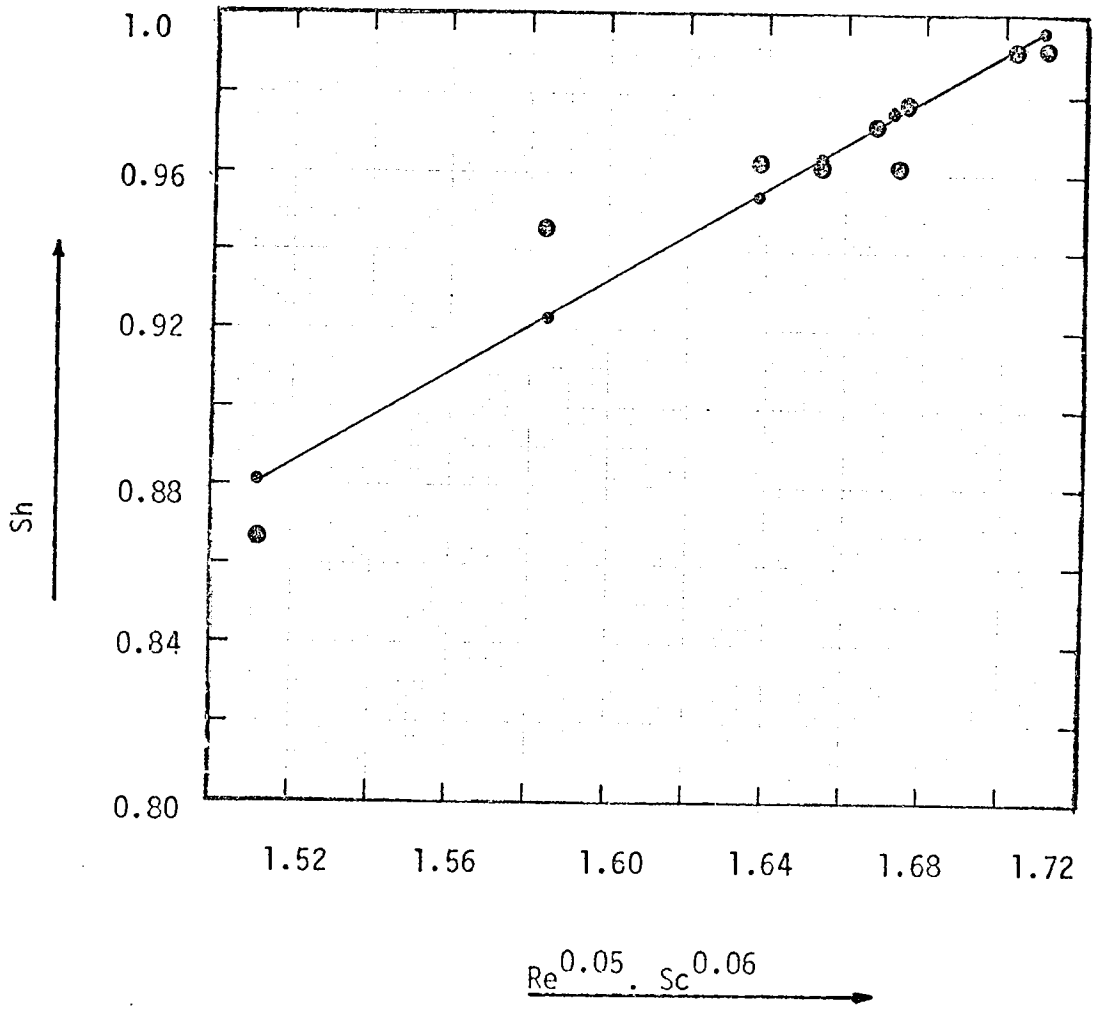

TABLE 5.9

Detergent Formulations.

Re	Sh		$Re^{0.05}$ $Sc^{0.06}$
	Experimental	Calculated	
632.7	0.963	0.964	1.65
521.5	0.973	0.973	1.67
485.7	0.992	0.997	1.71
450.0	0.978	0.977	1.68
488.2	0.993	0.993	1.70
632.7	0.963	0.955	1.64
531.7	0.962	0.976	1.67
471.6	0.946	0.923	1.58
479.3	0.867	0.881	1.51

5.4 Comparison of Experimental Mass Transfer Coefficients with Theoretical values for transfer through Particulate Slurry Drops.

Experimental mass transfer coefficients were calculated from a modified form of equation ((3.9));

$$K_E = \frac{R_c \; G \; \Delta H(T_{au} + 273.16)}{A. \; M_W \; (Ps - p)} \qquad ((3.9))$$

where k_G has been replaced by the overall mass transfer coefficient,

$A = 2\pi \; (R^2-(R-\beta)^2)/\varepsilon$, is the area for mass transfer; the porosity, ε , has been included to account for the increase in transfer path for the vapour from the interior to the exterior of the drop.

P_s, the saturation vapour pressure was obtained from experiments described in Appendix D, since the use of psychrometric charts for air-water systems was invalidated by the presence of dissolved or suspended solids.

Theoretical mass transfer coefficients were estimated from equation ((3.16)) after substituting equation ((3.21)) for the crust coefficient k_c. That is,

$$\frac{1}{K_T} = \frac{1}{k_G} + \frac{\beta}{D_M \cdot \varepsilon^{1.5}} \qquad ((5.23))$$

where K_T is the theoretical mass transfer coefficient;

k_G is the gas film mass transfer coefficient estimated from the proposed correlation for pure water drops, equation ((5.3)).

The transfer coefficients, as well as the percentage resistance to transfer, are tabulated in Tables 5.10 and 5.11, for aqueous sodium sulphate, and detergent drops, respectively.

Figure 5.30, which has a standard deviation of 0.164, and figure 5.31, with a standard deviation of 0.422, show conclusively that K_E and K_T compare favourably. Both figures confirm the applicability of the proposed correlation for pure water drops.

5.4.1 Resistance to Transfer.

For sodium sulphate drops, the experimental results show that 35.8% of the resistance lies in the gas film, while for detergent formulations, the resistance is 4.3%. This significant difference is due to the fact that sodium sulphate crusts are more porous and thinner than those of detergent formulations.

TABLE 5.10

Hydrated Sodium Sulphate Drops.

Mass Transfer Coefficient (cm/s)		Resistance (%)	
Experimental K_E	Theoretical K_T	Gas Film $\frac{(1/k_G)}{(1/k_G + 1/k_c)}$	Crust $\frac{(1/k_c)}{(1/k_G + 1/k_c)}$
1.71	1.20	47.2	52.8
1.41	1.54	25.2	74.8
1.58	1.63	34.9	65.1
1.74	1.73	31.0	69.0
1.87	1.90	41.4	58.6
2.20	2.64	31.0	69.0
2.93	2.40	45.5	54.6
2.35	2.05	45.1	54.9
3.48	3.50	37.1	62.9
3.00	3.00	37.6	62.4
2.16	2.42	27.3	72.7
1.84	1.54	29.4	70.6
3.57	3.53	34.1	65.9
2.91	2.90	35.5	64.5
2.11	2.12	30.6	69.4
1.29	1.16	31.2	68.8
2.77	2.78	45.6	54.4
2.12	1.91	39.0	61.0

TABLE 5.11.

Drops of Detergent Formulations.

Formulation	Mass Transfer Coefficient.		Per Cent Resistance (%)	
	Experimental K_E (cm/s)	Theoretical K_T (cm/s)	Gas Film $(1/k_G)/(\frac{1}{k_G} + \frac{1}{k_c})$	Crust $(1/k_C)/(\frac{1}{k_G} + \frac{1}{k_c})$
A	0.150	0.150	3.67	96.33
B	0.118	0.125	2.56	97.44
C	0.059	0.068	1.22	98.78
D	0.124	0.127	2.48	97.52
E	0.062	0.065	1.28	98.72
F	0.195	0.141	4.78	95.22
G	0.195	0.165	4.32	95.68
H	0.238	0.260	4.96	95.04
I	0.618	0.643	13.35	86.65

Figure 5.30.

Experimental versus Theoretical Mass Transfer Coefficients.

Sodium Sulphate Drops.

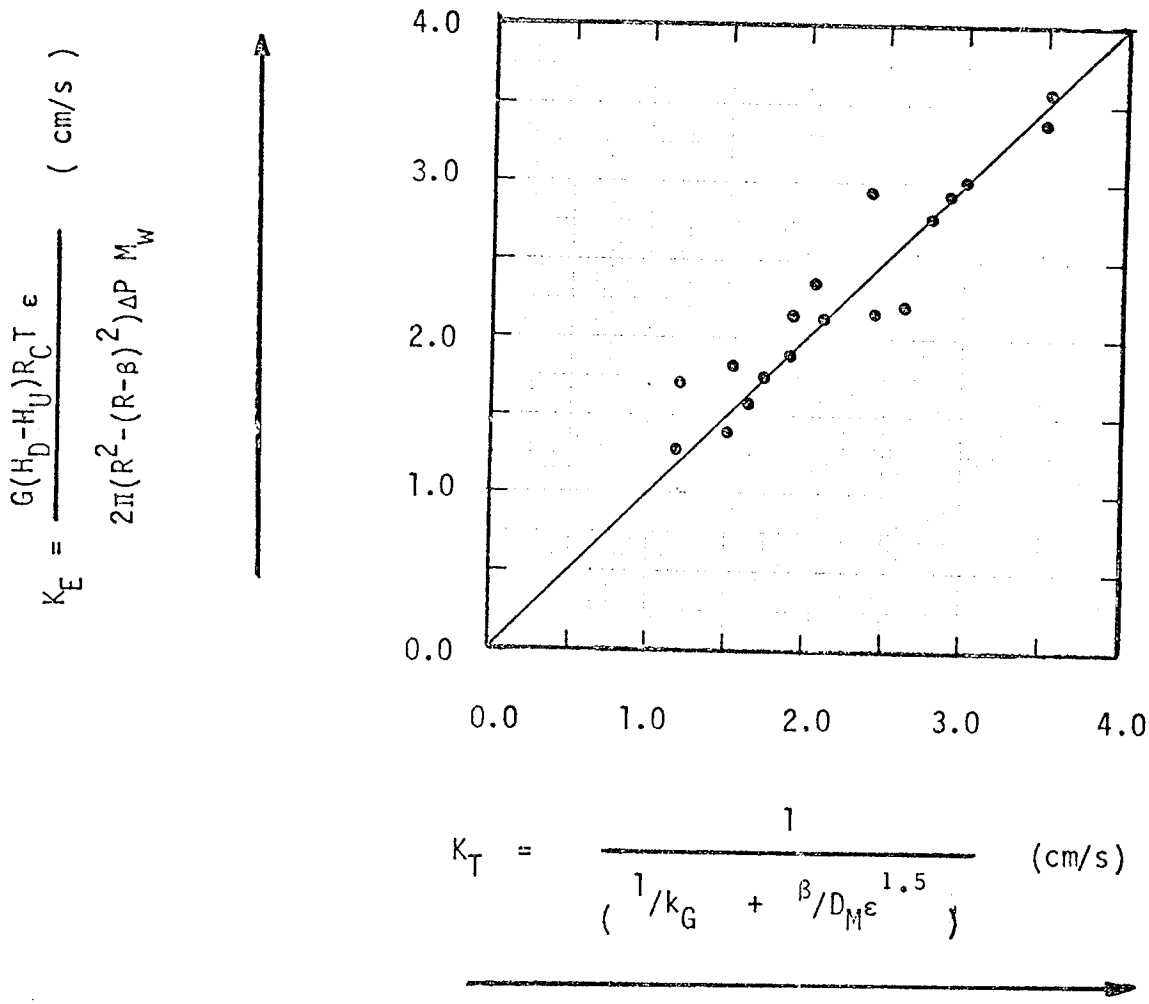

K_E = experimental mass transfer coefficient,

K_T = theoretical mass transfer coefficient.

Figure 5.31

Experimental versus Theoretical Mass Transfer Coefficients.

Detergent Formulations.

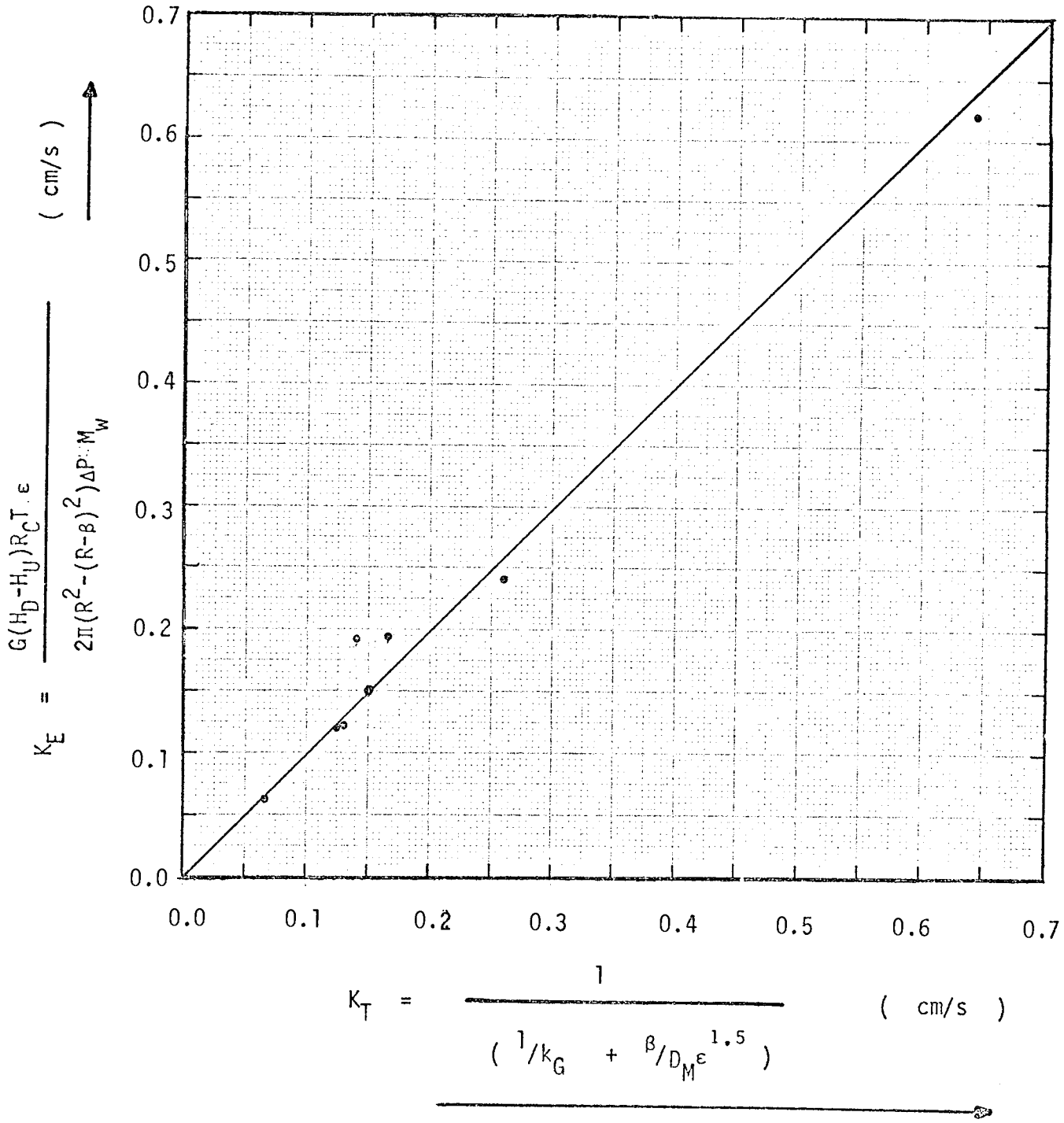

Section Six.

Discussion.

Chapter 6.1 Pure Water Drops.

Chapter 6.2 Aqueous Sodium Sulphate Decahydrate Drops.

Chapter 6.3 Detergent Slurry Drops.

Chapter 6.4 Comparison of Experimental Techniques.

6.1 Pure Water Drops.

6.1.1. Effect of Air Temperature on Mass Transfer Coefficient and Mass Transfer Rate:

Examination of figure 5.1 shows that both the mass transfer coefficient and mass transfer rate increase with increase in air temperature.

In the non-oscillating drop region, the mass transfer coefficient is influenced by the drop viscosity and internal circulation through their effect on the velocity surrounding the drop. As the air temperature rises, the drop viscosity decreases, internal circulation increases and the resistance to mass transfer is reduced. Hence, for a constant driving force, mass transfer rate should be expected to increase; but the driving force also increases, therefore the mass transfer rate increases.

Heertjes and de Nie (68) have shown that, where the circulation has completely developed, mass transfer amounts to 1.5 times that for stagnant drops.

6.1.2. Effect of Drop Diameter on Mass Transfer Coefficient and Mass Transfer Rate:

A review of the literature shows that, at zero relative velocity of fluid passed the drop, mass transfer occurs entirely by molecular diffusion through the surrounding phase and under these circumstances the corresponding Sherwood Number, Sh = 2.0; that is,

$$\frac{k_G \, d_p}{D_M} = 2.0 \qquad ((6.1))$$

where k_G = mass transfer coefficient (cm/s)

d_p = drop diameter (cm)

D_M = molecular diffusivity of water vapour (cm^2/s)

Since the air temperature is constant, the diffusion coefficient will be constant. Therefore, in accordance with equation ((6.1)), k_G must decrease when d_p increases.

The condition can be shown to exist when the relative velocity of the fluid passed the drop is finite. In this situation, the mass transfer coefficient can be correlated by,

$$\frac{k_G\ d_p}{D_M} = 2.0 + \Psi\left(\frac{\rho u d_p}{\mu}\right)^{0.5}\left(\frac{\mu}{\rho D_M}\right)^{0.33} \qquad ((6.2))$$

At constant temperature the Schmidt group, $\left(\frac{\mu}{\rho D_M}\right)^{0.33}$ is constant; and for a given value of the relative fluid velocity, equation ((6.2)) can be written as:

$$\frac{k_G}{D_M} = \frac{2.0}{d_p} + \phi\left(\frac{1}{d_p}\right)^{0.5} \qquad ((6.3))$$

If d_p is increased, the right hand side of equation ((6.33)) will decrease and hence k_G decreases.

Thus irrespective of the relative fluid velocity, the mass transfer coefficient decreases for an increase in the drop diameter. As expected, therefore, figures 5.2, 5.3 and 5.4 confirm the decrease in both the mass transfer coefficient and mass transfer rate as the drop diameter is increased.

6.1.3 Mass Transfer Correlations: The mass transfer correlations deduced by the least-squares curve-fitting technique in Section 5.1.3. have been shown to be temperature dependent, with the constant, Ψ , having different values for each temperature. In addition the values are different from those reported in the correlation of Ranz and Marshall (40), where Ψ is 0.6.

The temperature of the air in Ranz and Marshall's investigation varied over the range, $19.9 \leqslant T \leqslant 25.4^{o}C$, a condition where the change in the sensible heat contribution compared with the latent heat of vapourisation, would be negligible. This investigation, however, was carried out at air temperatures between $26.5 \leqslant T \leqslant 118.5^{o}C$. Thus in drying, where almost all the water is evaporated, the heat required for evaporation is large compared with the change in sensible heat and the latter is usually ignored. However, in the present investigation, all the water was not evaporated from the drop, and the drop-suspension device was designed so that, as drying progressed, the drop was continuously fed with make-up water at the appropriate temperature. Therefore what obtained in the system was analogous to the condition in a cooling tower where cooling took place by evaporation of a small proportion of the water, the latent heat being supplied by the changing sensible heat of the remainder. Consequently the sensible heat contribution, $(T_{au}-T_s)$, was included in the correlation of the mass transfer coefficients. The division of the sensible heat term by the ambient air temperature was introduced to provide a dimensionless term.

The Sherwood numbers corresponding to the operating conditions of Ranz and Marshall's investigation, were calculated from the correlation shown in equation ((5.13)), and compared with their experimental values. The standard deviation was found to be 2.27, and very similar to that obtained from this investigation. In addition the isothermal data shown in Table 5.5 were better.

6.2 Aqueous Sodium Sulphate Decahydrate Drops.

Crust formation presents an extra resistance to mass transfer, and unlike the drying of pure liquid drops, the controlling resistance is the transport through the crust, rather than the gas film surrounding the drop. The rate of drying, therefore, will be expected to vary with the crust thickness since the porosity was found to be virtually constant.

An examination of figure 5.11 shows that the crust thickness rate increases with increase in the air flow rate since drying occurs faster. A number of investigators (40, 45) showed that, as the drop was rotated, parts of the crust redissolved and then reformed at a different rate from the rest of the crust. This phenomenon of redissolving and reforming is more likely to vary with the air flow rate, that is, the rate of impingement of the air on the drop. As the air flow rate is increased, drying takes place more rapidly, and the effects of the above phenomenon will be minimal. Consequently, the crust thickness rate increases with

increase in air flow rate. Now, the thicker the crust, the greater is the resistance to mass transfer, therefore the rate of drying decreases for a corresponding increase in the crust thickness rate.

The overall mass transfer coefficient has been plotted against the crust thickness in figure 5.12 for two air flow rates. As the crust thickness increases, the resistance to mass transfer increases and hence the overall effect of increase in air flow rate increases the mass transfer coefficient, and thus the rate of drying increases.

Evaporation from drops of slurries containing dissolved solids takes place in the falling rate period where drying is controlled by the rate of migration of liquid to the internal surface of the crust at which evaporation occurs through the pores. The postulated mechanism (69) for this period is that the overall resistance to mass transfer increases as drying progresses, that is the mass transfer coefficient decreases. This mechanism has been confirmed as explained in the paragraph above, where the crust thickness rate increases as drying progresses, and thus reducing the mass transfer coefficient.

6.3 Detergent Slurry Drops.

Drying of detergent slurry drops also forms hollow crusts similar to the situation with sodium sulphate drops discussed in Section 6.2. However, the crusts are not as porous as those of sodium sulphate, and, in some cases, appear to be somewhat plastic in nature.

This has been borne out by the number of cracks and holes present on the crust surface when examined in the stereoscan. See plates 5.8 to 5.16.

It was shown in Section 3.2.3 that the following relation applies:

$$\frac{1}{K_{ca}} \approx \frac{1}{k_c} , \qquad ((3.16b))$$

when the gas film resistance, $(1/k_G)$, is very much smaller than the crust resistance $(1/k_c)$; that is, the controlling resistance to mass transfer is the crust rather than the gas film surrounding the drop. It was also explained in Section 2.2, by analogy to the Whitman Two-Film Theory (3), that the crust coefficient, k_c, is given by equation ((3.21)):

$$k_c = \frac{D_M \varepsilon^{1.5}}{\beta} \qquad ((3.21))$$

where D_M = molecular diffusivity (cm^2/s)

β = crust thickness (cm)

ε = porosity of crust (--)

From equation ((3.21)), therefore, the drying rate is proportional to the ratio $(\varepsilon^{1.5}/\beta)$ at a given temperature, since the diffusion coefficient is constant. However, the actual value of the ratio $(\varepsilon^{1.5}/\beta)$ is not important for a qualitative analysis; and the drying rate will be expected to increase as the ratio $(\varepsilon^{1.5}/\beta)$ or $\{\varepsilon/\beta\}$ increases.

Thus the trend, of the drying rate curves for the

nine detergent formulations, A to I, which were dried under the same air conditions, was explained in Section 5.3, on the basis of the ratio $\{\varepsilon/\beta\}$. As expected, the greater this ratio, the greater the rate of drying.

The analysis can be further justified by referring to Section 6.2 where it was shown that as the crust thickness rate increased, the drying rate decreased. For a highly porous crust, the effective diffusivity, $(D_M\varepsilon^{1.5})$, is large and hence more moisture diffuses into the air stream. But the mass transfer path, and hence the path length for effective diffusion, depends on the crust thickness. Therefore as the crust thickness increases, the mass transfer path will increase. Consequently a compromise of porosity and crust thickness can only be achieved through the ratio $\{\varepsilon/\beta\}$ since ε is independent of β. An effective increase in the ratio must lead to a decrease in the mass transfer resistance; hence the rate of drying increases.

The effects the additives have had on the drying characteristics have not been conclusive, and, unfortunately, there was no available literature to provide useful background information for discussing these effects. From the limited information obtained from this investigation, it can be stated that each additive does not have an independent effect on the rate of drying. However, in formulations containing high concentrations of active detergent and low concentrations of sodium sulphate, for example, formulations A and B, the addition of sodium carboxy methyl cellulose reduces the drying rate. But where the concentrations of sodium sulphate were high compared with active detergent, for example,

formulations E and F, the addition of sodium carboxymethyl cellulose improves the drying rate. Similarly sodium toluene sulphonate inhibits drying rate of formulations containing low concentrations of sodium sulphate compared with active detergent, and vice versa. However, the addition of coconut ethanol amide appears to improve drying.

6.4 Comparison of the Experimental Techniques.

No parallel work of this nature has been reported in the literature. Previous investigators (39, 40, 41, 45) studied the less complex situation of evaporation from single stationary liquid droplets suspended from glass filaments or thermocouple junctions, and others (41) used single stationary spheres, constructed from celite, (diatomaceous earth), with known porosities. Such techniques, though permitting measurement of the droplet weight as drying proceeds, are limited in application since the relative velocity of the drop, present in a spray drying tower, is non-existent. The suspension bead (45, 55) occupies an appreciable area of the droplet, and thus influences the shape of the drop. Although it has been claimed (45) that the heat conducted along the drop-suspension filament accounted for only 1% of the total heat input to the droplet, this extra heat does not arise for the continuous feed system used in the present study. This is due to the addition of the make-up liquid or slurry at the appropriate temperature, and the use of

PTFE nozzles. Also the flow of air was perpendicular to the drop suspension device, as opposed to the upward air flow reported in the literature (40, 45, 55). For an upward air flow, the drop-suspension filament is bound to be more in contact with the hot air rather than it is with the cross flow arrangement studied here.

The porosity of spray-dried slurry drops varies with the composition of the formulation, so that conclusive results on mass transfer in spray driers cannot be obtained from the evaporation of liquids from celite spheres of fixed porosity. Moreover, evaporation from such spheres, is analogous to evaporation from stationary, pure liquid drops where a continuous liquid interface is always in contact with the drying air. Furthermore, drying is from one side only, the drying rate being faster on the side incident to the air flow, and slower in the wake region. Therefore mass transfer is not uniform throughout the drop.

The technique adopted in this investigation was not chosen for its sophistication, but mainly because it simulated more closely the conditions of a droplet in a spray drier. The need for continuous feeding obviated substituting a mathematical expression (44, 45) for the amount of moisture necessary to maintain a constant drop size.

The main disadvantage of the present technique is the difficulty of measuring the droplet weight, especially for non-crust-forming liquid drops as drying proceeds.

Section Seven.

Conclusions and Recommendations.

Chapter 7.1 Conclusions.

Chapter 7.2 Recommendations.

7.1 Conclusions.

The results of this investigation have been presented and analysed in Section 5, and a detailed discussion followed in Section 6. In order to draw the conclusions into a more precise form, they are presented below in a numbered sequence.

7.1.1 Pure Water Drops:

(1) Mass transfer coefficient increases with increase in air flow rate and hence the rate of mass transfer also increases.

(2) Mass transfer coefficient decreases with increase in drop diameter and therefore the mass transfer rate also decreases.

(3) The value of Ψ reported by Ranz and Marshall (40) has been found to be temperature dependent. For a temperature range of $26.5 \leq T \leq 118.5^{o}C$, Ψ was found to lie in the range $0.38 \leq \Psi \leq 0.47$.

(4) The experimental data were well correlated by equation ((5.2))

$$Sh = 2.0 + 0.44 \left(\frac{T_{au}-T_s}{T_{amb}}\right)^{-0.008} . Re^{0.5} Sc^{0.33} \qquad ((5.2))$$

The correlation coefficient was 0.998 and the standard deviation was 2.27.

7.1.2 Aqueous Sodium Sulphate Drops:

(5) When a drop of aqueous sodium sulphate is dried, a hollow crust is formed. The crust thickness rate increases with increase in air flow rate, air temperature and the initial moisture content but increases with decrease in the initial drop radius.

(6) The crust provides 64.2% of the total resistance to mass transfer.

(7) The overall mass transfer coefficient, and hence the rate of mass transfer, increases or decreases with increase in air flow rate, depending on whether the initial drop radius is small or large.

(8) The driving force for mass transfer increases as drying progresses.

(9) The crusts are porous as revealed by stereoscan micrographs and hence pore diffusion is present. Porosity is independent of the solute concentration.

(10) The crusts appear to be smoother on the external than at the internal surface, thus supporting the findings of Charlesworth and Marshall (45), and, Duffie and Marshall (62). This observation confirms crystallisation and indicates evaporation at the core.

(11) The crystal structure associated with sodium sulphate is still present when crust formation is complete, see plate 5.4. Therefore no structural degradation or transformation occurred during drying of the drop.

(12) Some of the crusts cracked to release the internal pressure and formed blow holes. This phenomenon shown in plate 5.5 supports the findings of Charlesworth and Marshall (45), and Trommelen and Crosby (55).

(13) The crust thickness predicted from equation ((3.15)),

$$\beta = R - \left\{R^3 - \frac{3G}{2\pi C_o}\,(\Delta H_d - \Delta H_u)\Delta\theta\right\}^{1/3} \qquad ((3.15))$$

showed a good agreement, figure 5.28, with the experimental values evaluated from stereoscan micrographs shown in plates 5.1 and 5.2. The standard deviation of experimental values from prediction was found to be 1.5×10^{-6}.

7.1.3 Detergent Slurry Drops:

(14) The analysis of mass transfer data for particulate slurry drops with different porosities and crust thicknesses, can be based on the $\{\varepsilon/\beta\}$ ratio. Formulations having high $\{\varepsilon/\beta\}$ ratios dry better than those with low values.

(15) It was not possible to reach a qualitative conclusion on the effects of various additives, like sodium carboxy methyl cellulose and sodium toluene sulphonate, on the drying rate of detergent formulations. However, the addition of coco-nut ethanol amide appeared to improve drying.

(16) For the two complete detergent powder formulations, H and I, in formulation H, where the concentration of sodium sulphate was very low, and the active detergent paste was not added, the rate of drying

reduced considerably, compared with that of formulation I.

(17) The crusts were microporous, and thicker than those observed for sodium sulphate crusts. They formed larger cracks, and the surface was littered with punctures, thus suggesting that detergent crusts are plastic.

(18) The crusts were rougher on the external surface than observed for sodium sulphate crusts. The surface roughness tended to increase from formulation A through I; that is, formulation I appeared to be roughest.

(19) The mass transfer coefficients were well correlated by equation ((15.22)):

$$\frac{K_m \beta_m}{D_M \varepsilon^{1.5}} = 0.58 \left(\frac{\rho u d}{\mu}\right)^{0.05} \left(\frac{\mu}{D_M \varepsilon^{1.5}}\right)^{0.06} \qquad ((5.22))$$

The standard deviation was 0.036, with a correlation coefficient of 0.958.

(20) The agreement between the experimental and theoretical mass transfer coefficients shows, in addition to the above correlation, that the overall mass transfer coefficient can also be predicted from equation ((5.23)):

$$\frac{1}{K} = \frac{1}{k_G} + \frac{\beta}{D_M \varepsilon^{1.5}} \qquad ((5.23))$$

(21) The crust is the controlling resistance to transfer in particulate slurry drops, and accounts for 97.5% of the total resistance.

7.2 Recommendations.

(1) Drying characteristics of pure water drops and drops of sodium sulphate solutions have been studied extensively. The mathematical model, proposed for estimating crust thickness was tested and found satisfactory for sodium sulphate drops. This model should be further tested for other salts such as sodium phosphate with determinable properties.

(2) The correlation of mass transfer coefficients proposed here for detergent formulations should be applied to data obtained from a pilot size spray-drying tower.

(3) As discussed in Chapter 6.3, the effects of additives, such as sodium toluene sulphonate and sodium carboxy methyl cellulose, on the drying characteristics of detergent formulations, have not been conclusive although certain trends were observed. These effects should therefore be included in future investigations.

(4) Spray drying is not restricted to detergent slurries alone; an extension of this work to cover foodstuff, such as coffee extract and powdered milk is recommended.

(5) The effect of using high-humidity air as the drying medium should be investigated since only very low-humidity air was used here.

(6) The major disadvantage of the design of the drop-suspension device was the difficulty in measuring the change in droplet weight, especially for non-crust-forming solutions, as drying progressed. Therefore, a modification of the design should be considered.

(7) Surface structures and crust thickness were evaluated from stereoscan micrographs, but for microporous crusts of detergent formulations, this technique, sometimes, failed to provide all the information required due to the limited magnification range. Although the electron microscope has a larger magnification range, specimen preparation is very tedious, and only a very small portion of the crust, which could be unrepresentative of the whole surface, can be examined. However, if this investigation is extended to include 1-μ drops, then the technique is favoured. Nevertheless, the possibility of using other methods, such as x-rays, should be considered.

(8) Furthermore, the relationship between composition and porosity should be investigated.

NOMENCLATURE.

The symbols used in this thesis are listed below unless otherwise stated in the pertinent text.

A	mass transfer area	(m^2).
C	moisture content	(kg moisture/m^3 solution).
ΔC	concentration driving force	"
D	diffusion coefficient	(m^2/s).
d	diameter	(m).
G	dry air mass flow rate	(kg/s).
g	constant	
H	air humidity	(kg/kg).
K	overall mass transfer coefficient	(m/s).
k_G	film mass transfer coefficient	(m/s).
M	molecular weight	
N_A	mass transfer rate	(kg/m^2s).
P	total pressure	(atm).
p	partial pressure	(atm).
Δp	pressure driving force	(atm).
q	constant	
R	external radius of drop	(m).
r	internal radius of drop	(m).
R_c	universal gas constant	(0.08206 m^3.atm/kg mol deg K).
Re	Reynolds Number	$\rho u d_p/\mu$
S	specific surface area	(m^2/m^3).
Sc	Schmidt Number	$\mu/\rho D$
Sh	Sherwood Number	(mass transfer coefficient x d_p/D).
T	temperature	(deg K).
u	air velocity	(m/s).

W_c	mass transferred	(kg/m^2).
x	constant	
y	constant	
Z	constant	

GREEK SYMBOLS

β	crust thickness	(m).
ψ	constant	
ε	porosity of crust	
δ	constant	
θ	drying time	(s).
η	constant	
μ	air viscosity	(kg/m s).
ρ	air density	(kg/m^3).
ν	kinematic viscosity	(m^2/s).
π	constant = 3.1416	
σ	constriction factor	
τ	tortuosity factor	

SUBSCRIPTS.

a	air
amb	ambient condition
c	crust
d,D	downstream
e	equivalent-: relating to diffusion coefficient.
m	mean value
M	molecular-: relating to diffusion coefficient.

o	initial value
p	particle
s	saturation
u,U	upstream.

REFERENCES

The references listed below include those of particular relevance to the topics of the present investigation. However, some references, for which translations were unavailable, have been included. It is hoped that they will be useful to the reader.

1. Coulson, J.M., & Richardson, J.F.: Chemical Engineering, Vol 1, 2nd Edition, Pergamon Press, (1966).
2. Maxwell, J.C.: Coll. Sci. Papers, Cambridge, 11,625, (1890).
3. Whitman, W.G.: Chem. & Met. Eng., 29, 147, (1923).
4. Higbie, R.: Trans. Am. Inst. Chem. Eng., 31, 365, (1935).
5. Danckwerts, P.V.: Ind. Eng. Chem., 43, 1460, (1951).
6. Toor, H.L., & Marchello, J.M.: AIChE J., 4, 97, (1958).
7. Hinchley, J.W., & Himus, G.W.: Trans. Inst.Chem. Eng., 2, 57, (1924).
8. Colburn, A.P.: Ind. Eng.Chem., 22, 967, (1930).
9. Chilton, T.H., & Colburn, A.P.: ibid, 26, 1183, (1934).
10. Gilliland, E.R., & Sherwood, T.K.: ibid, 26, 516, (1934).
11. Maisel, D.S., & Sherwood, T.K.: Chem.Eng.Prog., 46, 131, (1950).
12. Sherwood, T.K., & Pigford, R.L.: Absorption and Extraction, McGraw-Hill, (1950).
13. Linton, W.H., & Sherwood, T.K.: Chem.Eng. Prog., 46, 490, (1950).
14. Sherwood, T.K.: Trans. Am. Inst. Chem. Eng., 36, 817,(1940).
15. Peck, R.E., & Kauh, J.Y.: AIChE J., 15, 85, (1969).

16. Harmathy, T.Z.: Ind.Eng.Chem.Fundamentals, 8, 92, (1969).

17. Keen, B.A.: J. Agric. Sci., 6, 456, (1914).

18. Fisher, E.A.: ibid, 13, 121, (1923).

19. " " : ibid, 17, 407, (1927).

20. Sherwood, T.K.: Ind. Eng. Chem., 21, 12, 976, (1929).

21. Sherwood, T.K.: Ind. Eng. Chem., 22, 132, (1930).

22. Sherwood, T.K.: ibid, 24, 307, (1932).

23. Sherwood, T.K., & Comings, E.W.: ibid, 25, 311 (1933).

24. Lewis, W.K.: ibid, 13, 427, (1921).

25. Tuttle, F: J. Franklin Inst., 200, 609, (1925).

26. Newman, A.B.: Trans. Am. Inst. Chem. Eng., 27, 203, 310, (1931).

27. Perry, J.H.: Chemical Engineers Handbook, 4th Edition, McGraw-Hill, (1936).

28. Hougen, O.A., McCauley, H.J., & Marshall, W.R.: Trans. Am. Inst. Chem. Eng., 36, 183, (1940).

29. Gurr, C.G., Marshall, T.J., & Hutton, J.T.: Soil Sci., 74, 335, (1952).

30. Kuzmak, J.M., & Sereda, P.J.: ibid, 87, 419, (1957).

31. Henry, P.S.H.: Proc. Roy. Soc., 171A, 215, (1939).

32. Cassie A.B.D., King, G., & Baxter, S.: Trans. Faraday Soc., 36, 445, 453, 458 (1940).

33. Walker, I.K.: New Zealand J. Sci., 4, 775, 796, (1961).

34. Coulson, J.M., & Richardson, J.F.: Chemical Engineering, Vol 2, 2nd Edition, Pergamon Press, (1968).

35. Gilliland, E.R.: Ind.Eng.Chem., 30, 406, (1938).

36. Wenzel, L., & White, R.R.: Ind.Eng.Chem.,43, 1829,(1951).

37. Kirk-Othmer : Encyclopedia of Chem. Tech., Vol 7, 2nd Edition.

38. Audu, T.O.K.: M.Sc. Dissertation, University of Aston-in-Birmingham, U.K., (1971).

39. Froessling, N.: Gerlands Beitre. Geophys., 52, 170, (1938).

40. Ranz, W.E., & Marshall, W.R., Jnr.: Chem.Eng.Prog., 48, 141, 173, (1952).

41. Pei, D.C.T., Narasimhan, C., & Gauvin, W.H.: 3rd Congress European Federation of Chemical Engineers, June, (1962).

42. Petersen, E.E.: Chemical Reaction Analysis, Prentice-Hall, (1965).

43. Wilson, M.P.: Ph.D. Thesis, University of Aston-in-Birmingham, U.K., (1971).

44. Schlünder, E.U.: Int. J. Heat Mass Transfer, 7, 49, (1964).

45. Charlesworth, D.H., & Marshall, W.R., Jnr.: AIChE J., 6, 9, (1960).

46. Tudose, R.Z.: Chim. et Ind. Genie Chimique, 104, 14, 1769, (1971).

47. Golli, S.El, Bricard, J., Turpin, P.Y., & Armaud, G.: Aerosol Science, 3, 255, (1972).

48. Ranz, W.E.: Trans. ASME., 78, 909, (1956).

49. Marshall, W.R., Jnr.: Trans. ASME., 77, 1377,(1955).

50. Hoffman, T.W., & Gauvin, W.H.: Can. J. Chem.Eng., 38, 129, (1960).

51. Downing, C.G.: AIChE J., 12, 760, (1966).

52. Toei, R., Okazaki, M., Kubota, K., Ohaski, K., & Mizata, K.: Chem. Eng. (Japan), 30, 43, (1966).

53. Hughmark, G.A.: AIChE J., 13, 1219, (1967).

54. Lee, K., & Ryley, D.J.: J. Heat Transfer, Trans. ASME, 90, 445, (1968).

55. Trommelen, A.M, & Crosby, E.J.: AIChE J., 16, 857, (1970).

56. Matlosz, R.L., Leipziger, S, & Torda, T.P.: Int. J. Heat Mass Transfer, 15, 831, (1972).

57. Dlouhy, J., & Gauvin, W.H.: AIChE J., 6, 29, (1960).

58. Manning, W.P., & Gauvin, W.H.: ibid, 6, 184, (1960).

59. Bose, A.K., & Pei, D.C.T.: Can. J. Chem.Eng., 42, 259, (1964).

60. Dickinson, D.R., & Marshall, W.R., Jnr.: AIChE J., 14, 541, (1968).

61. Narasimhan, C., & Gauvin, W.H.: Can. J. Chem.Eng., 46, 138, (1968).

62. Duffie, J.A., & Marshall, W.R., Jnr.: Chem.Eng.Prog., 49, 417, 480, (1953).

63. Abdul-Rahman, Y.A.K., Crosby, E.J., & Bradly, R.L.: J. Dairy Sci., 54, 1111, (1971).

64. Crosby, E.J., & Marshall, W.R., Jnr.: Chem. Eng. Prog., 54, 56, (1958).

65. Badger, W.L., & Banchero, J.T.: Introduction to Chemical Engineering, McGraw-Hill.

66. Glasstone, S., & Lewis, D.: Elements of Physical Chemistry, 2nd Edition, Macmillan, (1965).

67. Garner, F.H., & Keey, R.B.: Chem.Eng.Sci., 9, 119, (1958).

68. Heertjes, P.M., & De Nie, L.H.: Recent Advances in Liquid-Liquid Extraction, Chem.Eng.Sci., 21, 755, (1966).

69. Nonhebel, G., & Moss, A.A.H.: Drying of Solids in the Chemical Industry, Butterworths, (1971).

70. Beckett, R., & Hurt, J.: Numerical Calculations and Algorithms, McGraw-Hill.

71. Bratu, Em., Dimian, A., & Floarea, O.: Rev. Chim. (Bucharest), 7, 423, (1969).

72. Grigovlev, Yu. M.: Zh.Fiz. Khim., 44, 647, (1970).

73. Maletskaya, K.D.: Teplofiz Teplotekh, 16, 94, (1970).

74. Miura, K.: Kagaku Kogaku, 35, 643, (1971).

75. Kotelinee Kotei/'Nikov, A.R.: Khim. Prog., 49, 47,(1973).

APPENDICES.

APPENDIX A

A.1 Tables 1-4: Data for Evaluating Drying Characteristics of Pure Water Drops

A.1.1 Computational Algorithms for Least Squares Technique

(i) $Sh = 2.0 + \Psi Re^{0.5} Sc^{0.33}$ ((5.1))

(ii) $Sh = 2.0 + \delta \left(\frac{T_{au} - T_s}{T_{amb}}\right)^{\eta} Re^{0.5} Sc^{0.33}$ ((5.2))

A.1.1.1 "Basic 16" Program for Equation ((5.1))

A.1.1.2 "Basic 16" Program for Equation ((5.2))

A.1

TABLE 1

$T_{au} = 26.5^{oC}$, $T_s = 19.0^{oC}$

Air Flow Rate	Drop Diameter	Humidity		
		Upstream	Downstream	Saturation
$G \times 10^3$ kg/s	$d_p \times 10^2$ m	$H_U \times 10^4$ kg/kg	$H_D \times 10^4$ kg/kg	kg/kg
0.24	0.1	0.18	0.386	0.014
0.47	0.1	0.066	0.141	0.014
0.68	0.1	0.151	0.127	0.014
0.91	0.1	0.042	0.121	0.014
1.05	0.1	0.038	0.112	0.014
1.44	0.1	0.031	0.105	0.014
0.24	0.3	0.443	0.524	0.014
0.47	0.3	0.284	0.360	0.014
0.68	0.3	0.224	0.302	0.014
0.91	0.3	0.187	0.262	0.014
1.05	0.3	0.172	0.247	0.014
1.26	0.3	0.154	0.232	0.014
1.44	0.3	0.142	0.221	0.014
0.24	0.5	0.874	0.948	0.014
0.47	0.5	0.570	0.646	0.014
0.68	0.5	0.455	0.530	0.014
0.91	0.5	0.383	0.461	0.014
1.05	0.5	0.352	0.424	0.014
1.26	0.5	0.316	0.396	0.014
1.44	0.5	0.293	0.373	0.014

TABLE 2

T_{au} = 46.5, T_s = 32.4°C

Air Flow Rate	Drop Diameter	Humidity		
		Upstream	Downstream	Saturation
$G \times 10^3$ kg/s	$d_p \times 10^2$ m	$H_U \times 10^4$ kg/kg	$H_D \times 10^4$ kg/kg	kg/kg
0.24	0.1	0.1156	0.3480	0.031
0.47	0.1	0.1156	0.2590	0.031
0.68	0.1	0.1458	0.2560	0.031
0.91	0.1	0.1571	0.2440	0.031
1.05	0.1	0.1571	0.2380	0.031
1.26	0.1	0.2655	0.3360	0.031
1.44	0.1	0.3560	0.4240	0.031
0.24	0.3	0.1250	1.060	0.031
0.47	0.3	0.1290	0.7240	0.031
0.68	0.3	0.1458	0.6100	0.031
0.91	0.3	0.1525	0.5370	0.031
1.05	0.3	0.2500	0.6030	0.031
1.26	0.3	0.3095	0.6320	0.031
1.44	0.3	0.3438	0.6390	0.031
0.24	0.5	0.1069	1.940	0.031
0.47	0.5	0.1103	1.300	0.031
0.68	0.5	0.1290	1.070	0.031
0.91	0.5	0.1458	0.9270	0.031
1.05	0.5	0.2752	1.010	0.031
1.26	0.5	0.3059	0.9580	0.031
1.44	0.5	0.3519	0.9190	0.031

TABLE 3

$T_s = 32.4^{oC}$

$T_{au} = 85.0^{oC}$

Air Flow Rate	Drop Diameter	Humidity Upstream	Humidity Downstream	Humidity Saturation
$G \times 10^3$ kg/s	$d_p \times 10^2$ m	$H_U \times 10^4$ kg/kg	$H_D \times 10^4$ kg/kg	kg/kg
0.24	0.1	0.104	0.340	0.031
0.47	0.1	0.139	0.282	0.031
0.68	0.1	0.266	0.373	0.031
0.91	0.1	0.317	0.405	0.031
1.05	0.1	0.321	0.400	0.031
1.26	0.1	0.336	0.410	0.031
1.44	0.1	0.356	0.424	0.031
0.24	0.3	0.107	1.040	0.031
0.47	0.3	0.107	0.700	0.031
0.68	0.3	0.146	0.617	0.031
0.91	0.3	0.253	0.646	0.031
1.05	0.3	0.250	0.603	0.031
1.26	0.3	0.299	0.617	0.031
1.44	0.3	0.317	0.610	0.031
0.24	0.5	0.107	1.94	0.031
0.47	0.5	0.121	1.31	0.031
0.68	0.5	0.125	1.07	0.031
0.91	0.5	0.125	0.910	0.031
1.05	0.5	0.306	1.03	0.031
1.26	0.5	0.336	0.998	0.031
1.44	0.5	0.391	0.998	0.031

TABLE 4

$T_{au} = 118.5^{oC}$, $T_s = 32.4^{oC}$

Air Flow Rate	Drop Diameter	Humidity Upstream	Humidity Downstream	Humidity Saturation
$G \times 10^3$ kg/s	$d_p \times 10^2$ m	$H_U \times 10^4$ kg/kg	$H_D \times 10^4$ kg/kg	kg/kg
0.24	0.1	0.081	0.324	0.031
0.47	0.1	0.082	0.229	0.031
0.68	0.1	0.087	0.199	0.031
0.91	0.1	0.087	0.179	0.031
1.05	0.1	0.107	0.191	0.031
1.26	0.1	0.123	0.197	0.031
1.44	0.1	0.317	0.382	0.031
0.24	0.3	0.089	1.05	0.031
0.47	0.3	0.105	0.716	0.031
0.68	0.3	0.107	0.589	0.031
0.91	0.3	0.107	0.505	0.031
1.05	0.3	0.112	0.477	0.031
1.26	0.3	0.146	0.482	0.031
1.44	0.3	0.275	0.582	0.031
0.24	0.5	0.104	2.03	0.031
0.47	0.5	0.139	1.38	0.031
0.68	0.5	0.253	1.24	0.031
0.91	0.5	0.266	1.09	0.031
1.05	0.5	0.317	1.08	0.031
1.26	0.5	0.317	0.998	0.031
1.44	0.5	0.344	0.968	0.031

A.1.1 Computational Algorithm for Least Squares Technique

(i) Isothermal Data:

$$Sh = 2.0 + \Psi Re^{0.5} Sc^{0.33} \qquad ((5.1))$$

Equation ((5.1)) was rearranged to facilitate linearisation, thus:

$$(Sh-2) = \Psi Re^{0.5} Sc^{0.33} \qquad ((5.1a))$$

Taking logarithms of both sides of equation ((5.1a)) gives:

$$\log_e (Sh-2) = \log_e \Psi + \log_e (Re^{0.5} Sc^{0.33}) \qquad ((A.1))$$

or $Y = C + X$

where $Y = \log_e (Sh-2)$

$C = \log_e \Psi$

$X = \log_e (Re^{0.5} Sc^{0.33})$

The error between the given data and the approximating function at X_i is given by $e(X_i) = Y_i - C - X_i$ ((A.3))

The objective function, therefore, is to minimise the sum of the errors squared and hence determine the best value of the constant, C, from which Ψ can be evaluated. If the objective function is denoted S, then

$$S = \sum_{i=1}^{n} (Y_i - C - X_i)^2 \qquad ((A.4))$$

Differentiating S with respect to C, and setting the differential equal to zero, leads to

$$\frac{ds}{dc} = -2 \sum_{i=1}^{n} (Y_i - C - X_i) = 0 \qquad ((A.5))$$

Thus

$$\Sigma Y_i - nC - \Sigma X_i = 0 \qquad ((A.6))$$

Therefore

$$C = \frac{1}{n} (\Sigma Y_i - \Sigma X_i) \qquad ((A.7))$$

Ψ can then be evaluated from equation ((A.7)) by taking the antilogarithm of C, that is:

$$\Psi = \exp(C) \qquad ((A.8))$$

(ii) Proposed Correlation:

$$Sh = 2.0 + \delta \left(\frac{T_{au} - T_s}{T_{amb}}\right)^{\eta} Re^{0.5}\, Sc^{0.33} \qquad ((5.2))$$

Rearranging equation ((5.2)) leads to,

$$(Sh-2) = \delta \left(\frac{T_{au} - T_s}{T_{amb}}\right)^{\eta} Re^{0.5}\, Sc^{0.33} \qquad ((5.2a))$$

By taking logarithms of equation ((5.2a)),

$$\log_e(Sh-2) = \log_e\delta + \eta \log_e\left(\frac{T_{au} - T_s}{T_{amb}}\right) + \log_e(Re^{0.5} Sc^{0.33}) \qquad ((A.9))$$

Or

$$Y = C + X + BZ \qquad ((A.10))$$

Where

$$C = \log_e \delta$$

$$B = \eta$$

$$Z = \log_e \left(\frac{T_{au} - T_s}{T_{amb}}\right)$$

As explained in (i) above, the objective function is given by

$$S = \sum_{i=1}^{n} (Y_i - C - X_i - BZ_i)^2 \qquad ((A.11))$$

$$\frac{\partial S}{\partial C} = -2\, \Sigma(Y_i - C - X_i - BZ_i) = 0 \qquad ((A.12))$$

$$\frac{\partial S}{\partial B} = -2\, \Sigma Z_i\, (Y_i - C - X_i - BZ_i) = 0 \qquad ((A.13))$$

Equations ((A.12)) and ((A.13)) were solved for C and B and the solutions are:

$$B = \frac{n\,\Sigma(Z_i X_i) + \Sigma Y_i \Sigma Z_i - n\,(Y_i Z_i) - (X_i)(Z_i)}{(\Sigma Z_i)^2 - n\,\Sigma(Z_i)^2} \qquad ((A.14))$$

$$C = \frac{1}{n} (\Sigma Y_i - \Sigma X_i - B \ \Sigma Z_i) \qquad ((A.15))$$

Hence $\eta = B$ ((A.16))

and $\delta = \exp(C)$ ((A.17))

(iii) Coefficient of Correlation

Although in the least-squares approximation to a set of data points, the coefficient, or coefficients in the approximating function are chosen to make the sum of errors squared a minimum, the sum of errors squared is not a very good measure of fit (70). The index of correlation, which is a number that measures the fit of the approximation to the data, is defined so that a perfect fit gives an index of correlation equal to one. As the index of correlation becomes smaller, a poorer fit is indicated.

The coefficient of correlation is represented by,

$$r_{f,Y} = \left(1 - \frac{S}{n(\sigma_Y)^2} \right)^{\frac{1}{2}} \qquad ((A.18))$$

Where

S = sum of errors squared, equation ((A.4))

n = number of points in the collection Y

$(\sigma_y)^2$ = variance = $\frac{1}{n} \Sigma \ (Y - \overline{Y})^2$

$Y = \frac{1}{n} \Sigma Y_i$ = mean value of Y

The value of $r_{f,Y}$ is independent of the number of points in the collection.

A.1.1.1 "Basic 16" Program for Equation (5.1)

```
15      DIM Y(21),X(21)
20      B=2
21      N=21
22      M=3
25      S1=0
30      S2=0
35      S3=0
40      S4=0
42      FOR I1=1,M
43      READ Z
45      FOR I=1,N
50      READ Y(I)
52      NEXT I
53      FOR I=1,N
55      READ X(I)
60      NEXT I
65      FOR I=1,N
70      S1=S1+(Y(I)-B)*X(I)↑.5*Z↑.33
75      S2=S2+X(I)*X↑.67
80      NEXT I
85      A=S1/S2
90      PRINT
95      PRINT "Y=";B;"+";A"X↑.5";"Z↑.33"
100     PRINT
110     PRINT " RE        ...SH(EXP)...        ...SH(CALC)..."
115     S=0
120     S2=0
125     FOR I=1,N
130     Y1=B+A*X(I)↑.5*Z↑.33
135     S=S+Y(I)
140     S2=S2+(Y1-Y(I))↑2
145     PRINT X(I),Y(I),Y1
150     NEXT I
155     S=S/N
160     S1=0
165     FOR I=1,N
170     S1=S1+(Y(I)-S)↑2
```

```
175     NEXT I
180     S1=S1/N
185     C1=(I-S2/(N*S1))↑.5
190     PRINT "VARIANCE=";S1
195     PRINT "SUM OF ERRORS SQUARED=";S2
200     PRINT "COEFFICIENT OF CORRELATION=";C1
202     PRINT
203     PRINT
205     NEXT I1
210     END
```

A.1.1.2 "Basic 16" Program for Equation (5.2)

```
1Ø      DIM Y(1ØØ),Z(1ØØ),W(1ØØ)
2Ø      N=83
3Ø      S1=Ø
4Ø      S2=Ø
5Ø      S3=Ø
6Ø      S4=Ø
7Ø      S5=Ø
8Ø      S6=Ø
9Ø      FOR I=1,N
1ØØ      READ Y(I)
11Ø      NEXT I
12Ø      FOR I=1,N
13Ø      READ Z(I)
14Ø      NEXT I
15O      FOR I=1,N
16Ø      READ W(I)
17Ø      NEXT I
18Ø      FOR I=1,N
19Ø      S1=S1+LOG(Y(I)-2)
2ØØ      S2=S2+LOG(Z(I))
21Ø      S3=S3+LOG(W(I))
22Ø      S4=S4+(LOG(W(I)))*(LOG(Y(I)-2))
23Ø      S5=S5+(LOG(Z(I)))*(LOG(W(I)))
24Ø      S6=S6+(LOG(W(I)))↑2
25Ø      NEXT I
26Ø      B=(N*S5+S1*S3-N*S4-S2*S3)/(S3↑2-N*S6)
27Ø      X=(S1-S2-B*S3)/N
28Ø      X=EXP(X)
29Ø      PRINT
3OO      PRINT "SH=2+";X;"((TAY-TS)/TAMB)↑";B;"RE↑1/2.SC↑1/3"
31Ø      PRINT
32Ø      PRINT " SH(EXP)      SH(CALC)      ABSCISSA"
33Ø      PRINT
34Ø      S1=Ø
35Ø      S2=Ø
36Ø      FOR I=1,N
37Ø      U=W(I)↑B*Z(I)
```

```
38Ø        Y1=2+X*U
39Ø        S1=S1+Y(I)
4ØØ        S2=S2+(Y1-Y(I))↑2
41Ø        PRINT Y(I),Y1,U
42Ø        PRINT
43Ø        NEXT I
44Ø        S1=S1/N
45Ø        S3=Ø
46Ø        FOR I=1,N
47Ø        S3=S3+(Y(I)-S1)↑2
48Ø        NEXT I
49Ø        S3=S3/N
5ØØ        C1=(1-S2/(N*S3)))↑.5
51Ø        D1=S3↑.5
52Ø        PRINT
53Ø        PRINT
54Ø        PRINT "VARIANCE = ";S3
55Ø        PRINT
56Ø        PRINT "STANDARD DEVIATION = ";D1
57Ø        PRINT
58Ø        PRINT "SUM OF ERRORS SQUARED = ":S2
59Ø        PRINT
6ØØ        PRINT "COEFFICIENT OF CORRELATION = ";C1
61Ø        PRINT:
62Ø        END
```

APPENDIX B

B.1 Tables B5-B22: Data for Evaluating Drying Characteristics of Drops of aqueous Sodium Sulphate Decahydrate

B.2 ICL 1905 Fortran Program for calculating Crust Thickness Rates, Driving Forces and Mass Transfer Coefficients

B.3 Honeywell H316 "Basic 16" Computer Program for estimating Experimental and Theoretical Mass Transfer Coefficients and Percent Resistance in the gas phase and Crust phase

B.1

TABLE B5

Air Temperature, T_a = 129^oC
Mean Drop Temperature, T_s = 75^oC
Initial Moisture Content, C_o = $0.225 \times 10^3 Kg/m^3$
Air Flow Rate, G = $0.24 \times 10^{-3} Kg/s$
External Drop Radius, R = $0.374 \times 10^{-2} m$
Porosity ε = 0.389

TIME	AIR HUMIDITY Upstream	Downstream
mins	$H_U \times 10^4 Kg/Kg$	$H_D \times 10^4 Kg/Kg$
0	0.0508	0.0508
1	0.0508	0.6270
2	0.0508	0.4475
3	0.0508	0.3600
4	0.0508	0.3070
5	0.0508	0.2550
6	0.0508	0.2125
7	0.0508	0.1725
8	0.0508	0.1650
9	0.0508	0.1325
10	0.0508	0.1225
11	0.0508	0.1205
12	0.0508	0.1186
13	0.0508	0.1175
14	0.0508	0.1165
15	0.0508	0.1135
16	0.0508	0.1100
17	0.0508	0.1005
18	0.0508	0.0990
19	0.0508	0.0950
20	0.0508	0.0900
21	0.0508	0.0850
22	0.0508	0.0830

TABLE 35 Cont

23	0.0508	0.0800
24	0.0508	0.0785
25	0.0508	0.0757
26	0.0508	0.0732
27	0.0508	0.0712
28	0.0508	0.0710
29	0.0508	0.0700
30	0.0508	0.0695
31	0.0508	0.0671
32	0.0508	0.0642
33	0.0508	0.0631
34	0.0508	0.0620
35	0.0508	0.0615
36	0.0508	0.0600
37	0.0508	0.0600
38	0.0508	0.0585
39	0.0508	0.0580
40	0.0508	0.0572
41	0.0508	0.0565
42	0.0508	0.0561
43	0.0508	0.0552
44	0.0508	0.0543
45	0.0508	0.0543
46	0.0508	0.0542
47	0.0508	0.0542
48	0.0508	0.0542
49	0.0508	0.0542

TABLE B6

Air Temperature, T_a	=	$120.5^{o}C$
Mean Drop Temperature, T_s	=	$70.3^{o}C$
Initial Moisture Content, C_o	=	$0.353 \times 10^{3} Kg/m^{3}$
Air Flow Rate, G	=	$0.47 \times 10^{-3} Kg/s$
External Drop Radius, R	=	$0.263 \times 10^{-2} m$
Porosity, ε	=	0.390

	AIR HUMIDITY	
	Upstream	Downstream
mins	$H_U \times 10^{4} Kg/Kg$	$H_D \times 10^{4} Kg/Kg$
0	0.0433	0.0433
1	0.0433	0.8825
2	0.0433	0.7850
3	0.0433	0.6425
4	0.0433	0.6275
5	0.0433	0.4927
6	0.0433	0.4021
7	0.0433	0.3925
8	0.0433	0.3625
9	0.0433	0.2240
10	0.0433	0.1580
11	0.0433	0.1225
12	0.0433	0.1000
13	0.0433	0.0900
14	0.0433	0.0881
15	0.0433	0.0800
16	0.0433	0.0780
17	0.0433	0.0738
18	0.0433	0.0700
19	0.0433	0.0677
20	0.0433	0.0655
21	0.0433	0.0625

TABLE B6 Cont

22	0.0433	0.0600
23	0.0433	0.0515
24	0.0433	0.0473
25	0.0433	0.0446
26	0.0433	0.0443
27	0.0433	0.0442
28	0.0433	0.0442
29	0.0433	0.0442
30	0.0433	0.0442

TABLE B7

Air Temperature, T_a	= 121.0°C
Mean Drop Temperature, T_s	= 70.8°C
Initial Moisture Content, C_o	= 0.610 x 10^3 Kg/m^3
Air Flow Rate, G	= 0.47 x 10^{-3} Kg/s
External Drop Radius, R	= 0.375 x 10^{-2} m
Porosity, ε	= 0.385

AIR HUMIDITY

	Upstream	Downstream
mins	H_U x 10^4 Kg/Kg	H_D x 10^4 Kg/Kg
0	0.0184	0.0184
1	0.0184	0.1850
2	0.0184	0.1640
3	0.0184	0.1100
4	0.0184	0.1000
5	0.0184	0.0840
6	0.0184	0.0738
7	0.0184	0.0670
8	0.0184	0.0625
9	0.0184	0.0600
10	0.0184	0.0593
11	0.0184	0.0577
12	0.0184	0.0545
13	0.0184	0.0530
14	0.0184	0.0520
15	0.0184	0.0515
16	0.0184	0.0500
17	0.0184	0.0485
18	0.0184	0.0473
19	0.0184	0.0465
20	0.0184	0.0451
21	0.0184	0.0440

TABLE B7 Cont

22	0.0184	0.0440
23	0.0184	0.0440
24	0.0184	0.0440

TABLE B8

Air Temperature, T_a = 120.5°C
Mean Drop Temperature = 70.3°C
Initial Moisture Content, C_o = 0.5555×10^3 Kg/m^3
Air Flow Rate, G = 0.47×10^{-3} Kg/s
External Drop Radius, R = 0.263×10^{-2} m
Porosity ε = 0.380

AIR HUMIDITY

	Upstream	Downstream
mins	$H_U \times 10^4$ Kg/Kg	$H_D \times 10^4$ Kg/Kg
0	0.0249	0.0249
1	0.0249	0.1430
2	0.0249	0.1210
3	0.0249	0.1005
4	0.0249	0.0821
5	0.0249	0.0738
6	0.0249	0.0700
7	0.0249	0.0660
8	0.0249	0.0615
9	0.0249	0.0576
10	0.0249	0.0567
11	0.0249	0.0562
12	0.0249	0.0540
13	0.0249	0.0530
14	0.0249	0.0515
15	0.0249	0.0508
16	0.0249	0.0500
17	0.0249	0.0473
18	0.0249	0.0465
19	0.0249	0.0445
20	0.0249	0.0440
21	0.0249	0.0433
22	0.0249	0.0431

TABLE B8 Cont

23	0.0249	0.0430
24	0.0249	0.0425
25	0.0249	0.0423
26	0.0249	0.0423
27	0.0249	0.0423
28	0.0249	0.0423
29	0.0249	0.0423

TABLE B9

Air Temperature, T_a = 121.0°C
Mean Drop Temperature, T_s = 70.8°C
Initial Moisture Content, C_o = 0.555×10^{3} Kg/m^3
Air Flow Rate, G = 047×10^{-3} Kg/s
External Drop Radius, R = 0.375×10^{-2} m
Porosity, ε = 0.390

AIR HUMIDITY

	Upstream	Downstream
mins	$H_U \times 10^4$ Kg/Kg	$H_D \times 10^4$ Kg/Kg
0	0.0184	0.0184
1	0.0184	0.1520
2	0.0184	0.1250
3	0.0184	0.1100
4	0.0184	0.0950
5	0.0184	0.0821
6	0.0184	0.0745
7	0.0184	0.0695
8	0.0184	0.0640
9	0.0184	0.0615
10	0.0184	0.0610
11	0.0184	0.0585
12	0.0184	0.0577
13	0.0184	0.0545
14	0.0184	0.0537
15	0.0184	0.0515
16	0.0184	0.0500
17	0.0184	0.0485
18	0.0184	0.0473
19	0.0184	0.0465
20	0.0184	0.0460

TABLE B9 Cont

21	0.0184	0.0445
22	0.0184	0.0440
23	0.0184	0.0436
24	0.0184	0.0432
25	0.0184	0.0430
26	0.0184	0.0427
27	0.0184	0.0425
28	0.0184	0.0424
29	0.0184	0.0420
30	0.0184	0.0410
31	0.0184	0.0407
32	0.0184	0.0403
33	0.0184	0.0400
34	0.0184	0.0398
35	0.0184	0.0396
36	0.0184	0.0392
37	0.0184	0.0391
38	0.0184	0.0385
39	0.0184	0.0380
40	0.0184	0.0376
41	0.0184	0.0373
42	0.0184	0.0372
43	0.0184	0.0370
44	0.0184	0.0368
45	0.0184	0.0367
46	0.0184	0.0367
47	0.0184	0.0367
48	0.0184	0.0367
49	0.0184	0.0367

TABLE B10

Air Temperature, T_a = 120°C
Mean Drop Temperature, T_s = 65.5°C
Initial Moisture Content, C_o = 0.555×10^3 Kg/m^3
Air Flow Rate, G = 0.68×10^{-3} Kg/s
External Drop Radius, R = 0.225×10^{-2} m
Porosity ε = 0.384

	AIR HUMIDITY	
	Upstream	Downstream
mins	$H_U \times 10^4$ Kg/Kg	$H_D \times 10^4$ Kg/Kg
0	0.0385	0.0385
1	0.0385	0.0770
2	0.0385	0.0695
3	0.0385	0.0655
4	0.0385	0.0615
5	0.0385	0.0578
6	0.0385	0.0562
7	0.0385	0.0540
8	0.0385	0.0515
9	0.0385	0.0500
10	0.0385	0.0473
11	0.0385	0.0465
12	0.0385	0.0464
13	0.0385	0.0460
14	0.0385	0.0460
15	0.0385	0.0455
16	0.0385	0.0451
17	0.0385	0.0446
18	0.0385	0.0442
19	0.0385	0.0440
20	0.0385	0.0437

TABLE B10 Cont

21	0.0385	0.0436
22	0.0385	0.0435
23	0.0385	0.0430
24	0.0385	0.0430
25	0.0385	0.0430

TABLE B11

Air Temperature, T_a = 120.5 ^oC
Mean Drop Temperature, T_s = 70.3 ^oC
Initial Moisture Content, = 0.555 x 10^3 Kg/m^3
Air Flow Rate, G = 0.68 x 10^{-3} Kg/s
External Drop Radius, R = 0.263 x 10^{-2} m
Porosity ε = 0.380

	AIR HUMIDITY	
	Upstream	Downstream
mins	H_U x 10^4 Kg/Kg	H_D x 10^4 Kg/Kg
0	0.0585	0.0585
1	0.0585	0.1630
2	0 0585	0.1430
3	0.0585	0.1225
4	0.0585	0.1100
5	0.0585	0.1025
6	0.0585	0.0990
7	0.0585	0.0960
8	0.0585	0.0940
9	0.0585	0.0900
10	0.0585	0.0875
11	0.0585	0.0850
12	0.0585	0.0842
13	0.0585	0.0831
14	0.0585	0.0830
15	0.0585	0.0827
16	0.0585	0.0825
17	0.0585	0.0824
18	0.0585	0.0824
19	0.0585	0.0824
20	0.0585	0.0824

TABLE B12

Air temperature, T_a = 121.0 ^oC
Mean Drop Temperature, T_s = 70.8 ^oC
Initial Moisture Content, C_o = 0.555 x 10^3 Kg/m^3
Air Flow Rate, G = 0.68 x 10^{-3} Kg/s
External Drop Radius, R = 0.375 x 10^{-2} m
Porosity ε = 0.390

AIR HUMIDITY

	Upstream	Downstream
mins	H_U x 10^4 Kg/Kg	H_D x 10^4 Kg/Kg
0	0.0821	0.0821
1	0.0821	1.4000
2	0.0821	1.230
3	0.0821	0.7900
4	0.821	0.4950
5	0.0821	0.3550
6	0.0821	0.2940
7	0.0821	0.2400
8	0.0821	0.2250
9	0.0821	0.1980
10	0.0821	0.1880
11	0.0821	0.1850
12	0.0821	0.1750
13	0.0821	0.1670
14	0.0821	0.1630
15	0.0821	0.1600
16	0.0821	0.1590
17	0.0821	0.1550
18	0.0821	0.1530
19	0.0821	0.1528

TABLE B12 Cont

20	0.0821	0.1521
21	0.0821	0.1520
22	0.0821	0.1518
23	0.0821	0.1518
24	0.0821	0.1518
25	0.0821	0.1518

TABLE B13

Air Temperature T_a	$= 120.5^{o}C$
Mean Drop Temperature T_s	$= 70.3^{o}C$
Initial Moisture Content, C_o	$= 0.580 \times 10^{3} Kg/m^{3}$
Air Flow Rate, G	$= 0.68 \times 10^{-3} Kg/s$
External Drop Radius, R	$= 0.145 \times 10^{-2} m$
Porosity ε	$= 0.382$

AIR HUMIDITY

	Upstream	Downstream
mins	$H_U \times 10^{4} Kg/Kg$	$H_D \times 10^{4} Kg/Kg$
0	0.0128	0.0128
1	0.0128	0.5720
2	0.0128	0.4470
3	0.0128	0.4050
4	0.0128	0.3750
5	0.0128	0.3550
6	0.0128	0.3350
7	0.0128	0.3180
8	0.0128	0.3100
9	0.0128	0.3000
10	0.0128	0.2995
11	0.0128	0.2978
12	0.0128	0.2900
13	0.0128	0.2900
14	0.0128	0.2891
15	0.0128	0.2881
16	0.0128	0.2851
17	0.0128	0.2840
18	0.0128	0.2831

TABLE B13 Cont

19	0.0128	0.2831
20	0.0128	0.2831
21	0.0128	0.2831
22	0.0128	0.2831

TABLE B14

Air Temperature T_a	$= 121.5^{o}C$
Mean Drop Temperature T_s	$= 70.8^{o}C$
Initial Moisture Content, C_o	$= 0.555 \times 10^{3} Kg/m^{3}$
Air Flow Rate, G	$= 0.91 \times 10^{-3} Kg/s$
External Drop Radius, R	$= 0.225 \times 10^{-2} m$
Porosity ε	$= 0.385$

	AIR HUMIDITY	
	Upstream	Downstream
mins	$H_U \times 10^{4}$ Kg/kg	$H_D \times 10^{4}$ Kg/Kg
0	0.1540	0.1540
1	0.1540	0.7910
2	0.1540	0.6140
3	0.1540	0.5450
4	0.1540	0.5000
5	0.1540	0.4835
6	0.1540	0.4665
7	0.1540	0.4610
8	0.1540	0.4605
9	0.1540	0.4600
10	0.1540	0.4500
11	0.1540	0.4460
12	0.1540	0.4460
13	0.1540	0.4460
14	0.1540	0.4460
15	0.1540	0.4460
16	0.1540	0.4460
17	0.1540	0.4460

TABLE B15

Air Temperature T_a = 119.0°C
Mean Drop Temperature, T_s = 65.0°C
Initial Moisture Content, C_o = 0.550×10^3 Kg/m^3
Air Flow Rate, G = 0.91×10^{-3} Kg/s
External Drop Radius, R = 0.225×10^{-2} m
Porosity ε = 0.390

	AIR HUMIDITY	
	Upstream	Downstream
mins	$H_U \times 10^4$ Kg/Kg	$H_D \times 10^4$ Kg/Kg
0	0.0821	0.0821
1	0.0821	0.4665
2	0.0821	0.3500
3	0.0821	0.2500
4	0.0821	0.2000
5	0.0821	0.1750
6	0.0821	0.1625
7	0.0821	0.1540
8	0.0821	0.1525
9	0.0821	0.1475
10	0.0821	0.1460
11	0.0821	0.1455
12	0.0821	0.1450
13	0.0821	0.1442
14	0.0821	0.1441
15	0.0821	0.1438
16	0.0821	0.1436
17	0.0821	0.1433
18	0.0821	0.1427
19	0.0821	0.1427
20	0.0821	0.1427

TABLE B15 Cont

21	0.0821	0.1427
22	0.0821	0.1427
23	0.0821	0.1427

TABLE B16

Air Temperature, T_a = 121.5°C
Mean Drop Temperature, T_s = 70.8°C
Initial Moisture Content, C_o = 0.555×10^3 Kg/m^3
Air Flow Rate, G = 0.01×10^{-3} Kg/s
External Drop Radius, R = 0.338×10^{-2} m
Porosity ε = 0.385

	AIR HUMIDITY	
	Upstream	Downstream
mins	$H_U \times 10^4$ Kg/Kg	$H_D \times 10^4$ Kg/Kg
0	0.0403	0.0403
1	0.0403	0.5925
2	0.0403	0.3930
3	0.0403	0.2375
4	0.0403	0.1525
5	0.0403	0.1160
6	0.0403	0.0950
7	0.0403	0.0850
8	0.0403	0.0745
9	0.0403	0.0662
10	0.0403	0.0650
11	0.0403	0.0578
12	0.0403	0.0501
13	0.0403	0.0478
14	0.0403	0.0445
15	0.0403	0.0440
16	0.0403	0.0434
17	0.0403	0.0433
18	0.0403	0.0410
19	0.0403	0.0408
20	0.0403	0.0408
21	0.0403	0.0408

TABLE B16 Cont

22	0.0403	0.0408
23	0.0403	0.0408

TABLE B17

Air Temperature, T_a	$= 112.5^{o}C$
Mean Drop Temperature, T_s	$= 63.5^{o}C$
Initial Moisture Content C_o	$= 0.580 \times 10^{3} Kg/m^{3}$
Air Flow Rate, G	$= 1.05 \times 10^{-3} Kg/s$
External Drop Radius, R	$= 0.15 \times 10^{-2} m$
Porosity ε	$= 0.390$

	AIR HUMIDITY	
	Upstream	Downstream
mins	$H_U \times 10^{4}$ Kg/Kg	$H_D \times 10^{4}$ Kg/Kg
0	0.0127	0.0127
1	0.0127	0.0850
2	0.0127	0.0738
3	0.0127	0.0670
4	0.0127	0.0625
5	0.0127	0.0585
6	0.0127	0.0560
7	0.0127	0.0540
8	0.0127	0.0508
9	0.0127	0.0493
10	0.0127	0.0473
11	0.0127	0.0465
12	0.0127	0.0450
13	0.0127	0.0449
14	0.0127	0.0445
15	0.0127	0.0440
16	0.0127	0.0437
17	0.0127	0.0437
18	0.0127	0.0437
19	0.0127	0.0436
20	0.0127	0.0436
21	0.0127	0.0436

TABLE B18

Air Temperature T_a	$= 112.5^{o}C$
Mean Drop Temperature T_s	$= 63.5^{o}C$
Initial Moisture Content, C_o	$= 0.580 \times 10^{3} Kg/m^{3}$
Air Flow Rate, G	$= 1.05 \times 10^{-3} Kg/s$
External Drop Radius, R	$= 0.225 \times 10^{-2} m$
Porosity ε	$= 0.390$

AIR HUMIDITY

	Upstream	Downstream
mins	$H_U \times 10^{4} Kg/Kg$	$H_D \times 10^{4} Kg/Kg$
0	0.0125	0.0125
1	0.0125	0.0789
2	0.0125	0.0705
3	0.0125	0.0640
4	0.0125	0.0585
5	0.0125	0.0565
6	0.0125	0.0545
7	0.0125	0.0540
8	0.0125	0.0530
9	0.0125	0.0520
10	0.0125	0.0515
11	0.0125	0.0508
12	0.0125	0.0506
13	0.0125	0.0500
14	0.0125	0.0493
15	0.0125	0.0473
16	0.0125	0.0465
17	0.0125	0.0460
18	0.0125	0.0445
19	0.0125	0.0440

TABLE B18 Cont

20	0.0125	0.0433
21	0.0125	0.0433
22	0.0125	0.0433
23	0.0125	0.0433
24	0.0125	0.0433

TABLE B19

Air Temperature, T_a	$= 112.5^{o}C$
Mean Drop Temperature T_s	$= 63.5^{o}C$
Initial Moisture Content C_o	$= 0.500 \times 10^{3} Kg/m^{3}$
Air Flow Rate, G	$= 1.05 \times 10^{-3} Kg/s$
External Drop Radius, R	$= 0.30 \times 10^{-2} m$
Porosity ε	$= 0.385$

	AIR HUMIDITY	
	Upstream	Downstream
mins	$H_U \times 10^{4}$ Kg/Kg	$H_D \times 10^{4}$ Kg/Kg
0	0.0250	0.0250
1	0.0250	0.0900
2	0.0250	0.0780
3	0.0250	0.0746
4	0.0250	0.0730
5	0.0250	0.0705
6	0.0250	0.0662
7	0.0250	0.0640
8	0.0250	0.0615
9	0.0250	0.0610
10	0.0250	0.0600
11	0.0250	0.0585
12	0.0250	0.0580
13	0.0250	0.0577
14	0.0250	0.0570
15	0.0250	0.0565
16	0.0250	0.0563
17	0.0250	0.0560
18	0.0250	0.0552
19	0.0250	0.0550
20	0.0250	0.0545

TABLE B19 Cont

21	0.0250	0.0545
22	0.0250	0.0545
23	0.0250	0.0545
24	0.0250	0.0545
25	0.0250	0.0545

TABLE B20

Air Temperature, T_a	$= 69.0^{o}C$
Mean Drop Temperature, T_s	$= 39.6^{o}C$
Initial Moisture Content, C_o	$= 0.850 \times 10^{3} Kg/m^{3}$
Air Flow Rate, G	$= 1.05 \times 10^{-3} Kg/s$
External Drop Radius, R	$= 0.555 \times 10^{-2} m$
Porosity ε	$= 0.384$

AIR HUMIDITY

	Upstream	Downstream
mins	$H_U \times 10^{4} Kg/Kg$	$H_D \times 10^{4} Kg/Kg$
0	0.0410	0.0410
1	0.0410	0.1140
2	0.0410	0.1008
3	0.0410	0.0840
4	0.0410	0.0780
5	0.0410	0.0745
6	0.0410	0.0738
7	0.0410	0.0705
8	0.0410	0.0695
9	0.0410	0.0686
10	0.0410	0.0670
11	0.0410	0.0662
12	0.0410	0.0660
13	0.0410	0.0655
14	0.0410	0.0650
15	0.0410	0.0645
16	0.0410	0.0641
17	0.0410	0.0640
18	0.0410	0.0638

TABLE B20 Cont

19	0.0410	0.0637
20	0.0410	0.0636
21	0.0410	0.0636
22	0.0410	0.0636
23	0.0410	0.0636

TABLE B21

Air Temperature T_a	$= 94.0^{o}C$
Mean Drop Temperature, T_s	$= 60.5^{o}C$
Initial Moisture Content C_o	$= 0.722 \times 10^{3} Kg/m^{3}$
Air Flow Rate, G	$= 0.68 \times 10^{-3} Kg/s$
External Drop Radius, R	$= 0.25 \times 10^{-2} m$
Porosity ε	$= 0.390$

	AIR HUMIDITY	
	Upstream	Downstream
mins	$H_U \times 10^{4}$ Kg/Kg	$H_D \times 10^{4}$ Kg/Kg
0	0.0153	0.0153
1	0.0153	0.0820
2	0.0153	0.0780
3	0.0153	0.0745
4	0.0153	0.0720
5	0.0153	0.0695
6	0.0153	0.0670
7	0.0153	0.0661
8	0.0153	0.0655
9	0.0153	0.0630
10	0.0153	0.0615
11	0.0153	0.0609
12	0.0153	0.0592
13	0.0153	0.0587
14	0.0153	0.0580
15	0.0153	0.0576
16	0.0153	0.0570
17	0.0153	0.0562
18	0.0153	0.0560

TABLE B21 Cont

19	0.0153	0.0552
20	0.0153	0.0550
21	0.0153	0.0543
22	0.0153	0.0500
23	0.0153	0.0492
24	0.0153	0.0472
25	0.0153	0.0463
26	0.0153	0.0460
27	0.0153	0.0451
28	0.0153	0.0442
29	0.0153	0.0395
30	0.0153	0.0395
31	0.0153	0.0395
32	0.0153	0.0395
33	0.0153	0.0395

TABLE B22

Air Temperature, T_a	=	$94.0^{o}C$
Mean Drop Temperature, T_s	=	$60.5^{o}C$
Initial Moisture Content, C_o	=	$0.610 \times 10^{3} Kg/m^3$
Air Flow Rate, G	=	$0.68 \times 10^{-3} Kg/s$
External Drop Radius, R	=	$0.30 \times 10^{-2} m$
Porosity ε	=	0.390

	AIR HUMIDITY	
	Upstream	Downstream
mins	$H_U \times 10^4 Kg/Kg$	$H_D \times 10^4 Kg/Kg$
0	0.0224	0.0224
1	0.0224	0.1300
2	0.0224	0.1180
3	0.0224	0.1050
4	0.0224	0.0997
5	0.0224	0.0940
6	0.0224	0.0910
7	0.0224	0.0860
8	0.0224	0.0830
9	0.0224	0.0820
10	0.0224	0.0805
11	0.0224	0.0789
12	0.0224	0.0764
13	0.0224	0.0760
14	0.0224	0.0746
15	0.0224	0.0740
16	0.0224	0.0736
17	0.0224	0.0730
18	0.0224	0.0724
19	0.0224	0.0721
20	0.0224	0.0720

TABLE B22 Cont

21	0.0224	0.0715
22	0.0224	0.0712
23	0.0224	0.0695
24	0.0224	0.0686
25	0.0224	0.0684
26	0.0224	0.0680
27	0.0224	0.0678
28	0.0224	0.0670
29	0.0224	0.0661
30	0.0224	0.0651
31	0.0224	0.0650
32	0.0244	0.0645
33	0.0244	0.0641
34	0.0224	0.0640
35	0.0224	0.0640
36	0.0224	0.0639
37	0.0224	0.0639
38	0.0224	0.0639
39	0.0224	0.0639
40	0.0224	0.0639

B.2 ICL 1905 FORTRAN PROGRAM

```
      MASTER AUDUCRUST
      DIMENSION A(50),B(50),2(50),Y(50),H(50),RAD(50),EXPC(50),
      THEC(50),TIC(50),BETA(50),ODI(50),TOM(50)
      DC= 0.22              --------------- (molecular diffusivity at 0°C)
      DT=1.0*2.54  ----------- (equivalent diameter of wind tunnel)
      RHO=1.293E-03  ---------- (air density at 0°C)
      PI=3.1416
      TAMB=20.0+273.16  --------- (ambient temperature)
      READ(1.10)M
 10   FORMAT (12)
      DO 90 II=1.M
      WRITE (2.15) II
 15   FORMAT (1H1.4HSET , 12)
      READ(1.20)N
 20   FORMAT (12)
      READ(1.30)WOW,PRO,SLP,C1,G,R
 30   FORMAT (6F10.0)
      READ(1.40)T,TS
 40   FORMAT (2F10.0)
      READ(1.49)AA  ------------ (upstream air humidity)
 49   FORMAT (F10.0)
      AA=AA*.1E-03
      G=G/(1.0+AA) ----------  (dry air flow rate)
      READ(1.50)(B(I), I=1,N)  ------- (downstream air humidity)
 50   FORMAT(F10.0)
      BB=B(1)
      RHZ=RHO*273.16/(T+273.16)
      DIF=DC*((T+273.16(/273.16)**1.5
      SC=WOW/(RHZ*DIF) --------- (Schmidt Number)
      RE=8.0*G*R/(WOW*PI*DI**2)  ------ (Reynolds Number)
      FC=DIF*(2.0+0.6*RE**0.5*SC**0.33)/(2.0*R)
      FCC=DIF*(2.0+0.44*RE**0.5*SC**0.33*((T-TS)/TAMB)**(-0.008))/(2.0
      1*R    ------- (Film Mass Transfer Coefficient , kg)
```

```
      EFD=DIF*POR**1.5 -------  (Effective Diffusivity of water vapour)
      WRITE (2.64)G,RHZ,DIF,SC,RF,FC,FCC,EFD
 64   FORMAT (1HO,8F12.7)
      WRITE(2.65)
 65   FORMAT(19X,11HTHEORETICAL,6X,12HEXPERIMENTAL,8X,11HTHEORETICAL,10X
      1,12HEXPERIMENTAL
      WRITE(2.66)
 66   FORMAT(21X,8HMOISTURE,10X,8HMOISTURE,10X,12HOVERALL MASS, 8X,13H
      OV 1ERALL MASS,6X,15HCRUST THICKNESS)
      WRITE (2.67)
 67   FORMAT (22X,6HEVAPTD,12X,6HEVAPTD,11X,12HTRANS COEFF.,8X13H TRANS
      1COEFF.)
      WRITE (2.68)
 68   FORMAT (21X,8HGM/CU.CM,10X,8HGM/CU.CM.13X,6HCM/SEC.12X,6HCM/SEC,
      15X 1,3Hcm.)
      DO 70 I=2,N
      H(I)=BB-B(I)
      H(I)=H(I)*.1E-03  --------- (Kg water removed/Kg air)
      RAD(I)=(R**3-(90.0*G*H(I)/(PI*C1)))**(1.0/3.0)-(core  radius)
      BETA(I)= R-RAD(I)  -------- (Crust thickness)
      TCO(I)=FC*EFD)/(EFD+BETA(I)*FC)
      ODI(I)=(FCC+EFD)/(EFD+BETA(I)*FCC) --(OVerall Mass Transfer Coefficient
      TOM(I)=G*H(I)/(2.0*PI*ODI(I)*R**2) ----(driving force)
      THEC(I) =G*H(I)/(2.0*PI*TCO(I)*(R**2))
 70   WRITE (2.80)THEC(I),TOM(I),TCO(I),ODI(I),BETA(I)
 80   FORMAT (10X,5E20.5)
 90   CONTINUE
      STOP
      END
      FINISH
```

B.3 Honeywell H316 "Basic 16" Program for Estimating Experimental and Theoretical Mass Transfer Coefficients

```
20   L  = 18
30   R1 = 82.06          (universal gas constant)
40   R3 = 18.02          (molecular weight of water vapour)
50   R5 = 20 + 273.16    (ambient air temperature)
60   R7 = 2.54           (equivalent diameter of wind tunnel)
70   FOR I1 = 1,L:PRINT "SET";I1
80   READ T, H1, B, R2, R4, G, R, P2
     (T  = upstream air humidity)
     (H1 = downstream air humidity)
     (B  = crust thickness)
     (R2 = air temperature)
     (R4 = drop temperature)
     (G  = wet air flow rate)
     (R  = outside radius of drop)
     (P2 = saturation vapour pressure)
90   READ E              (porosity of crust)
100  G = G/(1 + H1)      (dry air flow rate)
110  A = 2 * 3.1416 * (R↑2 - (R-b)↑2)/E
                         (mass transfer area)
120  P1 = H1/(.622 + H1)(partial pressure of air)
130  R6 = .22 * (R2/273.16)↑1.5      (molecular diffusivity)
140  R8 = .1293E-02 * 273.16/R2      (air density)
150  R9 = .17E-03 * R2/273.16        (air viscosity)
160  A5 = R9/(R8 * R6)               (Schmidt number)
170  H3 = 8 * G * R/(R9 * 3.1416 * R7↑2)
                                     (Reynolds number)
180  PRINT H3
```

```
190  H4 = R6 * (2 + .44 * H3↑ .5 * A5↑.33 * ((R2-R4)/R5)↑(-.008))/(2 * R)
     (H4 = film mass transfer coefficient from the proposed
     correlation for pure waterdrops)
200  D = (T - H1)* G/A                    (mass transfer rate)
210  K = R1 * R2 * D/((P2 - P1) * R3)(experimental overall mass
                                          transfer coefficient)
220  W = H4 * K/(H4-K)                    (experimental crust coefficient)
230  A1 = 1/H4 : A2 = 1/W
240  A3 = 100 * A1/(A1 + A2)              (A3 = % gas film resistance)
250  A4 = 100 * A2/(A1 + A2)              (A4 = % crust resistance)
260  K1 = R6 * E↑1.5/B                    (theoretical crust coefficient)
270  K2 = H4 * K1/(H4 + K1)               (theoretical overall mass transfer
                                          coefficient)
280  PRINT : PRINT
290  PRINT D, W, H4, K1 : PRINT
300  PRINT K, K2, A3, A4
310  PRINT
320  NEXT I1
330  END
```

APPENDIX C

C.1 Table C.1: Pressure Drop Data for Estimating Porosity of Drops from Detergent Formulations

C.2 Honeywell H316 "Basic 16" Computer Program for Estimating Drying Characteristics of Detergent Drops; also, Experimental and Theoretical Mass Transfer Coefficients

C.3 Computational Algorithm for Least Squares Technique for Proposed Correlation for Particulate Slurries

$Sh = gRe^{x}Sc^{y}$ ((5.21))

C.3.1 "Basic 16" Program for Least Squares Technique

C.1 TABLE C.1

Pressure Drop Through Crusts

Formulation	ΔP $g/(cm.S^2)$	Air Flow Rate $\times 10^3$ (g/s)
A	3420	1.23
B	3500	0.416
C	7950	0.350
D	9900	0.483
E	7200	0.399
F	1550	0.932
G	3740	0.333
H	1850	0.932
I	550	1.30

C.2 Honeywell H-316 "Basic 16" Computer Program

```
5     REM  ESTIMATION OF DRYING CHARACTERISTICS OF DETERGENT DROPS
10     DIM T(19),W(19),D(19),K(19)
15     DIM Z(19)
20     N=19
30     M=9
60     H1=.501E-05
65     G=.68/(1+H1)
80     P1=H1/C.622+H1)
110     R1=82.06
120     R2=98+273.16
121     R4=81+273.16
122     R5=20+273.16
123     R6=.22*(R2/273.16)↑1.5
124     R7=.1293E-02*273.16/R2
125     R8=.21E-03/(R7*R6)
130     R3=18.02
140     FOR I=1,N
150     READ T(I)
160     NEXT I
165     S=0
166     S6=0
170     FOR I1=1,M: PRINT I1
171     READ R,B,P2:P2=P2/760:P3=P2-P1
173     R9=8*G*R/(.21E-03*3.141*2.54↑2)
174     H3=R6*(2+.44*R9↑.5*R8↑.33*(R2-R4)/R5)↑(-.8E-02))/(2*R)
175     PRINT
176     PRINT H3,R9
177     PRINT
178     READ F
179     READ E:A=2*3.1416*(R↑2-(R-B)↑2/E
180     E=E↑1.5
181     K1=R6*E/B
182     K2=H3*K1/(H3+K1)
183     A1=E↑(1/1.5)/B
185     FOR I=1,N
190     READ W(I)
196     A2=W(I)/A
```

```
200     D(I)=W(I)/(T(I)*A)
210     K(I)=(R1*R2*D(I))/(P3*R3)
215     Z(I)=H3K(I)/(H3-K(I))
216     PRINT
217     PFINT W(I),D(I),A1,A2: PRINT
220     NEXT I
240     FOR I=1,N
241     S6=S6+Z(I)
242     S=S+K(I)
243     NEXT I
244     S6=S6/N:C1=H3*R6*E/(R6*E+B*H3)
247     S=S/N
249     S1=2*S*R/(R6*E)
250     S2=.21E-03/(R7*R6*E)
251     S3=2*S6*R/(R6*E)
252     PRINT S1,S2,S3,R6,R7
253     PRINT
255     PRINT S6,K1,C1,S,K2
256     PRINT : NEXT I1
260     END
```

C.3 Computational Algorithm for Least Squares Technique in Terms of Equation ((5.21))

$$Sh = gRe^{x}\ Sc^{y} \qquad ((5.21))$$

Equation ((5.21)) was linearised by taking logarithms, thus

$$\log_e Sh = \log_e g + x \log_e Re + y \log_e Sc \qquad ((C.1))$$

or

$$Y = C + xU + yZ \qquad ((C.2))$$

where

$$Y = \log_e Sh$$

$$C = \log_e g$$

$$U = \log_e Re$$

$$Z = \log_e Sc$$

The objective function becomes:

$$S = \Sigma(Y_i - C - xUi - yZi)^2 \qquad ((C.3))$$

$$\frac{\partial S}{\partial C} = -2\Sigma(Y_i - C - xUi - yZi) = 0 \qquad ((C.4))$$

$$\frac{\partial S}{\partial x} = -2\Sigma U_i(Y_i - C - xUi - yZi) = 0 \qquad ((C.5))$$

$$\frac{\partial S}{\partial y} = -2\Sigma Z_i(Y_i - C - xUi - yZi) = 0 \qquad ((C.6))$$

The three simultaneous equations to be solved for C, x and y are:

$$\Sigma Y_i - nC - x\Sigma U_i - y\Sigma Z_i = 0 \qquad ((C.7))$$

$$\Sigma U_i Y_i - C\Sigma U_i - x\Sigma U_i^{\ 2} - y\Sigma U_i Z_i = 0 \qquad ((C.8))$$

$$\Sigma Z_i Y_i - C\Sigma Z_i - x\Sigma Z_i U_i - y\Sigma Z_i^2 = 0 \qquad ((C.9))$$

The solutions are: ((5.21))

$$x = \frac{(\Sigma U_i \Sigma Z_i - n\Sigma U_i Z_i)(n\Sigma Z_i Y_i - \Sigma Y_i \Sigma Z_i) - ((\Sigma Z_i)^2 - n\Sigma Z_i^2)(n\Sigma U_i Y_i - \Sigma U_i \Sigma Y_i)}{((\Sigma Z_i)^2 - n\Sigma Z_i^2)((\Sigma U)^2 - n\Sigma U_i^2) - (\Sigma U_i \Sigma Z_i - n\Sigma U_i Z_i)^2} \qquad ((C.10))$$

$$y = \frac{\Sigma Y_i \Sigma U_i - n\Sigma U_i Y_i - ((\Sigma U_i)^2 - n\Sigma U_i^2)x}{\Sigma U_i \Sigma Z_i - n\Sigma U_i Z_i} \qquad ((C.11))$$

$$C = (\Sigma Y_i - x\Sigma U_i - y\Sigma Z_i)/n \qquad ((C.12))$$

and

$$g = \exp(C) \qquad ((C.13))$$

The nature of fit of the regression, equation ((C.2)) to the experimental points was determined from the index of correlation explained in Section (iii) of Appendix A.1.1.

C.3.1 "Basic 16" Program for Least Squares Technique

```
5       PRINT "PROPOSED CORRELATION FOR DETERGENT FORMULATION"
6       PRINT : PRINT
10       DIM E(10),T(10),P(10),Q(10)
20       DIM X(10),Z(10),U(10)
25       D2=.348449
30       N=9
40       S1=0
50       S2=0
60       S3=0
70       S4=0
80       S5=0
90       S6=0
100      S7=0
110      S8=0
112      FOR I=1,N
114      READ E(I)
115      NEXT I
120      FOR I=1,N
130      READ X(I)
132      NEXT I
134      FOR I=1,N
135      READ T(I)
140      NEXT I
150      FOR I=1,N
160      READ Z(I)
170      NEXT I
180      FOR I=1,N
190      READ U(I)
195      U(I)=U(I)*T(I)/(D*E(I)↑1.5)
200      NEXT I
210      FOR I=1,N
220      S1=S1+LOG(X(I))
230      S2=S2+LOG(Z(I))
240      S3=S3+LOG(U(I))
250      S4=S4+LOG(X(I)))↑2
260      S5=S5+(LOG(Z(I)))↑2
270      S6=S6+(LOG(X(I)))*(LOG(Z(I)))
```

```
280    S7=S7+LOG(U(I)))*(LOG(Z(I)))
290    S8=S8+(LOG(U(I)))*(LOG(X(I)))
300    NEXT I
310    C1=N*S8-S1*S3
320    C2=S2↑2-N*S5
330    C3=N*S7-S2*S3
340    C4=S1*S2-N*S6
350    C5=S1↑2-N*S4
360    B=(C1*C2-C3*C4(/(C4↑2-C5*C2)
370    C6=-(C1+C5*B)/C4
380    K=(S3-B*S1-C6*S2)/N
390    K=EXP(K)
400    PRINT
410    PRINT "SH =";K;"(RE)↑";B;"(SC)↑";C6
412    PRINT
415    PRINT "RE      SH(EXP)      SH(CALC) ";RE↑";B;"SC↑";C6
420    S1=0
430    S2=0
440    FOR I=1,N
450    Y1=K*X(I)↑ B*Z(I) ↑C6
460    S1=S1+U(I)
470    S2=S2+(Y1-U(I))↑2
475    Y2=X(I)↑B*Z(I)↑C6
480    PRINT X(I),U(I),Y1,Y2
490    NEXT I
500    S1=S1/N
510    S3=0
520    FOR I=1,N
530    S3=S3+(U(I)-S1)↑2
540    NEXT I
550    S3=S3/N
555    D3=S3↑(1/2)
560    C=(1-S2/(N*S3))↑.5
565    PRINT
570    PRINT " VARIANCE = ";S3
572    PRINT
574    PRINT "STANDARD DEVIATION = ":D3
575    PRINT
580    PRINT " SUM OF ERRORS SQUARED = ";S2
```

```
585     PRINT
590     PRINT " COEFFICIENT OF CORRELATION = ";C
595     PRINT
625     FOR I=1,N
630     P(I)=U(I)*D*E(I)↑1.5/T(I)
635     Q(I)=K*X(I)↑B*Z(I)↑C6*D*E(I)↑1.5/T(I)
640     PRINT
645     PRINT P(I),Q(I)
650     PRINT
652     NEXT I
655     END
```

APPENDIX D

Vapour Pressure Experiments and Results

D.1 Vapour Pressure Experiments

The apparatus shown in plate D.1 was adopted owing to the inadequacy of conventional (66) methods for vapour pressure determinations.

The solution, or slurry was introduced to an an evacuated flask, A, in a water bath, and allowed to reach the operating temperature. After steady state had been achieved, the pressure reading on the mercury manometer was recorded. A control experiment, with distilled water, was set up simultaneously to calibrate the apparatus.

Vapour pressures of hydrated sodium sulphate solutions, and detergent formulations are recorded below:

TABLE D.1

Sodium Sulphate Solutions (Na_2So_4 10 H_2O)

Temperature (oC)	39.6	60.5		63.5		65.0
C_o ($\frac{g\ water}{cm^3\ solution}$)	0.85	0.61	0.722	0.50	0.58	0.55
Vapour pressure (atm)	0.011	0.016	0.027	0.027	0.04	0.033

cont

70.3		70.8	75.0
0.56	0.58	0.56	0.225
0.04	0.04	0.041	0.0042

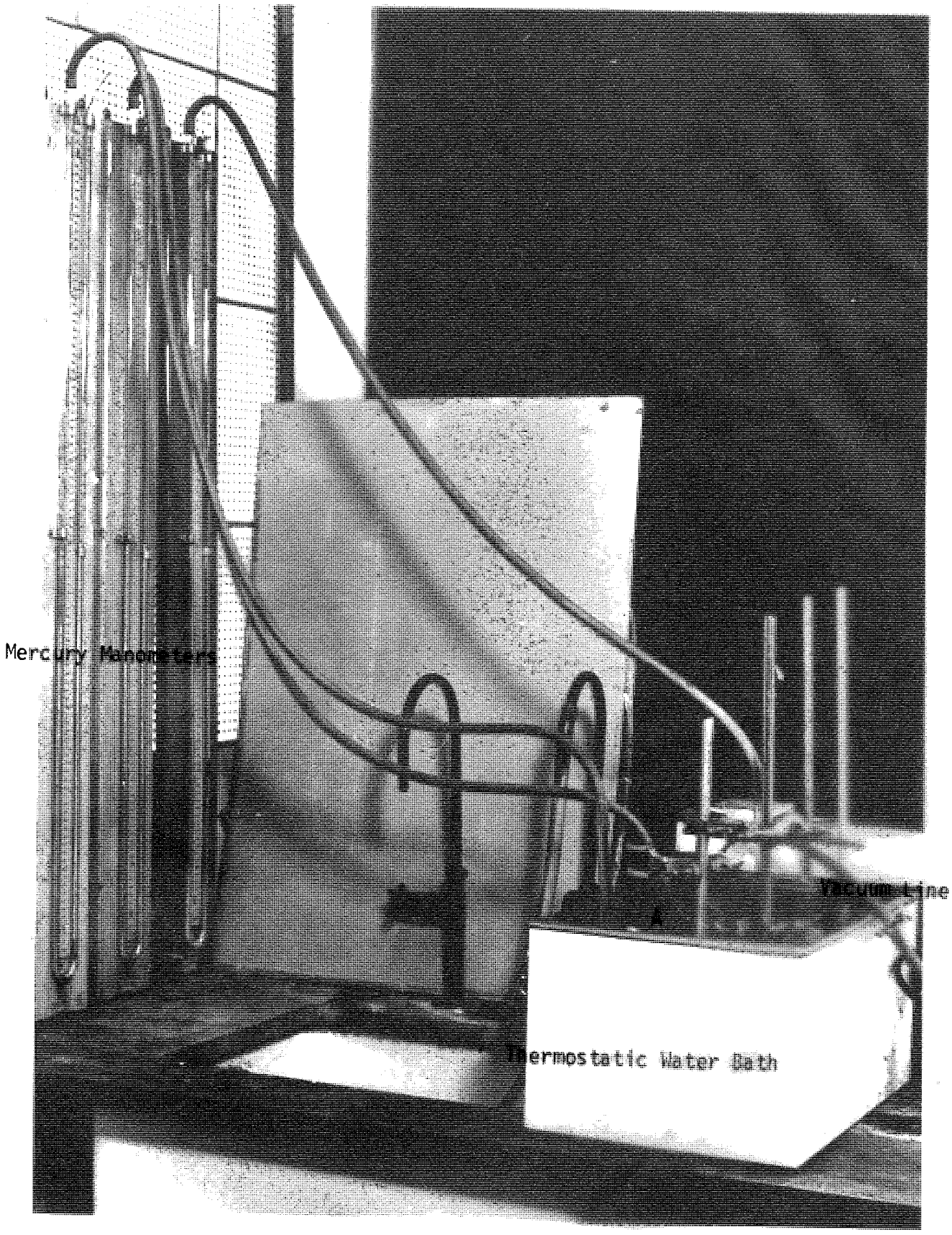

Plate D.1 Vapour Pressure Apparatus.

TABLE D.2

Detergent Formulations

Temperature of slurry = 81.0 ^{oC}

Formulation	A	B	C	D	E	F	G	H	I
Vapour Pressure (atm)	0.101	0.092	0.089	0.084	0.079	0.064	0.096	0.092	0.092

FIGURE 5.28

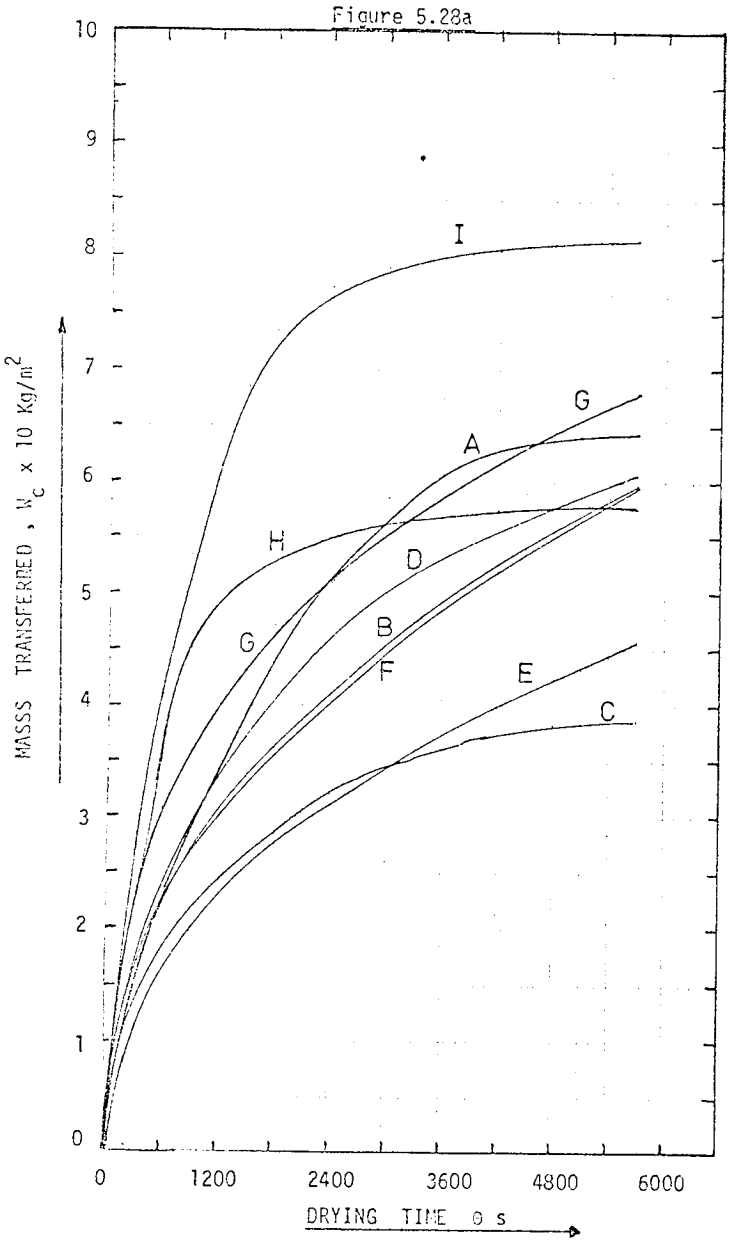
Figure 5.28a
MASSS TRANSFERRED , N_c x 10 Kg/m^2
DRYING TIME θ s
0
1200
2400
3600
4800
6000
0
1
2
3
4
5
6
7
8
9
10
I
G
A
H
D
G
B
F
E
C

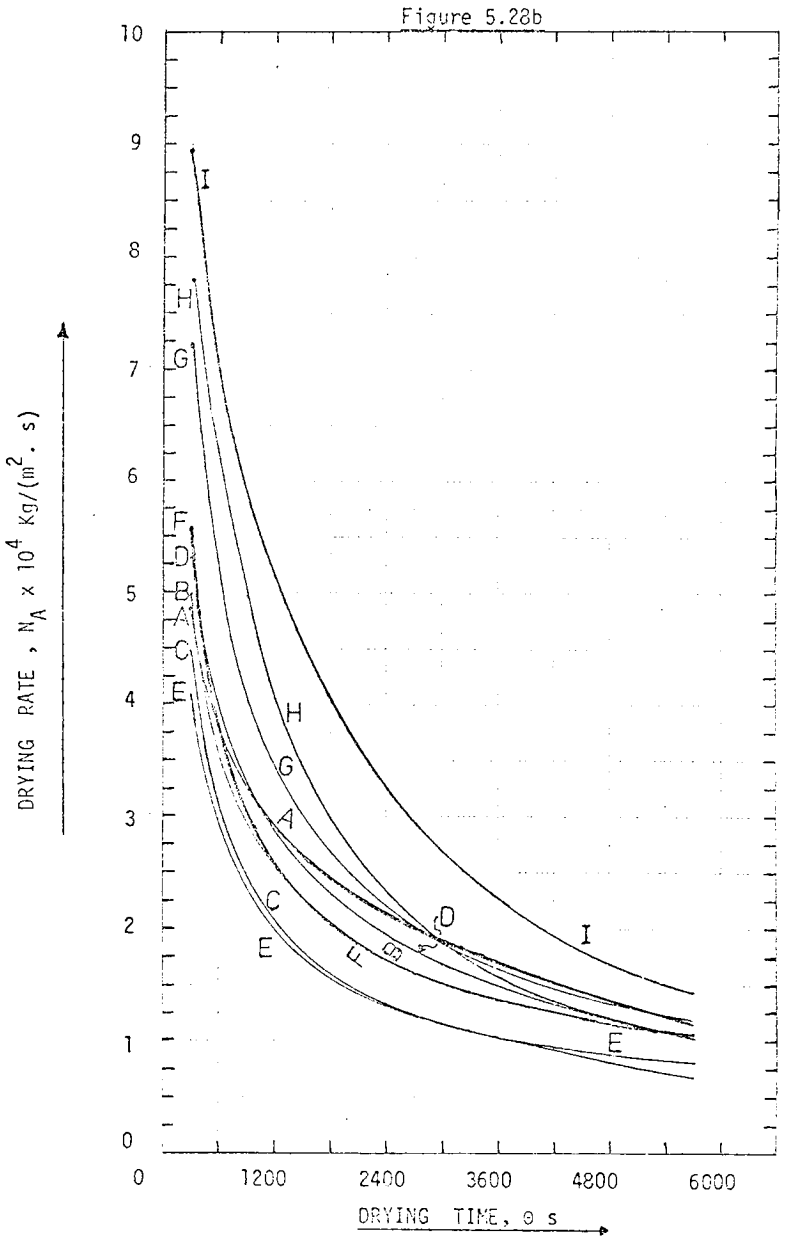
Figure 5.28b
DRYING RATE , N_A x 10^4 Kg/(m^2. s)
DRYING TIME, θ s
0
1200
2400
3600
4800
6000
0
1
2
3
4
5
6
7
8
9
10
I
H
G
F
D
B
A
C
E
H
G
A
D
I
C
E
B
E